

In presenting this thesis in partial fulfillment of the requirements for an advanced degree at Idaho State University, I agree that the Library shall make it freely available for inspection. I further state that permission to download and/or print my thesis for scholarly purposes may be granted by the Dean of the Graduate School, Dean of my academic division, or by the University Librarian. It is understood that any copying or publication of this thesis for financial gain shall not be allowed without my written permission.

Signature _____

Date _____

Migration of Fission Products in Nuclear Fuel Compact Matrix Material

by

Theodore C Pollock

A thesis
submitted in partial fulfillment
of the requirements for the degree of
Master of Science in the Department of Nuclear Engineering
Idaho State University
Fall 2015

To the Graduate Faculty:

The members of the committee appointed to examine the thesis of Theodore C Pollock find it satisfactory and recommend that it be accepted.

Dr. Mary Lou Dunzik – Gougar, Adviser

Dr. George Imel, Committee Member

Dr. Rene Rodriguez, Graduate Faculty Representative

Whenever I am not completely sure about what I am doing, I think back to TOF-SIMS measurement at Montana State University. While trying to get a \$1.5M piece of equipment to operate correctly, I heard the following:

“NO!! NOOOO MOHAMMED!! DON’T DO THAT!! ... Oh, wait, do that again Mohammed”

- Recep Avci Ph.D

Without moments like these, nothing would ever get done.

Table of Contents

List of Figures	vi
List of Tables	vii
Abstract:	viii
Chapter 1 Introduction and Purpose	1
Chapter 2 A Review of the Concepts and Relevant Research	6
2.1 Diffusion in Porous Media	6
2.2 Fick’s Laws and Flux	10
2.3 Knudsen Diffusion	14
2.3.1 Introduction	14
2.3.2 Effect of Tortuosity	15
2.3.3 Knudsen Number.....	20
2.4 Adsorption of Fission Products to VHTR Materials	24
2.5 Graphite Diffusion Coefficients	27
Chapter 3 Modeling Fission Product Migration in Matrix Graphite	35
3.1 MATLAB Model for Knudsen Number.....	35
3.2 MATLAB Model For Diffusion Depth	40
Chapter 4 Measuring Fission Product Migration in Matrix Graphite.....	46
4.1 Experimental Work	46
4.2 Suggestions for Further Experimentation	61
4.3 Alternate Mechanism for Silver Migration – Thermal Diffusion	64
4.3.1 Soret Effect in Nuclear Applications.....	65
4.3.2 Thermal Diffusion in Non-Nuclear Applications.....	69
Chapter 5 Conclusions	75
References.....	78
Appendix 1 MATLAB Scripts.....	81
Final V2.m.....	81
Depth V2.m	83
BoyleData.m.....	87
Appendix II One Practical Solution for the Diffusion Equation.....	88
Appendix III TOF-SIMS Files Linear and Log Y-axis Scales	93

List of Figures

Figure 2.1 Diffusing Metal	13
Figure 2.2 Tortuosity.....	15
Figure 2.3 Knudsen Number vs. Diffusion Coefficient.....	18
Figure 2.4 Expected Concentration vs. Depth for Graphite.....	31
Figure 2.5 Silver Concentration vs. Depth HTC #4.....	33
Figure 3.1 Knudsen Number Low Pressure.....	38
Figure 3.2 Knudsen Number High Pressure.....	39
Figure 3.3 Silver Vapor Pressure.....	41
Figure 3.4 Silver Concentration vs. Depth.....	45
Figure 4.1 Aluminum Jig.....	48
Figure 4.2 Denton Desktop Pro.....	50
Figure 4.3 Graphite Sample Before Coating.....	51
Figure 4.4 Coated Graphite Sample.....	52
Figure 4.5 Sample 74 TOF-SIMS Surface.....	55
Figure 4.6 Sample 74 TOF-SIMS 5 Minute Sputter.....	56
Figure 4.7 Sample 75 TOF-SIMS Surface.....	57
Figure 4.8 Sample 75 5 Minute Sputter.....	58
Figure 4.9 Sample 76 Surface.....	59
Figure 4.10 Sample 76 10 Minute Sputter.....	60
Figure 4.11 Carbon Concentration vs. Temperature.....	71
Figure 4.12 Hydrogen Distribution in Zirconium.....	73

List of Tables

Table 1.1 HTGR Information.....	4
Table 2.1 Neutron Activation Analysis Data Boyle	32

Migration of Fission Products in Nuclear Fuel Compact Matrix Material

Abstract: In support of next generation nuclear reactor fuel development, the nature of fission product migration through fuel compact matrix material was investigated. An analytical model for bulk and Knudsen diffusion were built in MATLAB in order to predict the behavior of fission product surrogates migrating through nuclear fuel compact matrix material similar to A3-3. The model graphically shows where the Knudsen regime may or may not be applicable for user-specified temperature and pressure parameters. Model output is consistent with Knudsen diffusion occurring at conditions expected in a very high temperature gas-cooled reactor (VHTR). In parallel with the theoretical analyses, experiments were conducted to investigate diffusion processes at very low concentrations of diffusant species in order to promote Knudsen diffusion. Graphitic matrix material similar to A3-3 matrix was coated via physical vapor deposition with a thin layer of silver followed a thicker layer of silicon carbide intended to prevent silver movement away from the matrix material. Samples were heated to 700 C or 1000 C and subsequently analyzed to determine silver location and concentration. Though results were not as expected, valuable lessons were learned to inform future experiments.

Chapter 1 Introduction and Purpose

Since the first human-controlled fission of a uranium nucleus in the Chicago Pile 1 on December 2 1942, fission products have been generated in nuclear systems ranging from power plants to nuclear weapons. When a nuclear weapon detonates, the fission products are scattered instantly and are of relatively little concern in comparison to the destructive blast force (“Hiroshima, Nagasaki”, 2015). For nuclear power systems, however, the containment of fission products is of paramount importance. The United States fleet of pressurized water reactors and boiling water reactors are required by 10 CFR 50.34 regulations to contain the fission products generated by their low enriched uranium fuel even during accident conditions (United States, 2015). The first form of fission product containment is the zirconium alloy fuel cladding that surrounds the uranium fuel pellets (Duderstadt & Hamilton, 1976). Thousands of reactor operation hours have been logged and are a testament to the effectiveness of zirconium alloy cladding’s ability to contain the fission products. Occasionally, fuel rod cladding will develop a crack or other defect and release a small amount of fission product gas into the water coolant. In most circumstances, a cladding breach is monitored and the reactor can continue to operate as long as the concentration of fission products in the coolant remains sufficiently low. Individual fuel assemblies are checked for cladding breaches by sipping techniques during refueling outages (Tsoulfanidis, 2013).

The mechanisms of fission product release for light water reactor fuels are relatively simple compared to some other reactor designs. If the Zircaloy cladding remains intact, fission products will be contained. If the cladding develops a crack or pinhole, fission products will be released. Studies on zirconium alloy cladding have been

extensive and have provided a wealth of information on the topic. The same cannot be said for non-water moderated reactor designs that use graphite-encapsulated fuel and gas coolant.

There were two gas-cooled reactors operated in the United States that used graphite-encapsulated fuel and helium coolant. The first of these reactors was Peach Bottom Unit 1 near Harrisburg, Pennsylvania, which operated from 1966 to 1974 (Kingrey, 2003). This reactor was a proof of concept plant intended to test the merits of a gas-cooled reactor while producing a maximum of 40 MWe for the power grid. The reactor had two cores during its lifetime – core 1 operated from 1966 to 1970 and core 2 operated from 1970 through close of Unit 1 in 1974. Both cores used graphite fuel rods with uranium and thorium embedded in the graphite. The rods were 12 feet long and 3.5 inches in diameter and contained a fission product trap in the center made of activated carbon from coconut shells. In the first core, approximately 90 fuel elements failed and were cause for replacing the core at half of its expected lifetime. Fuel particle coating was improved in the rods for core 2 and the result was a much lower failure rate.

The second gas-cooled reactor in the United States, operated from 1979 – 1989, was the Fort Saint Vrain Nuclear Generating Station in Platteville Colorado (Copinger & Moses, 2003). Like the Peach Bottom Unit 1 that preceded it, Fort Saint Vrain operated with a uranium – thorium fuel cycle, graphite moderator, and helium coolant. The main differences between PB1 and FSV were the scale of operation and core design. FSV generated 8.5 times the electrical power at 330 MWe. The core was a prismatic design opposed to PB1's rods. The prismatic design had 1482 hexagonal blocks 14 inches from flat-to-flat and 31 inches high stacked in 247 columns. Each hexagonal block was drilled

to accept coolant passages. Fuel particles were composed of uranium and thorium carbide coated with pyrolytic carbon and silicon carbide. Commercial operation ceased at FSV when cracks were observed in the steam generator main steam ringheaders and the cost of repair was deemed not feasible.

Other countries have operated gas cooled – graphite moderated reactors over the past half century (Beck & Pincock, 2011). The UK has relied on a fleet of 14 Advanced Gas Reactors (AGR) with carbon dioxide coolant and outlet temperatures around 650 C since 1976 (Nonbol, 1996). The UK and other nations have developed their own high temperature gas cooled reactor (HTGR) designs for experimental and commercial purposes, but none of these designs has achieved the widespread deployment of AGR, PWR, or BWR. Table 1.1 highlights some of the key features of high temperature gas cooled reactors that have been built outside the United States, excluding the AGR program.

Table 1.1 HTGR information for reactors outside the United States and AGR program (Beck & Pincock, 2011)

List of Past and Currently Operational High Temperature Gas Cooled Reactors					
Country	Reactor Name	Operational Years	Thermal Power [MW]	Coolant	Core Design
United Kingdom	Dragon	1964 - 1975	21.5	Helium	Prismatic
West Germany	AVR	1967 - 1988	46	Helium	Pebble Bed
West Germany	THTR	1985 - 1991	750	Helium	Pebble Bed
Japan	HTTR	1998 -	30	Helium	Prismatic
People's Democratic Republic of China	HTR - 10	2000 -	10	Helium	Pebble Bed

Thirteen countries including the United States, Canada, the People’s Republic of China and the Russian Federation participate in the Generation IV International Forum, the objective of which is to design the next generation of reactors, including a gas cooled – graphited moderated very high temperature reactor (VHTR) (Beck & Pincock, 2011). Prismatic and pebble bed Gen IV VHTR designs both use TRISO coated fuel particles surrounded by graphite matrix material. Pebble bed designs use softball-sized pebbles composed of TRISO-coated fuel particles in matrix material rather than prismatic blocks. It is known that fission products will escape from the fuel in small quantities and migrate throughout the reactor (Beck & Pincock, 2011). To further the development of the VHTR, it is necessary to understand how the fission products migrate.

The particular focus of this research was the mechanism(s) of fission product migration away from the particle fuel and through the graphite matrix material. Historically, this migration has been roughly modeled as diffusion and quantified with empirical diffusion coefficients (IAEA, 1997). However, post-irradiation analyses of the materials do not support classical diffusion theory. Because diffusing species tend to move away from the region of highest species' concentration, a concentration gradient is created. Such gradients in fission product species' concentrations are not seen surrounding the particle fuel in post irradiation graphitic matrix material. In fact, for certain species, especially fission product silver, it has been suggested that migration occurs as individual atoms in the gas phase finding their way through pores and along grain boundaries in materials. This type of movement was described by Knudsen (Knudsen, 1934) and is commonly, though inaccurately, referred to as Knudsen Diffusion.

It was the objective of the research presented here to elucidate the mechanism of silver migration through graphitic matrix material.

Chapter 2 A Review of the Concepts and Relevant Research

2.1 Diffusion in Porous Media

Gaseous diffusion has been studied since the 1800s and since that time there have been numerous theories proposed to describe how gases diffuse and reach an equilibrium state. Some of these theories have held up better than others over time and have been experimentally verified. Early models assumed that the most important interactions for diffusion were between gas molecules or atoms themselves and not the wall or container that the gasses inhabited. For high pressures and large volumes, this approximation is valid because the overwhelming majority of interactions are between the gas particles and not the walls. As gas pressure decreases and concomitantly mean free path increases, the number of wall collisions relative to gas particle collisions increases and becomes more of a factor influencing diffusion. This phenomenon led to the treatment of wall effects as perturbations to the ideal system where only molecule – molecule collisions were considered.

Martin Knudsen and contemporary researchers began to experiment with porous media at the turn of the 20th century and quickly realized that more than a perturbation theory was necessary to explain how gases traveled through porous structures. Knudsen (1934) published The Kinetic Theory of Gases, which was developed from Boltzmann's work (Knudsen, 1934). Since then, hundreds of other researchers have proposed modified solutions to bring the purely mathematical kinetic theory closer to real porous systems. As mentioned earlier, there have been several methods proposed that explain gaseous diffusion without wall effects. Adding the uncertainty in diffusion caused by porous structure only complicated matters further. Understanding all the facets of porous

diffusion can be daunting and the following explanation is intended to provide an overview of the mechanisms and their applicability to diffusion in porous materials (Cunningham & Willimas, 1980).

The parameters of utmost importance are the mean free path of gas and the size of the pores. In the first case where the mean free path (λ) of the gas is much less than the pore diameter (d), it is assumed that molecule – molecule interactions are important and molecule – pore interactions are not important. Within this first category, there are two subtypes of diffusion – viscous and molecular. Viscous diffusion occurs when the mean free path of the gas relative to the size of the gas molecules or atoms is small, or in another way of thinking, approaches the liquid state. In the viscous regime, the gas interacts with a pore wall and it will immediately rebound and interact with a gas molecule and has no chance of reaching another pore wall. This explanation has more relevance to granular type porous materials and should not be prevalent in graphite matrix material. Molecular diffusion occurs when the mean free path of a gas is both significantly larger than the collision diameter of the gas itself (this will be explained later) and smaller than the pore diameter. This scenario is applicable to macroporous materials such as graphite matrix material in a reactor because the mean free path of helium gas contaminated with trace amounts of fission products will be significantly larger than the collision diameter of helium – fission product gas but significantly smaller than macropores on the order of 1 micron.

Molecular diffusion exists when conditions favor interactions between gas particles rather than gas – pore interactions. When the mean free path increases due to a pressure decrease or the pore diameter decreases, gas particles will have more

interactions with pore walls. When a gas becomes so rarified and / or the pore diameter becomes so small that only gas – pore interactions take place, this is assumed to be in the Knudsen regime ($\lambda \gg d_{pore}$). In a real porous system, it would be erroneous to assume that gases diffuse strictly by molecular diffusion or strictly within the Knudsen regime. For this reason, certain cutoff values that take into account the gas behavior and porous character can be designated by an experimenter to approximate where molecular, transition, and Knudsen diffusion are taking place within a system. The transition region, also known as the “slip region” usually occurs when the Knudsen number (which will be explained later) is somewhere between of 0.1 – 10.

If the pore diameter becomes so small that it is near the size of the gas particle, configurational diffusion can occur. This phenomenon was originally observed when large organic dye molecules passed through porous polymer structures. In a nuclear reactor scenario, there are no large gas molecules diffusing and structural data for matrix material on the order of angstroms is scarce, so this type of diffusion has been ignored in further analysis.

The final consideration for porous diffusion has to deal with adsorption and wall properties. Adsorption occurs when gas molecules adhere to pore walls by van der Waals forces instead of rebounding from the walls and behaving as a gas. This occurs when gas enters a pore at a high temperature and then the temperature decreases. This is why fission products are detected in matrix graphite when the sample is removed from a reactor and analyzed. Most fission products will adsorb at much lower temperatures than helium and this is why fission products are left behind while helium will retain enough kinetic energy at room temperature so that it leaves matrix material pores and only the

adsorbed fission products are left behind. Although this may seem intuitive, the less understood characteristic of porous material diffusion is the pore wall structure. It is impossible to have a completely smooth pore wall, but the degree of roughness influences both adsorption properties and the transfer of momentum of gas particles. The roughness and irregularities of pore walls can cause incoming gas particles to rebound against a concentration or pressure gradient and this complicates the basic assumption of hard sphere momentum transfer. Although the effect of pore roughness on gas particle momentum transfer is negligible for a steady state system that operates for long periods of time, roughness will influence the retention of fission product gases within matrix material pores.

From the preceding explanation, it should be clear that the two main factors for porous media diffusion are mean free path of the gas and pore characteristics. The first component is easily understood by the kinetic theory of gas, but the second component is still far from completely understood. The pore structure of many materials, including nuclear graphites and matrix materials are poorly characterized. Traditionally, nuclear graphite characterization has focused on neutronic and durability properties. Porosity mainly affects fission product migration and retention. So long as reactors operated with minimal fission product release, there was little reason for concern. The final disposal of these materials, along with most other end-of-life considerations for reactor designs has been a secondary priority and therefore porosity characterization has been lacking. The combination of incomplete pore structure knowledge and the inherent complexity of porous media diffusion has created the current situation in nuclear research where the mechanisms of fission product migration are not understood and quantification of fission

product dispersion in graphitic materials is scarce. The following sections attempt to explain some of the factors that have been a part of diffusion research for nuclear applications.

2.2 Fick's Laws and Flux

Most heat and mass diffusion problems have traditionally been described by Fick's first and second laws. The first law describes a steady state system where the flux is proportional to a concentration gradient. The second law describes how concentration within a medium changes with time. Both equations can be manipulated to provide useful solutions for diffusion in real systems. An example of a practical solution is derived in Appendix II. Here, the basic equations will be explained.

Fick's first law states that the flux of component 1 (J_1) can be described by

$$J = D \left[\frac{\partial C}{\partial x} \right]_t \quad (2.1)$$

with units of

$$\frac{\text{mass}}{\text{Length}^2 t} = \frac{\text{Length}^2}{t} \left[\frac{\text{mass}/\text{Length}^3}{\text{Length}} \right] \quad (2.2)$$

where D is the diffusion coefficient, x is the axis parallel to the concentration gradient, and t is time. As the specimen becomes homogeneous and the concentration gradient disappears, the flux, J , will approach zero. Additionally, the diffusion coefficient, D , or alternately, the ratio of the flux to concentration gradient, is independent of the magnitude of the gradient.

An experimental method used for determining the parameters for Fick's first law was explained by Smith in 1953 (Shewmon, 1989). He used a hollow iron cylinder with length, l , and radius, r , in a constant temperature furnace. A carburizing gas was introduced through the center of the sphere and a decarburizing gas passed over the outside of the sphere. When the carbon concentration ceased to change with time within the cylinder's wall, the amount of carbon (q) passing through the wall per unit time was constant.

$$J = \frac{q}{2\pi r l t} \quad (2.3)$$

Combining Fick's first law and equation (2.3) for flux, J , yields an equation for the quantity of carbon that passed through the cylinder during time t .

$$q = -D(2\pi l t) \frac{dc}{d(\ln(r))} \quad (2.4)$$

For this type of experiment, q , l , and t can be measured. If the concentration of carbon inside the cylinder wall can be measured by some chemical method, the diffusion coefficient, D , can be determined by plotting the concentration, c , vs. the natural log of the cylinder wall radius, r . If the diffusion coefficient does not change when the ratio of *carbon/iron* changes, the plot should be linear. It has been proven experimentally by Smith that the diffusion coefficient does change as the ratio of *carbon/iron* increases and therefore the plot of c vs. $\ln(r)$ is not linear. The data obtained for the iron cylinder at 1000 C yielded a diffusion coefficient range of $2.5 * 10^{-7} \frac{cm^2}{s}$ at 0.15 wt% carbon to $7.7 * 10^{-7} \frac{cm^2}{s}$ at 1.4 wt% carbon (Shewmon, 1989).

When non-steady state conditions exist for the concentration of diffusant inside some media, Fick's first law is still valid but not convenient to use. For non-steady state conditions, Fick's second law is used more often. To illustrate Fick's second law, it is useful to imagine a rod with its central axis along the x -axis and a differential thickness Δx somewhere in the rod. At this spot, Δx , there will be a flux of material, J_1 , entering and a flux of material, $-J_2$, leaving. Assuming that Δx is very thin, the two fluxes can be related by

$$J_1 = J_2 - \Delta x \frac{\partial J}{\partial x} \quad (2.5)$$

Assuming that $J_1 \neq J_2$ the concentration of material inside the thickness Δx will change with time. The amount of material accumulation or loss within Δx can be expressed as

$$J_1 - J_2 = \Delta x \frac{\partial c}{\partial t} = -\Delta x \frac{\partial J}{\partial x} \quad (2.6)$$

This physical representation of Fick's second law can be better understood in graphical form

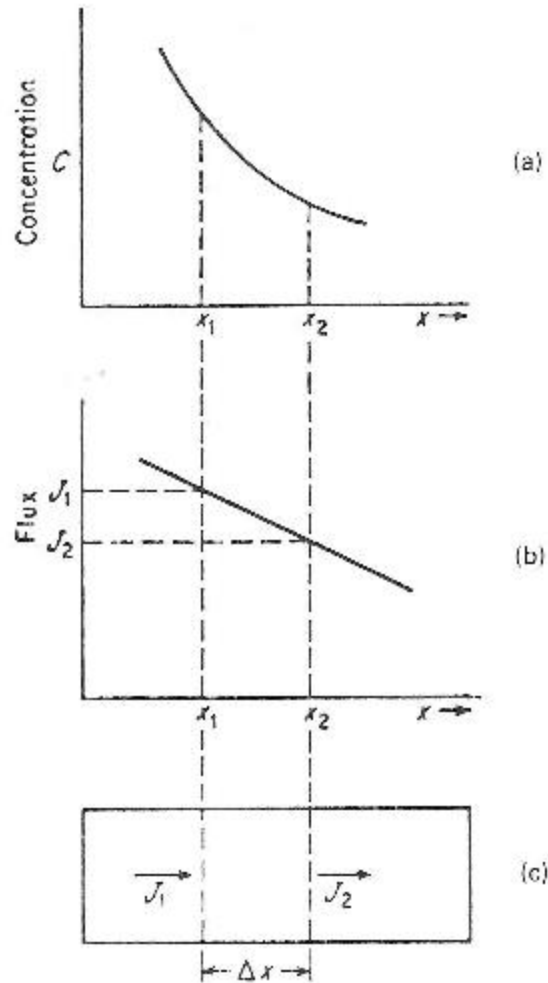


Figure 2.1 Plots (a) and (b) show the concentration and flux, respectively, of diffusing material within thickness Δx . Plot (c) is the bar with thickness Δx . (Shewmon, 1989)

Fick's second law

$$\frac{\partial C}{\partial t} = D \frac{\partial}{\partial x} \left[\frac{\partial C}{\partial x} \right] \quad (2.7)$$

is useful for conditions of non-steady state diffusant concentration.

2.3 Knudsen Diffusion

2.3.1 Introduction

When the pore diameter or the pressure decreases so that the pore diameter is smaller than the mean free path of the gas, Knudsen diffusion can occur (Breitkopf, 2008). The diffusion coefficient in the Knudsen regime can be written as in equation 2.8 or 2.9, where v is the velocity of the gas

$$D_{Knudsen} = \frac{1}{3} d_{pore} \sqrt{\frac{8RT}{\pi M_{gas}}} \quad (2.8)$$

$$D_{Knudsen} = \frac{1}{3} v d_p \quad (2.9)$$

When the pore diameter, d_p , is constant and the pressure decreases, there will be a transition region between molecular diffusion and Knudsen diffusion. For this region there is a separate diffusion coefficient, D^* .

$$\frac{1}{D^*} = \frac{1}{D_{Molecular}} + \frac{1}{D_{Knudsen}} \quad (2.10)$$

If a material does not have a uniform pore size distribution, “complex models are necessary” to evaluate the migration of material through the solid (Breitkopf, 2008). In this case, some small pores may be transporting material by Knudsen diffusion and larger pores or material defects may be transporting via molecular diffusion.

The effective diffusion coefficient that should be used for calculation in a specific regime is modified by accounting for the porosity of the bulk material and the tortuosity. This effective diffusion coefficient is written as in equation 2.11, where ε is the porous fraction of the material and τ is the tortuosity of the pore.

$$D_{Kn-eff} = \frac{\varepsilon}{\tau} D_{Knudsen} \quad (2.11)$$

Tortuosity is a unitless quantity described by figure 2.2 and equation 2.12, which describes a pore's deviation from a straight channel.

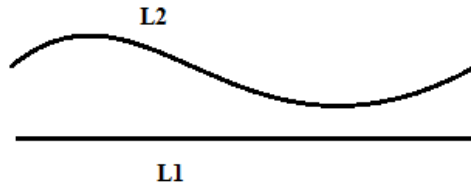


Figure 2.2 Physical representation of tortuosity

$$\tau = \frac{L2}{L1} \quad (2.12)$$

2.3.2 Effect of Tortuosity

Tortuosity is one factor that influences the migration of gases through porous media. The definition of tortuosity is the ratio of real-to-apparent pore length (Bacos et al., 1999). It is rare that perfectly straight pores are formed in porous materials such as graphitic matrix material and therefore the tortuosity of such materials will have a value greater than 1. When a gas is forced to migrate through an increasingly tortuous

pathway, it will experience more resistance than in a straight cylinder. For this reason, tortuosity is in the denominator of equation 2.11 and reduces the effective diffusion coefficient. Most of the current published material regarding nuclear graphite acknowledges the need to account for tortuosity, but stops short at quantifying it rigorously (Mays et al., 1995). A journal article published in 2008 reports an investigation of the effect of oxidation on graphite structural material for HGTRs (Xinli et al., 2008). The researchers investigating the deterioration of HGTR graphite structural material used tortuosity models from Bacos et al. who investigated carbon / carbon composite oxidation.

Although it has been widely recognized that tortuosity is an important factor for migration of liquids and gases through various types of porous media, measuring tortuosity can be difficult especially for carbonaceous and graphitic materials. Mercury porosimetry, helium pycnometry and gas adsorption can provide morphological characterization and permeability data, but these methods do not yield any insight into tortuosity (Bacos et al., 1999).

In a series of publications on coated carbon / carbon composite material oxidation, Bacos et al explained how tortuosity measurements could be made for multi-layer composite materials. This may have some applicability for the carbon matrix material used to make high temperature gas-cooled reactor fuels. First, the pores of an uncoated carbon composite material were filled with electrochemical nickel and analyzed with enhanced SEM. The nickel clearly showed the pore shape and the tortuosity value for the uncoated sample was determined through image analysis. Then, when the permeability of the coated sample, morphological parameters of the uncoated sample, and

pore volume and thickness of the coating material were all known, pore radius and tortuosity of the coating material could be determined by equation 2.13

$$\frac{e_t}{K_t} = \sum_{i=1}^n \frac{e_i}{K_i} \quad (2.13)$$

where

e = thickness of material

$$K = \text{permeability [m}^2\text{]} = \frac{\varepsilon r_p^2}{8 \tau^2} \left(1 + \frac{\beta_s \mu}{r_p P} \sqrt{\frac{R T}{M}} \right)$$

ε = pore volume fraction

β_s = gas – wall interaction coefficient (5 for diffuse surface)

The method of tortuosity quantification described by Bacos et al. may have some limitations for nuclear applications. First, the method was used for layered composite materials in which pore tortuosity would be apparent on a 2D plane in either the longitudinal or transverse direction. In a non-layered material where tortuosity does not follow a plane, the method of looking at a pore on a SEM image like a line on a piece of paper may not be effective. Secondly, depending on the pore size of the nuclear matrix material in question, filling the sample with electrochemical nickel for enhanced SEM analysis may not be a viable option. In the composite materials tested by Bacos et al., the mean pore radius was 2.12 micrometers. Despite these possible shortcomings, Xinli et al. (2008) used the equations to model HTGR graphite oxidation as Bacos used them for

carbon composites. These equations were originally published by Carman in 1956 (Carman, 1956).

In the literature discussed thus far, tortuosity has been defined as a geometric material property based on pore shape alone. There has been some research that suggests tortuosity may affect the migration of material through porous media differently in the Knudsen and bulk regimes (Vasenkov, Geir, & Karger, 2003). For zeolite beds, there was a discrepancy for the experimentally measured diffusion coefficient vs. the diffusion coefficient calculated from gas kinetic theory. These results are shown in figure 2.3

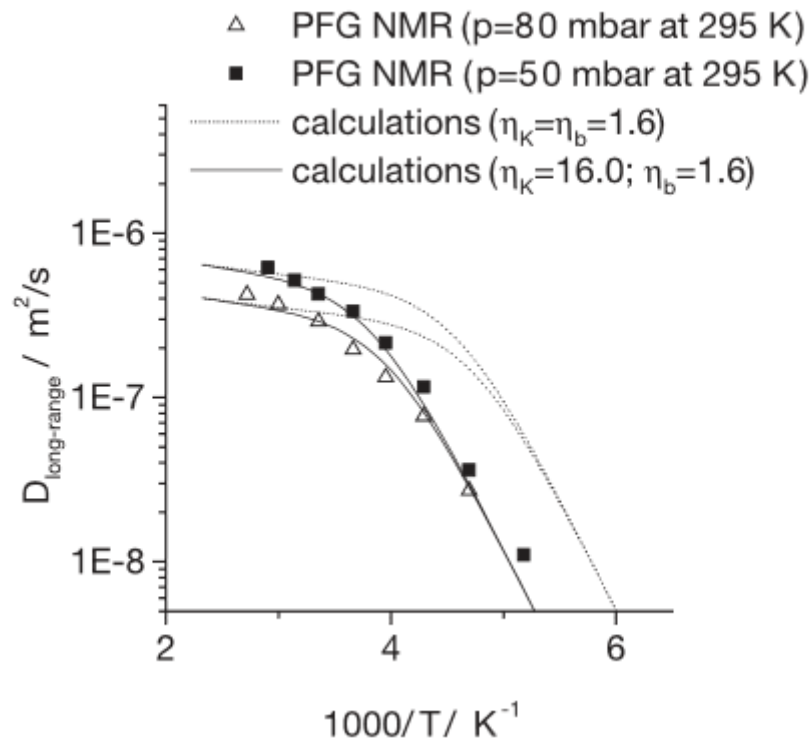


Figure 2.3 Experimentally determined and gas kinetic calculated diffusion coefficients vs. temperature. Note “backwards” temperature on the X axis – left side of x -axis is bulk, right side of x -axis is Knudsen.

When the diffusion coefficients were calculated with gas kinetic theory and constant tortuosity $\tau = 1.6$, the calculated and experimentally measured diffusion

coefficients matched well in the high temperature bulk regime. When the temperature decreased and the Knudsen regime dominated, the calculated values for the diffusion coefficient were significantly higher than the experimental values. The temperature dependence of the results in this particular experiment is confusing, because increased temperature typically means Knudsen regime. In this case, however, the zeolite bed trapped most of the ethane at low temperatures and released the ethane at higher temperatures. The result was fewer ethane gas molecules at lower temperatures (rarified gas – Knudsen regime) and more ethane gas molecules at higher temperatures (bulk regime). In order to correct for the discrepancy in calculated vs. experimental data, the tortuosity in the Knudsen regime was increased by an order of magnitude to $\tau = 16.0$ for the second round of calculations shown by the solid lines in figure 2.3. Increasing the tortuosity by a factor of 10 in the Knudsen regime led to better agreement between experimental and calculated diffusion coefficients.

It may be possible that a given material affects diffusing gases differently based on how rarified the gas is (Vasenkov et al., 2003). The primary explanation for this phenomenon is that rarified gases migrating in the Knudsen regime interact with walls more than in the bulk regime, so irregularities on pore wall surfaces will have an effect on migration. Although the research was conducted with ethane in zeolite beds, the concept of pore wall irregularities affecting the migration of rarified gases may be a factor for fission product gases migrating through matrix material. Regardless, if there is a factor of 10 difference in the tortuosity factors for Knudsen and bulk regimes, it remains an important factor in porous media diffusion and has received limited attention in nuclear graphite research.

2.3.3 Knudsen Number

In 2008, a German study was performed to investigate the effect of the Knudsen number and pore shape on material diffusion. Argon and helium gasses were used over 10 orders of Knudsen magnitude and it was concluded that the diffusion coefficient and the Knudsen number are related. (Gruener & Huber, 2008)

Researchers have discussed how pore tortuosity affects diffusion and have proposed different ways to modify the Knudsen equation with a tortuosity *factor*. Gruener and Huber took a different approach and tried to eliminate the problem posed by tortuosity and the uncertainty in quantifying it. Instead, they used nanomachining to produce silicon wafers with nearly uniform, straight channels that correspond with Knudsen's ideal theory rather than naturally occurring porous materials, which have irregularly shaped tortuous pores.

In this experiment, helium and argon were allowed to diffuse through single crystalline silicon machined with parallel, linear channels with diameter 12 nanometers and length 200 micrometers over a temperature range of $40 \text{ K} < T < 300 \text{ K}$. These parameters correspond to a Knudsen number range of $10^2 < Kn < 10^7$. It should be noted that this range of Knudsen numbers is well within the Knudsen regime. The Knudsen regime is usually considered to be $Kn > 1$, but there is some variability on this point in the literature. Some sources suggest that the Knudsen regime exists only where the Knudsen number is significantly greater than unity (Ziarani & Aguilera, 2012).

Species migration in macroscopic systems at low pressure or high temperature is typically described by Knudsen diffusion, with $Kn > 1$. For ambient pressure and temperature, helium migration should be in the Knudsen regime for a 10 nm pore according to Gruener and Huber. Mean free path (λ) and the Knudsen number (Kn) are found with equations 2.14 and 2.15.

$$\lambda = \frac{kT}{\sqrt{2}\pi d^2 p} \quad (2.14)$$

where

$$k = \text{boltzman constant} = 1.38 \times 10^{-23} \left[\frac{m^2 kg}{s^2 K} \right]$$

$$T = \text{temperature [K]}$$

$$d = \text{hard sphere gas atomic diameter [m]}$$

$$p = \text{pressure [Pa]}$$

$$Kn = \frac{\lambda}{d_{pore}} \quad (2.15)$$

where

$$d_{pore} = \text{diameter of the pore [m]}$$

A sample calculation for helium gas migrating through silicon nanochannels is shown in equations 2.16 and 2.17. The two equations are equivalent, but written with different variants of the Boltzmann constant – 2.16 already has been divided by Avogadro's number and 2.17 shows the division.

$$\lambda = \frac{kT}{\sqrt{2}\pi d^2 p} = \frac{1.38 \times 10^{-23} (297)}{\sqrt{2} (3.14) (62 \times 10^{-12})^2 (101325)} = 2.37 \times 10^{-6} m \quad (2.16)$$

$$\begin{aligned} \lambda &= \frac{RT}{\sqrt{2}\pi d^2 N_A p} = \frac{(0.008314)(297)}{\sqrt{2} (3.14) (62 \times 10^{-12})^2 (6.02 \times 10^{23}) (101)} \\ &= 2.37 \times 10^{-6} m \end{aligned} \quad (2.17)$$

$$\text{pressure } (p) = 1 \text{ bar}$$

$$\text{temperature } (T) = 297 \text{ K}$$

$$\text{helium diameter } (d) = 62 \times 10^{-12} m$$

Gruener and Huber calculated a λ -value of 118 nanometers for helium at 1 bar and 297K. The Knudsen numbers for $\lambda = 2.37 \times 10^{-6}$ and $\lambda = 118 \times 10^{-9} m$ are calculated in equations 2.18 and 2.19.

$$Kn = \frac{118 \times 10^{-9}}{10^{-9}} = 118 \quad (2.18)$$

$$Kn = \frac{2.37 \times 10^{-6}}{10^{-9}} = 2370 \quad (2.19)$$

Regardless of the discrepancy in mean free path values, the Knudsen number for each case is significantly greater than 1 and, therefore, is in the Knudsen regime. Finally, the researchers calculated the ideal Knudsen diffusion coefficient (for an unspecified temperature somewhere in their experimental range of 40 K – 300 K) and a pore diameter of 12 nm and obtained $5 \frac{mm}{s}$.

$$D_{Knudsen}(273K) = \left(\frac{1}{3}\right) (12 \times 10^{-9}) \sqrt{\frac{(8) (8314) (273)}{(3.14) * (4)}} = 4.809 \frac{mm^2}{s} \quad (2.20)$$

$$D_{Knudsen}(300K) = \left(\frac{1}{3}\right) (12 \times 10^{-9}) \sqrt{\frac{(8) (8314) (300)}{(3.14) (4)}} \quad (2.21)$$

$$= 5.041 \frac{mm^2}{s}$$

Experimentally, the researchers determined that the Knudsen-number-independent diffusion coefficient was $3.76 \pm 0.8 \frac{mm^2}{s}$. The empirical coefficient deviated from the theoretical coefficient because the pores were not perfectly circular, even with the precise nanomachining techniques. To correct for non-circular pores, $D_{Knudsen}$ was modified by replacing the pore diameter, d , by a value, G , which is a function of the pore cross sectional area and perimeter. It was assumed that the irregularity in the circular pore would carry through the entire depth of the pore. This assumption seems reasonable for a machined material, but is probably invalid for naturally occurring porous materials.

$$\frac{1}{G} = \frac{1}{4L} \int_0^L \frac{o(l)}{A(l)} dl \quad (2.22)$$

where

$o(l)$ = pore cross section perimeter as a function of pore length

$A(l)$ = pore cross sectional area as a function of pore length

L = length of pore

Using TEM, 20 of the channels were analyzed to determine the perimeter and area of the pores. From this, 20 G - values were calculated and averaged to give 9.9 nm compared to G -value of 12 nm resulting from the assumption of perfectly circular pores. Using the new G -value rather than d , to calculate the new diffusion coefficient that results in a value that more closely matches the experimental value.

$$\begin{aligned}
 D_{Knudsen}(300K) &= \left(\frac{1}{3}\right) (9.9 \times 10^{-9}) \sqrt{\frac{(8) (8314) (300)}{(3.14) (4)}} \\
 &= 4.159 \frac{mm^2}{s}
 \end{aligned}
 \tag{2.23}$$

2.4 Adsorption of Fission Products to VHTR Materials

Branney (2010) reported work on fission product surrogate adsorption onto VHTR structural materials.

The purpose of this research was to determine how fission products adsorb to the materials found in VHTR cores. Typical diffusion studies quantify the extent to which one material will migrate through another bulk material. Adsorption should not be confused with diffusion, because, although they both describe the interaction between a bulk and a trace material, adsorption is a surface and bonding phenomenon while diffusion is more of a penetrating process. If a fission product were to escape the fuel in a VHTR, it would come into contact with the moderator and structural components of the core. Upon escape from a TRISO fuel particle, a fission product, silver, for example, would need to migrate through the graphite matrix material in fuel prisms or pebbles. In a prismatic reactor design, it would subsequently migrate through the fuel block graphite

before entering the coolant gas. The fission product gas would then be a trace gas mixed in with the coolant and free to interact with the structural components of the core. At this point, the fission product may adsorb onto stainless steel, graphite, and other materials in the core. The extent and rate of this adsorption process was the principal subject of this research.

Because the focus was not on diffusion, there was no mention of the Knudsen regime or depth of penetration of fission products. In fact, no solid graphite was used in this study. Instead, graphite powder and stainless steel plates were the two materials used. Nonetheless, the results of this work are valuable for diffusion-type studies because gas phase species were used in the experiments, rather than solid or liquid, and the measurement techniques provide useful guidance.

Silver was mentioned as being a material of interest for this work, but it was not used for experimentation. Instead, cesium and iodine vapors were produced and passed over stainless steel plates or through Inconel columns packed with graphite powder. Because the purpose of the experiments was to adsorb the vapor on to the materials of interest, attention was paid to preventing the vapor from plating onto the experimental equipment. A tube furnace with argon flowing through the tube was used to heat the cesium and iodine to suitable temperatures to induce vaporization. Electrical heat tape was used extensively on connecting tubing between the site of vapor generation and the samples of stainless steel or columns of powdered graphite. Generating cesium vapor was of special concern considering cesium's propensity to explode when it encounters moisture. For this reason, argon was used to create an inert environment, and a special stainless steel vessel was constructed in order to safely break open the glass ampules that

contained the cesium metal. Although cesium and iodine have significantly higher vapor pressures than silver and required a lesser degree of heating than silver needs to form a vapor, the use of electrical tape could provide a solution for reducing the plating of silver onto experimental equipment.

An interesting aspect of the experiments was the simplicity of generating vapor. Although cesium required construction of a custom-made vessel, the vapor was generated with a regular tube furnace and argon. A dilution tube was added after the tube furnace so that extra argon could be added and the concentration of fission product surrogate that reached the stainless steel or graphite samples could be controlled. No gas analyzers were used in this experiment, instead, a thorough study of literature values for vapor pressure was conducted and a basic thermocouple monitored the temperature in the tube furnace. This way, Branney was able to determine the concentration of cesium or iodine vapor in argon with some acceptable amount of uncertainty. It was noted that data for silver vapor pressure was scarce compared to cesium and iodine.

Because the anticipated deliverable from these experiments was quantification of the species' onto graphite and stainless steel, it was necessary to measure the amount of the fission product surrogate adhered to the graphite or structural material. In theory, the difference between pre- and post- experiment masses of graphite and stainless steel samples would show how much fission surrogate material plated onto the surfaces. This approach was attempted with a thermo gravimetric analyzer (TGA), which is a sophisticated mass balance capable of measuring to the microgram level. This method provided some preliminary results, but the accuracy was less than desired and the instrument sensitivity was not sufficient for experimental mass differences in the

nanogram range. In order to obtain more accurate results, the samples were analyzed via NAA and ICP-MS. NAA allowed back-calculation to determine the mass of adsorbed material in graphite (with some degree of error) and ICP-MS was reportedly able to detect nanogram per gram levels for cesium on stainless steel. The method for translating ICP-MS data to a mass basis was not explained and warrants further study.

Adsorption data were successfully obtained from these experiments. It was concluded that more vapor was adsorbed at lower temperatures (500 C) and the mass adsorbed decreased with increasing system temperature (up to 800 C). Additionally, the data indicated an absorption maximum as the vapor concentration reached the 700 – 900 ppb range at 500 C and 600 C. This newly produced data contradicts earlier work that resulted in a lower values for saturation levels at a higher temperature.

The type of graphite used in this experiment was not identified. No characterization or citation of graphite properties was given. The Knudsen regime was not mentioned in this work, but that is appropriate considering the focus was adsorption rather than diffusion. Despite these shortcomings, the use of fission product surrogate in the vapor phase and description of measurement techniques could be valuable for future work.

2.5 Graphite Diffusion Coefficients

Boyle (2010) describes an experimental method to obtain diffusion coefficients for silver in graphite. Valuable information was provided about what experimental methods were successful and the limits of detection for different types of silver measurement equipment (Boyle T. R., 2010) (Boyle T. R., 2013). Boyle obtained some

useful data and estimated the diffusion coefficient for silver vapor in graphite. There was no identification or discussion about the specific diffusion mechanism.

Boyle used four variations of machined graphite cylinders that were hollow in the middle and sealed with a screw-on graphite cap/plug. Each of these graphite jar-like samples was known as a high temperature cell (HTC). The first HTC was machined with a cylindrical hollow inner chamber with a flat surface opposite the cap. This HTC was put into the tube furnace with the axis of the hollow chamber parallel to the furnace's tube. The problem with the first HTC experiment was that there was a liquid – gas silver mixture that impinged upon the intended diffusion surface opposite the cap. The second HTC was identical to the first, but the hollow cylindrical axis was positioned vertically in the tube furnace such that only silver vapor would come into contact with the surface of the intended diffusion medium. The problem with the second HTC was that the silver vapor did not penetrate the graphite surface but rather formed a precipitate where the cylinder wall met the flat “roof” of the hollow chamber. The third HTC was identical to the second, but rather than a perfectly cylindrical hollow cavity containing the silver flakes, the “roof” was machined into a hemisphere to remove the sharply angled material on which silver precipitation had occurred. As with the previous two experiments, the vapor concentration was too low and, therefore, did not migrate into the graphite.

With the experience gained from these first three CT-imaged HTC experiments, the experiment design was changed to increase the silver vapor concentration. Silver flakes were replaced with silver-infused graphite powder, which was produced by soaking plain graphite powder in silver nitrate solution and then allowing the mixture to dry. After a day of drying at room temperature, the powder was further dried by heating

at 700 C for several hours in a tube furnace with constant argon flow through the tube. The resulting dried silver-infused graphite powder was then immediately placed into the fourth HTC and sealed with GraphiBond sealant. Boyle estimated that this powder method increased the silver vapor inside the HTC from 0.1 femtogram/ μm^3 with shavings to 1 picogram/ μm^3 , although an explanation of these estimates was not provided.

After the fourth HTC was filled with the graphite powder and heated at 1150 C for four days, it was carefully cut open so that it could be sectioned and analyzed for silver concentration. Diamond paste, sand paper, a drill press, and jigs were used to create thin graphite samples for neutron activation analysis.

To estimate the extent of silver diffusion in the experiments, a simple model derived from Fick's first and second laws was used with some reference values for silver in graphite from IAEA TECDOC 978 (1997). Starting with the equation

$$D(T) = D_o e^{\left(-\frac{Q}{RT}\right)} \quad (2.24)$$

where

$$D(T) = \text{diffusion coefficient} = 1.17 \times 10^{-14} \left[\frac{\text{m}^2}{\text{s}} \right]$$

$$D_o = \text{preexponential magnitude} = 5.3 \times 10^{-9} \left[\frac{\text{m}^2}{\text{s}} \right]$$

$$R = \text{gas constant} = 8.3145 \left[\frac{\text{J}}{\text{K mol}} \right]$$

$$Q = \text{activation energy} = 1.54 \times 10^5 \left[\frac{J}{mol} \right]$$

$$T = \text{temperature} = 1423 [K]$$

The diffusion coefficient calculated using equation 2.24 is used in equation 2.25, with a heating duration of 4 days (3.456 e5 seconds).

$$C(x, t) = C_o \operatorname{erfc} \left(\frac{x}{\sqrt{2Dt}} \right) \quad (2.25)$$

where

C = concentration of diffusant

x = distance into diffusing medium

t = time

$$\operatorname{erfc}(x) = 1 - \operatorname{erf}(x) = \frac{2}{\sqrt{\pi}} \int_0^x \exp(-\lambda^2) d\lambda \quad (2.26)$$

where

λ = variable of integration (no physical significance)

The resulting normalized concentration profile is shown in figure 2.4

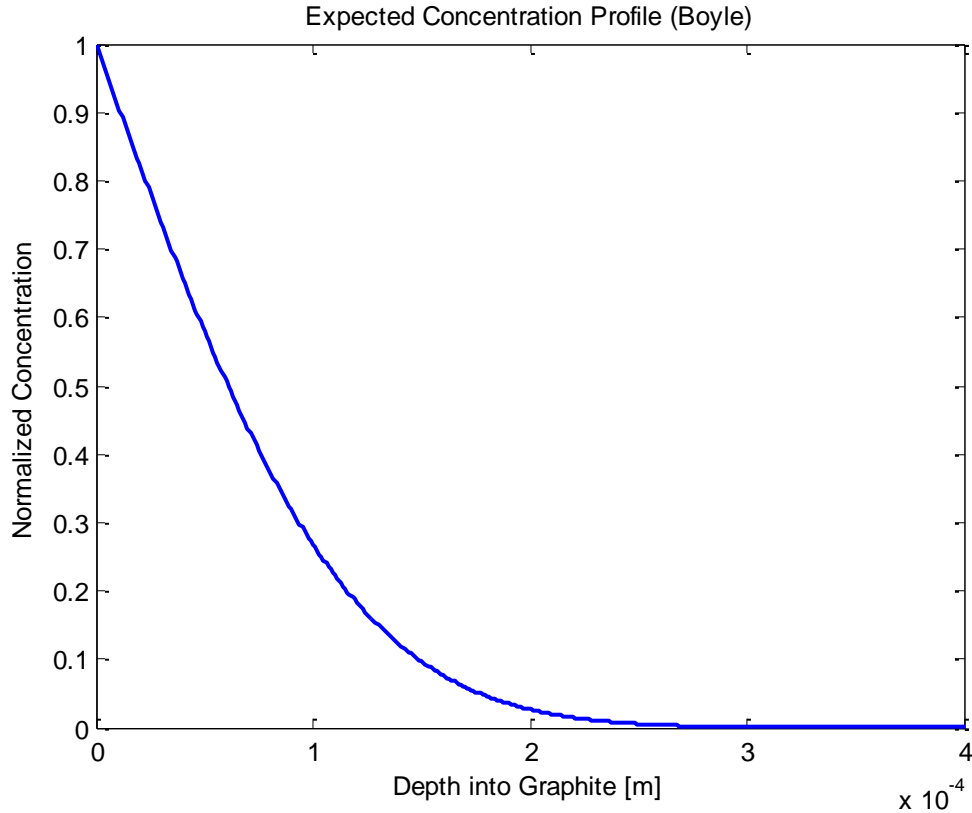


Figure 2.4 Expected silver concentration profile as calculated by equation 2.2

Boyle's experimental data produced a curve less smooth than in figure 2.4. The data are summarized in table 3.1 and plotted in figure 2.5. The main source of error noted by Boyle was uncertainty in the graphite sample thickness. The procedure for removing graphite material from the HTC for analysis was accomplished with a drill press, micrometer, and 1600 grit sandpaper. There was another source of error that the author did not address, but probably adversely affects the results of this experiment. The surface of the diffusion material was the hemispherical "roof" of the chamber that contained the silver-laden graphite powder. It was assumed that silver migrated through the hemisphere as it would a slab of material because the radius of the hemisphere was much greater than the expected depth of penetration. This approximation seems valid, but the

method of sectioning caused problems. Sections of graphite were sanded off as flat planes, which crossed through the hemisphere. This method of taking flat sections from the hemisphere would cause samples to contain a disproportionately lower silver concentration at the top of the hemisphere and disproportionately higher silver concentration towards the base of the hemisphere. This problem could only be eliminated by taking gradually larger hemispherical sections starting at the inside of the original hemisphere and working out. Sample geometry was not mentioned by the author (Boyle, 2010 and 2013), but clearly it is a problem that would require a more sophisticated sectioning method.

Table 2.1 Data collected from NAA, HTC #4

Section Number	Xi [μm]	Xj [μm]	ΔX [μm]	Xav [μm]	volume [mm ³]	Ag mass [μg]	C(Ag) [μg/mm ³]	σc [μg/mm ³]
1	0	9	9	4.5	0.8742	7.98	9.1282	1.4390
2	9	18	9	13.5	0.8742	4.02	4.5984	0.7316
3	18	31	13	24.5	1.2628	5.11	4.0467	0.4473
4	31	44	13	37.5	1.2628	4.22	3.3419	0.3721
5	44	54	10	49.0	0.9714	4.34	4.4680	0.6403
6	54	60	6	57.0	0.5828	3.53	6.0568	1.4379
7	60	68	8	64.0	0.7771	3.06	3.9378	0.7079
8	68	75	7	71.5	0.6799	2.28	3.3532	0.6933
9	75	81	6	78.0	0.5828	1.51	2.5909	0.6343
10	81	89	8	85.0	0.7771	0.76	0.9780	0.2155
11	89	96	7	92.5	0.6799	0.54	0.7942	0.2177
12	96	101	5	98.5	0.4857	0.59	1.2148	0.4006
13	101	103	2	102.0	0.1943	0.34	1.7501	1.3403
14	103	108	5	105.5	0.4857	0.36	0.7412	0.2939
15	108	119	11	113.5	1.0685	0.17	0.1591	0.0958

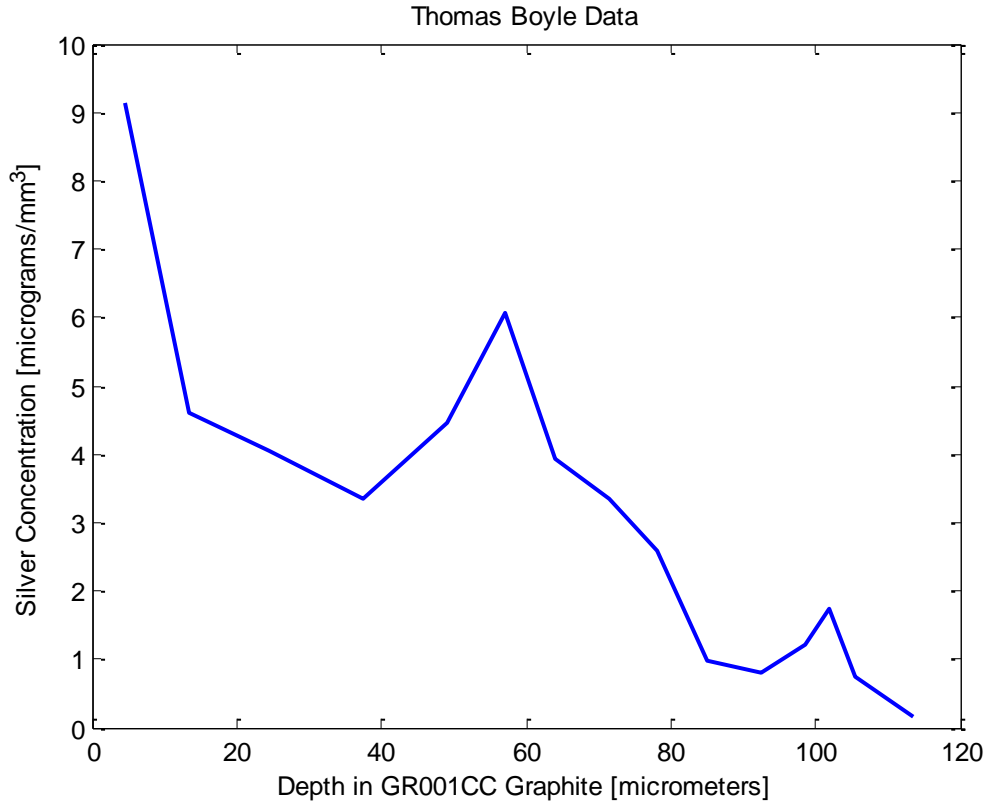


Figure 2.5 Silver concentration vs. depth for HTC #4

From the HTC 4 data, the diffusion coefficient for silver in commercial grade GR001CC graphite at 1150 C was found to be $2.385 \times 10^{-15} \frac{m^2}{s}$. Other conclusions reached by the author included that the use of less dense graphite and better equipment, specifically a vacuum furnace for heating the HTC, would improve the results. The furnace change would allow for an inert experimental environment and higher temperatures (1600 C) to simulate an accident scenario. Boyle also claimed that better HTC sectioning equipment could provide better samples for analysis, especially from the first 100 μm into the sample, which he considered critical. The final, and most interesting, suggestion for future work was to use the HTC design, but instead of a

threaded plug for the “cap of the jar”, use an irradiated graphite plug so that the silver vapor could diffuse into a graphite structure more closely resembling reactor graphite.

Chapter 3 Modeling Fission Product Migration in Matrix Graphite

3.1 MATLAB Model for Knudsen Number

In order to better understand and visualize some of the diffusion phenomena being investigated, some simple MATLAB scripts were built. Both scripts are attached as appendices. The first script FinalV2.m calculates and plots the mean free path of a silver – helium mixture for specified temperature and pressure conditions. Mean free path is important to know because it can be compared to characteristic dimensions of bulk materials, in this case the crack and pore structure of matrix carbon. A mixture of silver and helium gas was chosen to mimic the conditions that exist in a VHTR reactor with helium coolant and trace levels of fission products. The meshgrid command sets up an X-Y plane of temperature – pressure (x,y) points specified by the user. The temperature and pressure upper and lower bounds as well as the interval between successive points can also be supplied by the user.

The mean free path for a binary gas mixture is (Chapman & Cowling, 1970)

$$\lambda = \frac{KT}{\pi \left(P_1 \sigma_{11}^2 \sqrt{2} + P_2 \sigma_{12}^2 \sqrt{1 + \frac{m_1}{m_2}} \right)} \quad (3.1)$$

where

$$K = \text{Boltzmann Constant} = 1.38 \times 10^{-23} \frac{m^2 kg}{s^2 K}$$

$$T = \text{temperature [K]}$$

$$P_1 = \text{He pressure [Pa]}$$

$$P_2 = \text{Ag pressure [Pa]}$$

$$\sigma_{11} = \text{He} - \text{He collision diameter} = (2) (31 \times 10^{-12}) = 62 \times 10^{-12} \text{ m}$$

$$\sigma_{12} = \text{He} - \text{Ag collision diameter} = (31 + 144) \times 10^{-12} = 175 \times 10^{-12} \text{ m}$$

$$m_1 = \text{He atom mass} = 4 \text{ amu}$$

$$m_2 = \text{Ag atom mass} = 107 \text{ amu}$$

Equation 3.1 takes into account the partial pressure of the gas constituents expected in the reactor or experimental environment. The sum of the partial pressures in a gas mixture accounts for the total pressure in a system. If a gas mixture of helium and a very dilute amount of silver exists at atmospheric pressure, say 5 part per million of silver (5ppm Ag) the pressures of helium and silver are

$$P_{He} = \left(\frac{10^6 - 5}{10^6} \right) (100000) = 99999.5 \text{ Pa} \quad (3.2)$$

$$P_{Ag} = \left(\frac{5}{10^6} \right) (100000) = 0.5 \text{ Pa} \quad (3.3)$$

Then, the mean free path of the gas mixture with 5ppm Ag at atmospheric pressure is

$$\begin{aligned} \lambda &= \frac{K \ 293}{\pi \left((99999.5) (62 \times 10^{-12})^2 (\sqrt{2}) + (0.5) (175 \times 10^{-12})^2 \sqrt{1 + \frac{4}{107}} \right)} \quad (3.4) \\ &= 0.000002 \text{ m} \end{aligned}$$

The Knudsen number is inversely proportional to the pore diameter and there is a wide range of pore diameters that exist for the nuclear fuel matrix material. It is known that when A3-3 matrix material is produced, it contains micropores $d < 2$ nm, mesopores $2 \text{ nm} < d < 50$ nm, and macropores $50 \text{ nm} < d$ (Delle, 1983). It has also been reported that the most frequently occurring pores in A3-3 matrix material are between 1 and 2 nanometers (Robens, 1983). The pore diameter for matrix material can be several orders of magnitude higher, with over 10% of porosity being greater than 1 micrometer up to 5 micrometers (Krautwasser, 1983). For the purpose of this sample calculation, a pore size of 1.5 nm ($1.5 \times 10^{-9}m$) will be used because it is in this size pore that Knudsen diffusion is most likely to occur.

$$KN = \frac{0.000002m}{1.5 \times 10^{-9}m} = 1333 \quad (3.5)$$

For the conditions of room temperature, atmospheric pressure, 5ppm Ag in helium, and pore diameter of 1.5 nanometers it is obvious that silver transport through graphite is occurring in the Knudsen regime because the Knudsen number is much greater than 1.

The sample calculation shows the approach used for calculating the Knudsen number, but engineers are typically interested in ranges of applicability. The MATLAB program FinalV2.m performs the basic calculations for varying ranges of temperature and pressure, and user specified silver concentration (ppm in helium) and pore diameter in order to show graphically how the parameters affect each other and the movement of the gaseous species.

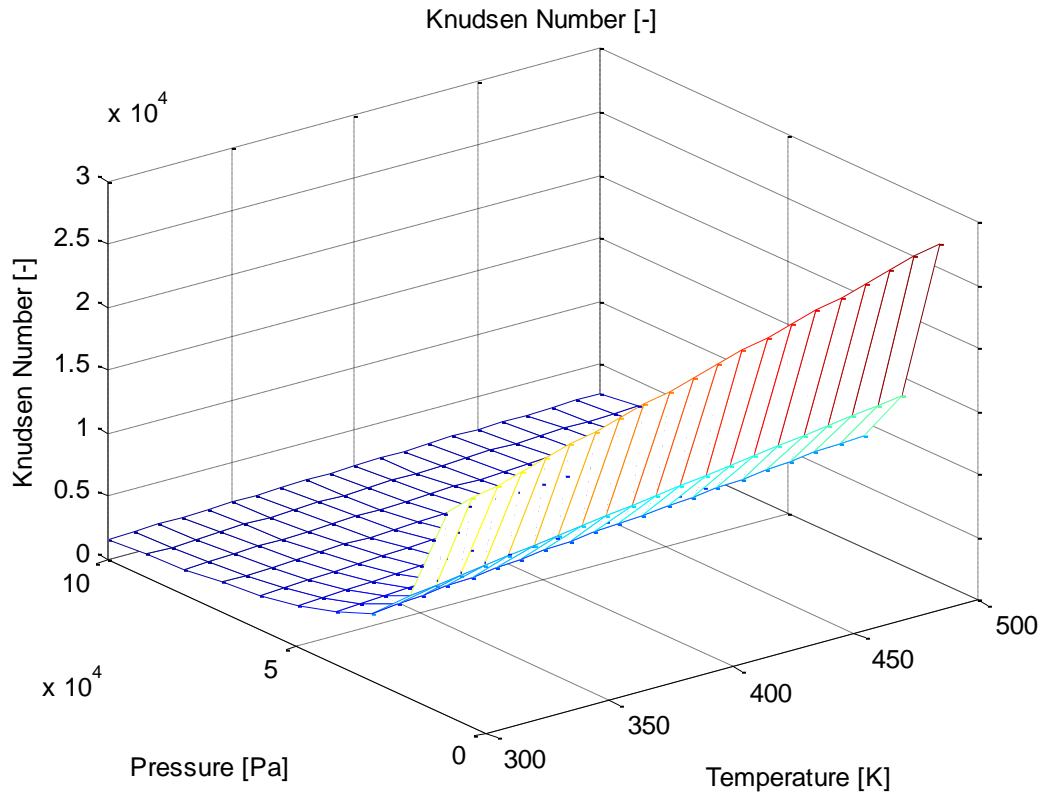


Figure 3.1 Knudsen number for the following conditions
 Temperature 300 – 500 K, 10 degree increment
 Pressure 10,000 – 100,000 Pa (100,000 Pa = atmospheric), 10,000 Pa increment
 10 ppm Ag in He
 Pore diameter 1.5 nanometers

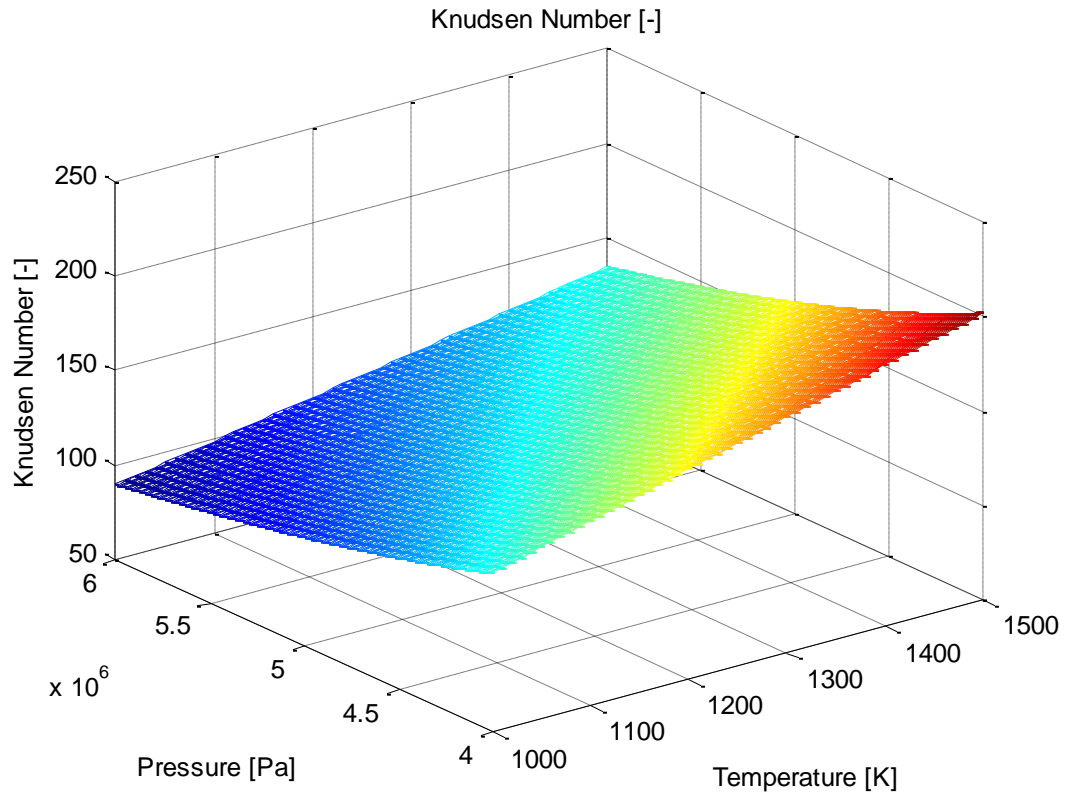


Figure 3.2 Knudsen number for the following conditions
 Temperature 1000 – 1500 K, 10 degree increment
 Pressure 4×10^6 – 6×10^6 Pa (reactor pressure), 10,000 Pa increment
 10 ppm Ag in He
 Pore diameter 1.5 nanometers

Figure 3.1 shows the Knudsen number for pressures ranging from vacuum to atmospheric pressure and temperatures ranging from ambient to slightly heated. The Knudsen number trend can clearly be seen by the pressure and temperature range in figure 3.1 where the Knudsen number decreases at low temperature and high pressure. The same trend is evident in figure 3.2 but the pressure and temperature ranges have been changed to mimic the conditions found near the fuel in a VHTR. The interval size of the meshgrid was reduced significantly in figure 3.2 which explains why the surface plot looks more like a plane of color instead of a grid. For very small pores, in this case 1.5 nanometers, figure 3.2 shows that Knudsen diffusion is occurring.

3.2 MATLAB Model For Diffusion Depth

The second MATLAB script, DepthV2.m, was written to predict the concentration of silver in nuclear fuel matrix material under various experimental conditions. The motivation for this model was to aid in experiment design. In preliminary experiments, fuel matrix material was sputter coated with a very thin layer of Ag, followed by a sputter-coated layer of SiC (intended to keep the silver with the matrix material, rather than vaporizing into the furnace during heating.) Unfortunately, all the silver was lost during heating and none was found in the matrix material. As a result of those experiments, other sample preparation techniques and geometries were considered. The tactic for any further experimentation would be to produce a silver vapor and put that vapor in contact with matrix material to allow silver transport into the material.

As with most metals, silver has a low vapor pressure, which means that only a small amount of silver can exist in the gas phase in equilibrium with the solid and / or liquid phase. This maximum amount of silver that can exist in the gas phase in equilibrium with its other phases is the saturation concentration. Because there is no silver production inside the matrix material for the experiment in question, it follows that the maximum concentration of silver will be that of the gas that is in contact with the matrix material. The silver in the vapor phase will migrate through the matrix material and the silver concentration will decrease as penetration depth increases. The objective is to measure the silver concentration vs. depth in the matrix material after the experiment; therefore, it is necessary for silver to be present at detectable levels inside the matrix material. The concentration of silver in the gas that surrounds the matrix material must

be sufficient to result in a measurable quantity of silver migrating into the material. In this section, silver vapor pressure data will be used to provide some preliminary indications about what can be expected from a silver vapor on matrix graphite experiment.

The vapor pressure data for the MATLAB program covers a temperature range of 958K – 1503K and came from experimental results originally published in the Journal of Chemical and Engineering Data in 1961 (Panish, 1961). When the program runs, the user can select any temperature in that range, and the correct vapor pressure will be selected according to which data point is nearest to the selected temperature. A sample of the vapor pressure data set is shown in figure 3.3

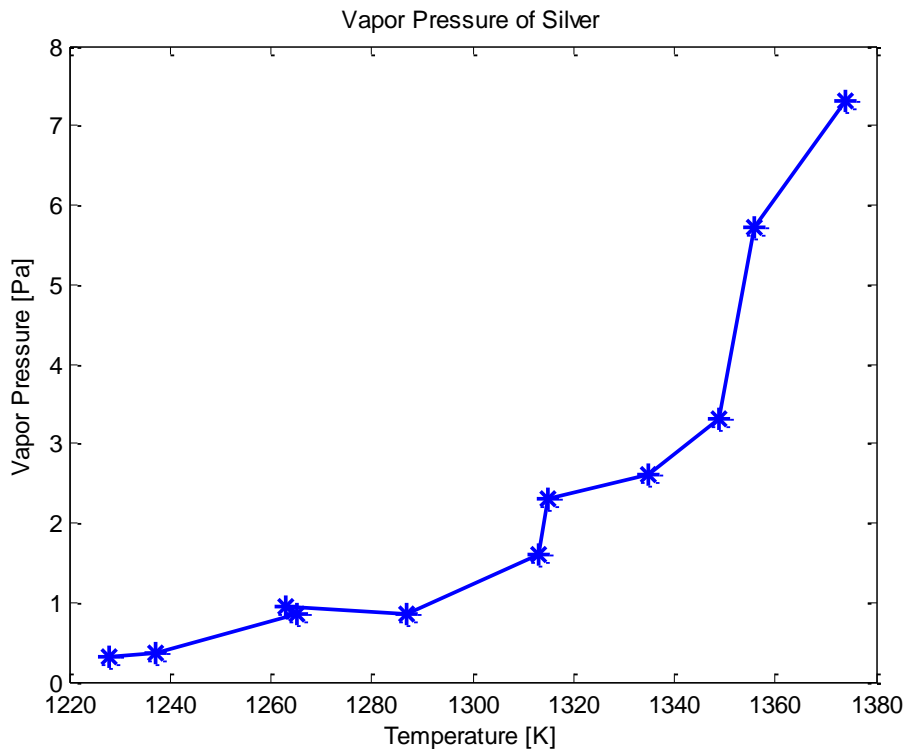


Figure 3.3 Sample of the experimentally determined vapor pressure data for silver, converted from original [mmHg] to [Pa].

With the correct vapor pressure, the equilibrium saturation concentration of silver gas is calculated with a modified ideal gas law equation

$$C = \frac{P}{RT} \quad (3.6)$$

Where

$$C = \text{concentration of silver in the gaseous phase} \left[\frac{g}{cm^3} \right]$$

$$R = \text{ideal gas constant} = 8314 \frac{g \text{ m}^2}{s^2 \text{ mol K}}$$

The sample calculations will be done for 1300K, atmospheric pressure (100,000 Pa), 24-hour sample heating time, and matrix material porosity assumed to be 1.5 nanometers. These parameters reflect a temperature attainable in a laboratory tube furnace, an acceptable experiment run time, and porosity that has been reported in literature.

$$C = \frac{0.8512 \text{ Pa}}{(8.314)(1300)} \frac{107 \text{ g}}{\text{mol}} \frac{m^3}{1000000 \text{ cm}^3} = 8.42 \times 10^{-9} \frac{g \text{ Ag}}{cm^3} \quad (3.7)$$

Next, the mean free path is calculated in a similar manor as equation 3.1

$$\lambda = \frac{KT}{\pi \left((P_{total} - VP_{Ag}) \sigma_{He}^2 \sqrt{2} + VP_{Ag} \sigma_{He-Ag}^2 \sqrt{1 + \frac{m_{He}}{m_{Ag}}} \right)} \quad (3.8)$$

MFP

$$= \frac{(1.38 * 10^{-23})(1300)}{3.14 \left((100000 - 0.8512) (62 \times 10^{-12})^2 \sqrt{2} + (0.8512) (175 \times 10^{-12})^2 \sqrt{1 + \frac{4}{10}} \right)} \quad (3.9)$$

$$= 1.05 \times 10^{-10} [m]$$

The Knudsen number can then be calculated assuming a pore diameter of 1.5 nanometers for the matrix material

$$KN = \frac{1.05 \times 10^{-10}}{1.5 \times 10^{-9}} = 0.07 \quad (3.10)$$

Because the Knudsen number in this case is significantly less than one, silver would be traveling through the matrix material via molecular diffusion. The MATLAB program accounts for different transport regimes according to the Knudsen number of the system. A Knudsen number less than one indicates pure molecular diffusion, a number greater than 5 indicates pure Knudsen diffusion and numbers 1 through 5 are the transition regime. The molecular, transition, and Knudsen diffusion coefficients are calculated as

$$D_M = \frac{\epsilon}{\tau} \frac{\lambda}{3} \sqrt{\frac{8RT}{\pi M}} \quad (3.11)$$

$$D_T = \frac{1}{\frac{1}{D_M} + \frac{1}{D_K}} \quad (3.12)$$

$$D_K = \frac{\epsilon}{\tau} \frac{d}{3} \sqrt{\frac{8RT}{\pi M}} \quad (3.13)$$

It can be seen that the diffusion coefficients for the molecular and Knudsen regime are nearly identical, varying only by the spatial dimension of gas movement – mean free path vs. pore wall diameter. Because the Knudsen number previously calculated clearly indicated molecular diffusion, the diffusion coefficient for a porosity of 20% and tortuosity of 2 becomes

$$D_M = \left(\frac{0.2}{2}\right) \left(\frac{1.05 \times 10^{-10}}{3}\right) \sqrt{\frac{(8)(8314)(1300)}{(3.14)(107)}} = 1.77 \times 10^{-9} \frac{m^2}{s} \quad (3.14)$$

The final step is to estimate the concentration of silver vs. depth in matrix material. The equation used to model this kind of experiment is the dimensional form of the non-dimensional equation derived in Appendix II.

$$C(x, t) = C_o \operatorname{erfc} \left(\frac{x}{2\sqrt{Dt}} \right) \quad (3.15)$$

Using 24-hour heating time, Equation 3.7 was solved and the results plotted in figure 3.4

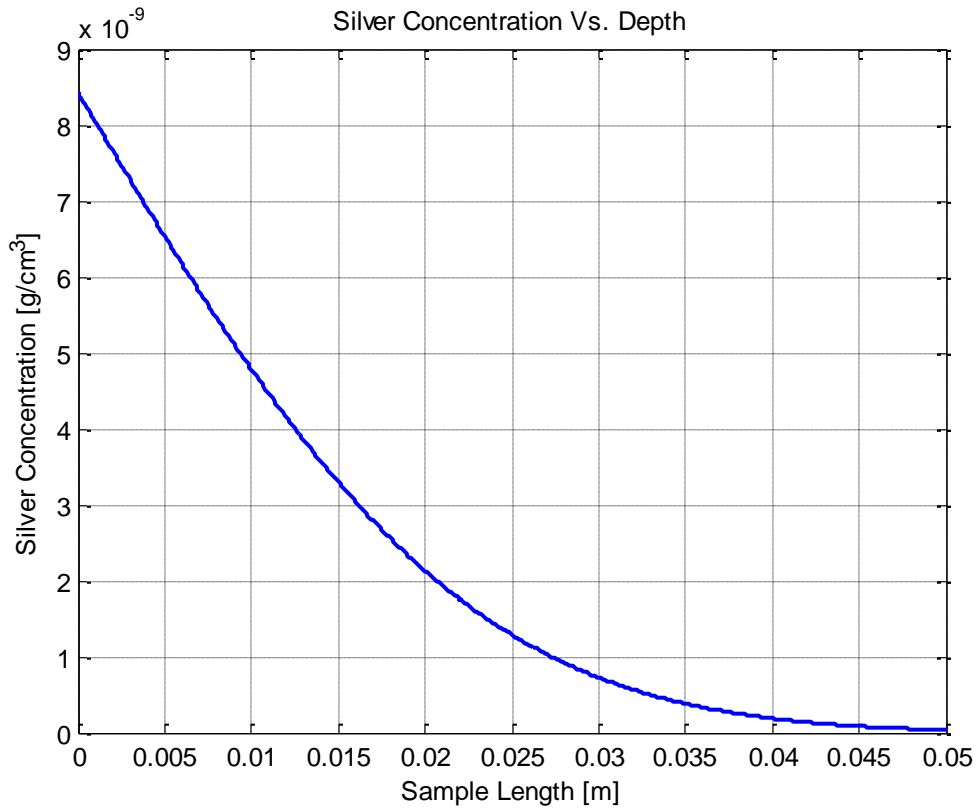


Figure 3.4 Calculated silver concentration as a function of depth in A3-3 type matrix material for a 24 hour heating time.

It can be seen in Figure 3.4 that the silver concentration diminishes within the first 5cm into the surface of the matrix material. At approximately 2.75cm, the silver concentration is only 1ppb.

Obviously, the concentration of a diffusing species will eventually drop below the level of detection of even the most sensitive instrument. However, it is important to design the experiment such that sufficient data can be collected well above the level of detection. Empirical diffusion coefficients are only as representative of the system as the data used to calculate them.

Chapter 4 Measuring Fission Product Migration in Matrix Graphite

4.1 Experimental Work

Attempts were made at ISU to provide experimental data for silver migrating through matrix material. The original motivation for this work was to provide a new type of experimental data that had not been pursued in traditional diffusion studies. Most diffusion studies use some variant of the “sandwich” technique where a solid piece of silver is placed between two slabs of graphite and then both are heated in an oven. Although this type of experiment will allow diffusion to occur, it does not resemble what is happening in a reactor. Inside the core of a reactor, fission product species do not diffuse from such large source terms. Each atom that fissions in a reactor is a source term for the release of fission products. On a macroscopic level, each TRISO particle is a small source for the generation of fission product gases that will exist in low concentrations surrounding the uranium fuel pellet. These are the conditions that should be of interest to the nuclear community – gas diffusion in low concentrations instead of large concentrations of fission products in diffusion couple sandwiches.

There were 18 cylindrical shaped graphitic samples to work with that were believed to be close to A3-3 grade matrix material. The samples ranged from 1.21 – 1.36 inches in length and all were 0.6 inches in diameter. The original sample container was labeled 73 – 90 and this numbering scheme was used to keep track of the samples as they were sectioned and analyzed.

Literature on the subject suggested that it might be possible to detect silver migration on the order of millimeters into graphitic materials. Regardless of what experimental procedures would be deemed necessary, it was apparent that the samples were all too large and would need to be cut into smaller pieces. Early on, it seemed like contamination from cutting blades would ruin any kind of experiment and information about cutting graphite without introducing contamination was limited. This led to two semi-successful methods of cutting the samples. The first involved using the hydraulic cutter at Premier Technology in Blackfoot Idaho. This water jet produced a rough cut and would have required some sort of surface modification before experimentation. The second method was an aluminum jig that was designed to hold a full size sample in place in order to be cut by a laser. The jig worked well, but the laser was difficult to control and produced a rough cut as well. Both methods were supposed to minimize contamination entering the graphite by a cutting blade, but probably ended up by contaminating the graphite anyways. The hydraulic jet used Blackfoot Idaho drinking water and the laser clipped the edges of the jig and shot aluminum through the cut.



Figure 4.1 Aluminum jig used for holding graphite cylinder sample for hydraulic and laser cutting.

When the hydraulic jet and laser delivered less than acceptable results, it was decided to use a clean, unused hacksaw blade instead. When used carefully, the cuts were clean and precise. In order to clean up the flat surface where silver would be applied, a manual polisher was used with fine 1000 grit silicon paper at the Center for Advanced Research Studies (CAES) in Idaho Falls. This method of clean hacksaw blade and polisher produced small enough samples with smooth, uniform surfaces ready for vapor deposition.

Because the objective was to use as little silver as possible in order to mimic conditions in a reactor, silver was applied to the flat polished surface of the matrix material cylinder by physical vapor deposition. A Denton Desktop Pro model physical vapor deposition unit was used to consistently apply layers of 20 – 35 nanometers of

silver onto the matrix material. During the silver application, the rest of the matrix material was shielded with masking tape. After the silver layer was applied, the masking tape was removed and a silicon carbide layer about 400 nanometers was applied to the entire cylinder to provide an encapsulating layer similar to the structure of TRISO particles.

Before silver and silicon carbide were applied to matrix material, several deposition experiments were performed with glass slides at varying pressures and voltages in order to produce repeatable uniform results. For silver application, the purpose was to find the right combination of parameters that would allow for the thinnest possible, but still repeatable, film deposition. The films were tested with a profilometer that was able to detect deposition thickness to ~2 nanometers. It was determined that silver deposition layers in the 20 – 30 nanometer range were reproducible, but thinner layers were not repeatable and were sometimes uneven. The objective for silver deposition was to apply the thinnest layer possible with the equipment available, but Silicon Carbide was the opposite scenario. The purpose of the silicon carbide was to provide a silver encapsulation layer, so a thick layer would be preferable. Silver was deposited on one end of the cylindrical sample and silicon carbide was deposited on all surfaces of the cylinder. The difficult part of silicon carbide deposition is the current mode. Silver and most other conducting metals typically use DC power, which is easily controlled. Insulating materials such as silicon carbide will not sputter with DC power and require radio frequency (RF) power instead. The RF controller at ISU is a manual unit and is difficult to operate. If the sputtering target is set up correctly, the shutter is closed, and the lights in the room are turned off, it is possible to create a plasma. When

the plasma forms, layers of 300 nanometers or greater can be deposited for a 30 minute run.

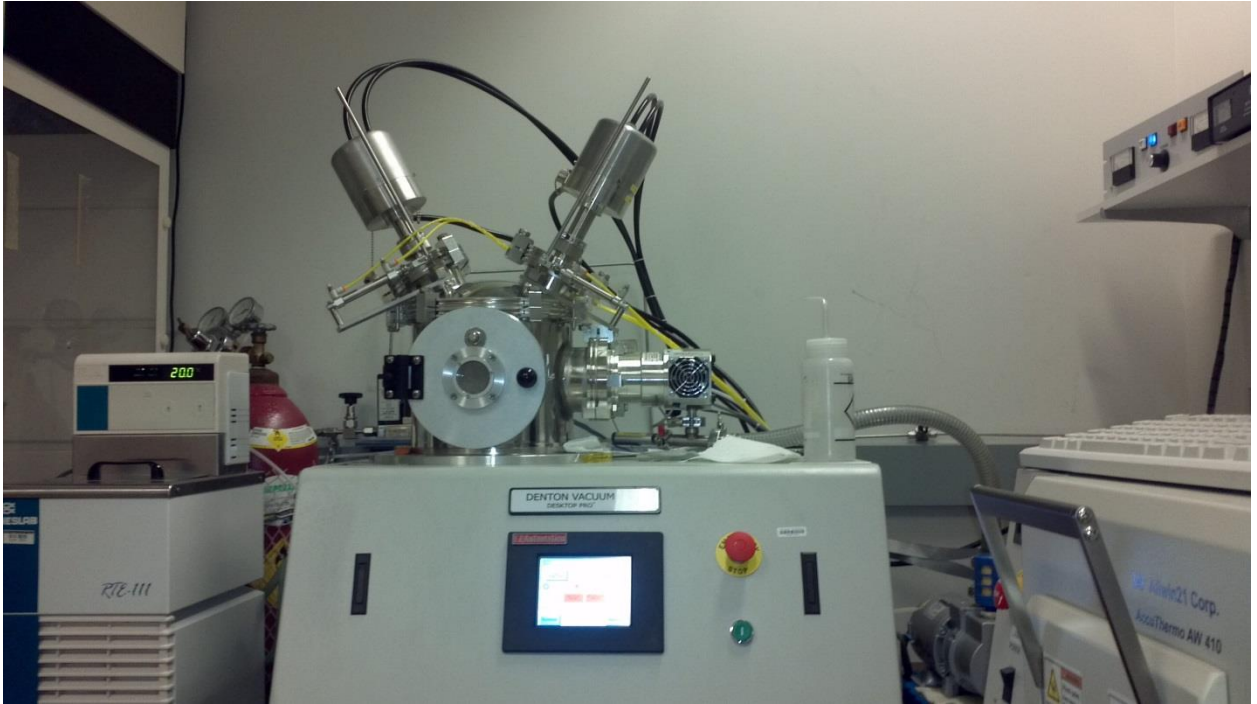


Figure 4.2 Denton Desktop Pro physical vapor deposition unit at Idaho State University.

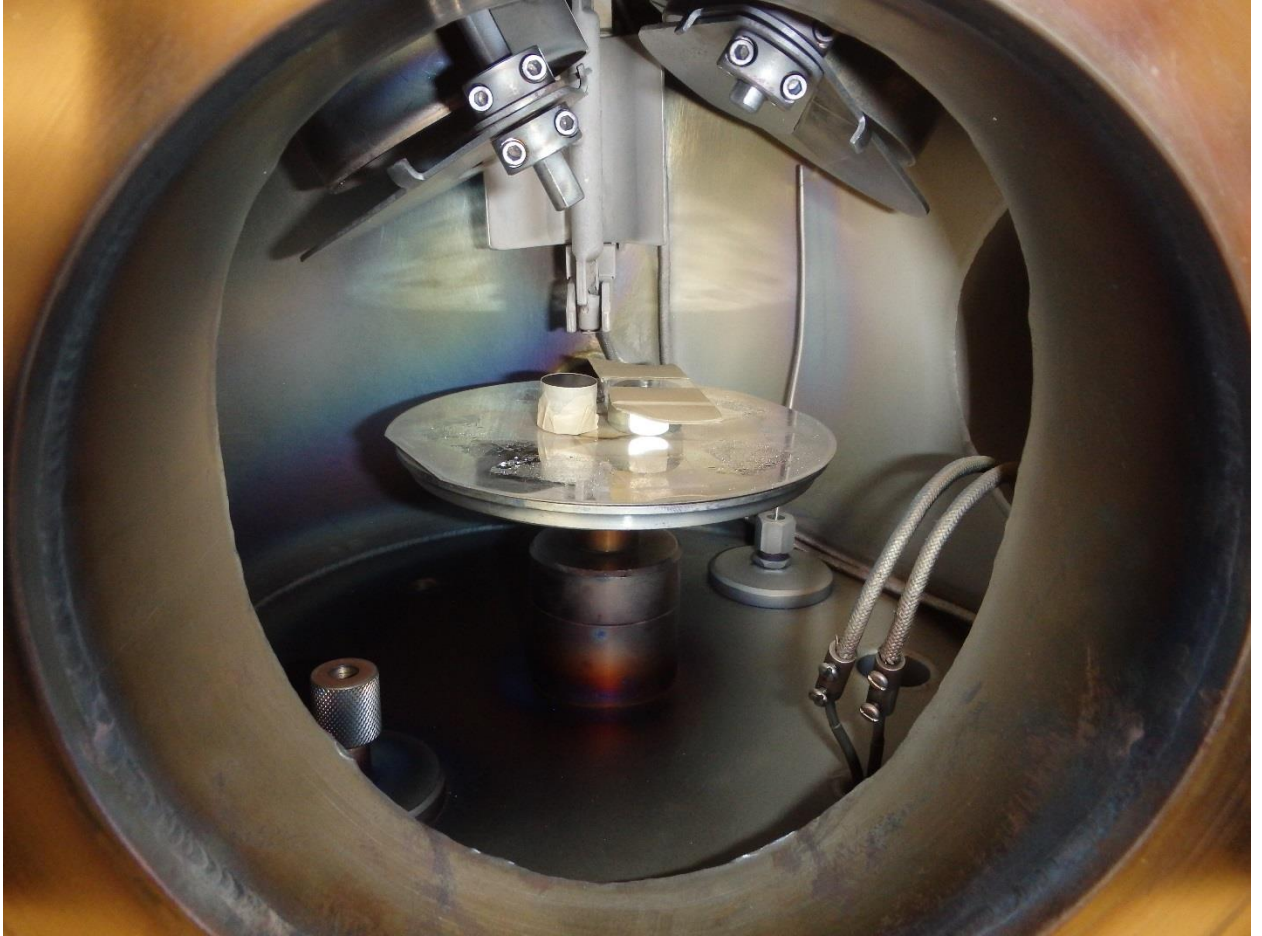


Figure 4.3 Sample with taped glass witness plate inside Denton PVD unit ready to be coated.



Figure 4.4 Completed samples coated with SiC

A preliminary experimental run was completed with four heated samples and a fifth non-heated sample for comparison. Results of this run were to provide a baseline for further experiments of similar configuration. Instead of acquiring baseline results, the first four samples proved the limitations of the intended experimental procedure. The five samples were prepared identically - ~25 nanometers of silver on the flat surface of the cylinder and ~350+ nanometers of SiC encapsulating the cylinder. One sample was not heated in order to provide a standard of comparison for the heated samples. Two of the four heated samples were heated at 1000 C for 12 hours in a tube furnace purged with argon. One of the samples was placed in the furnace with the silver-coated face of the

cylinder pointing up and the other sample was placed in the furnace with the silver-coated face pointing down. The other two samples were heated in a similar fashion but the maximum temperature was only 700 C.

The non – heated sample was sent to the University of Montana so that the equipment operators could adjust the time-of-flight secondary ion mass spectroscopy (TOF-SIMS) equipment to accept the heated samples that would come later. The non-heated sample displayed the expected layers of SiC, then Ag, then carbon. Problems arose when the first of the 1000 C heated samples was placed in the machine for analysis. SiC could be detected, but there was no silver found in the top layer of matrix material. The equipment operators suggested that an experimental error had been made and no silver was deposited on the sample. Although their concerns were valid, there was silver deposited on each sample. A “witness plate” was placed in the deposition chamber for each deposition run to record exactly how much material was deposited. The witness plate was half of a microscope slide with a strip of exposed glass in the middle and masking tape on the edges. This plate and the matrix material had the same amount of material deposited onto each other, and the thickness of the deposition was measured by removing the masking tape and running the slide through the profilometer.

It was observed by TOF – SIMS that silver had been completely vaporized (or otherwise removed) from the matrix material for 1000 C heated samples. SiC could be detected on the outside of the samples, so it appears that the SiC did not perform its intended purpose of keeping the silver inside the sample. After it was determined that the two 1000 C samples had the same problem, the 700 C samples were analyzed with the hopes that silver would be present. It seemed feasible that silver would be present

because 700 C is approximately 300 C less than the melting point of silver.

Unfortunately, the same problem was encountered with the 700 C samples. The only sample that showed trace amounts of silver was the sample that was placed in the furnace with the silver face down. Even for this sample, the silver did not diffuse into the matrix material, there was just a trace amount found near the SiC – matrix material boundary.

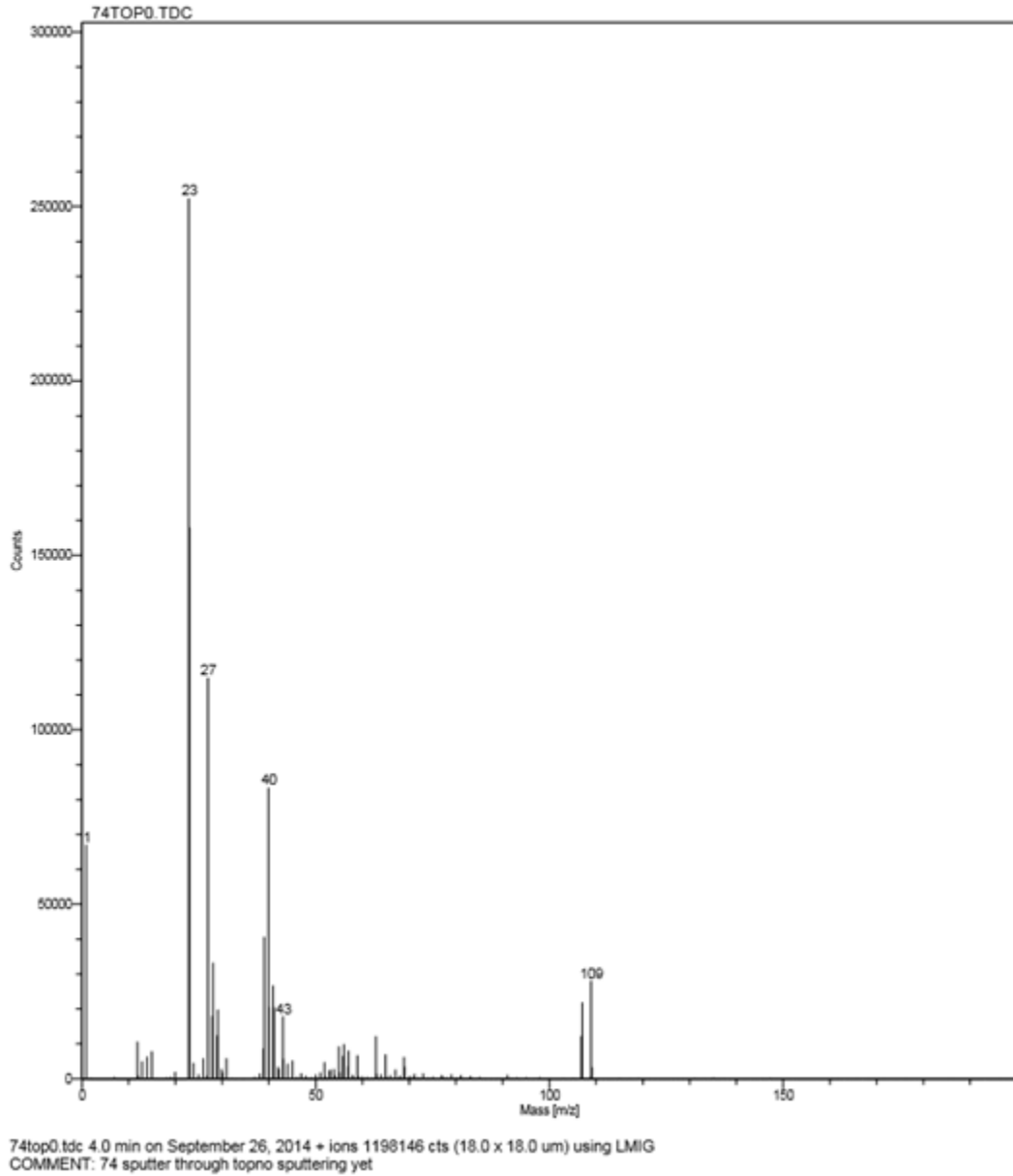


Figure 4.5 Sample 74 TOF-SIMS analysis. No sputtering. This sample was coated with silver and silicon carbide but NOT heated. Silver is clearly visible at 109 as well as SiC at 40.

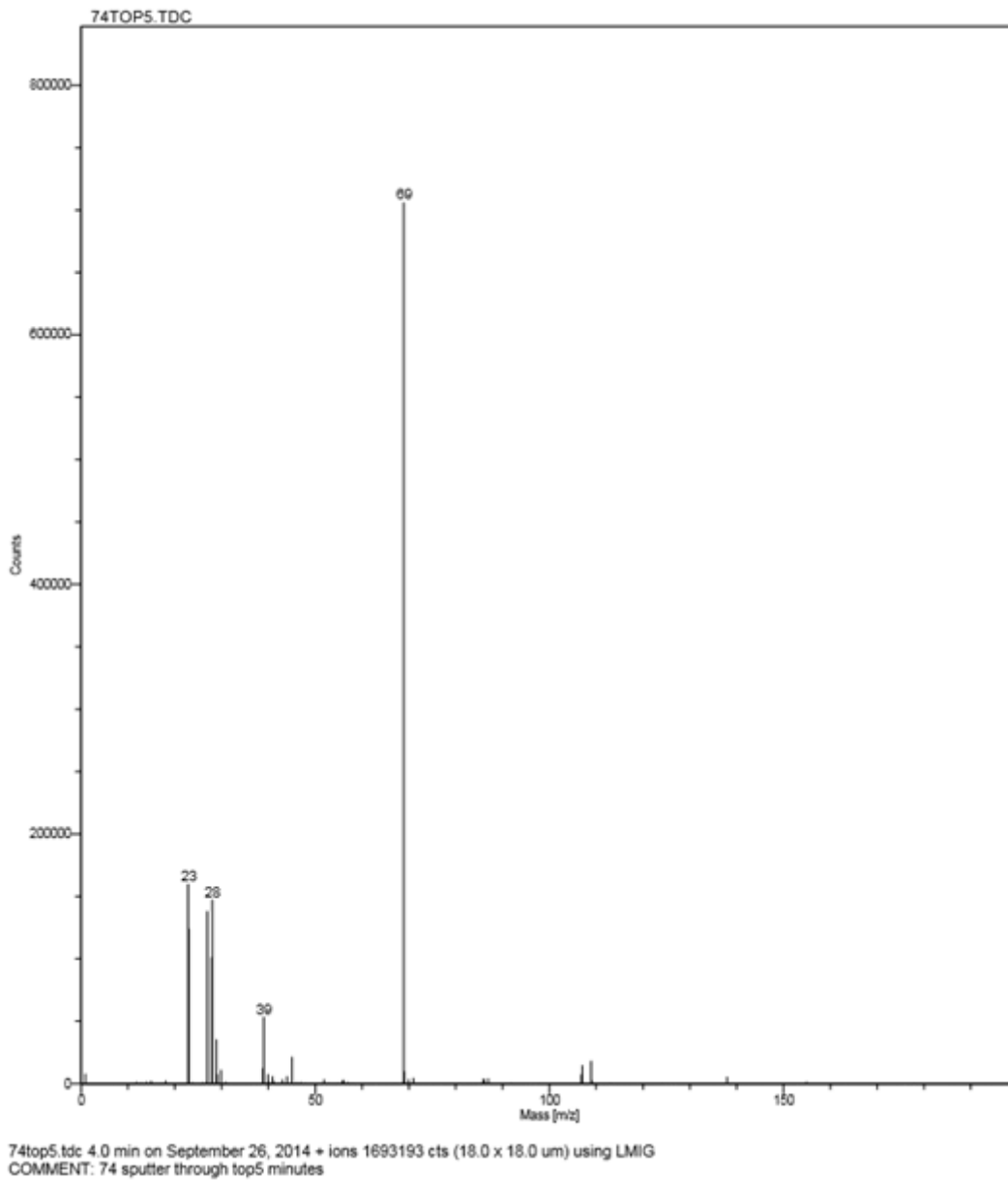


Figure 4.6 Sample 74 TOF-SIMS analysis. 5 minutes of sputtering = $0.94\mu\text{m}$. Silver and SiC still present (notice y axis scale). Peak at 69 amu likely from GaCa, possibly from sandpaper.

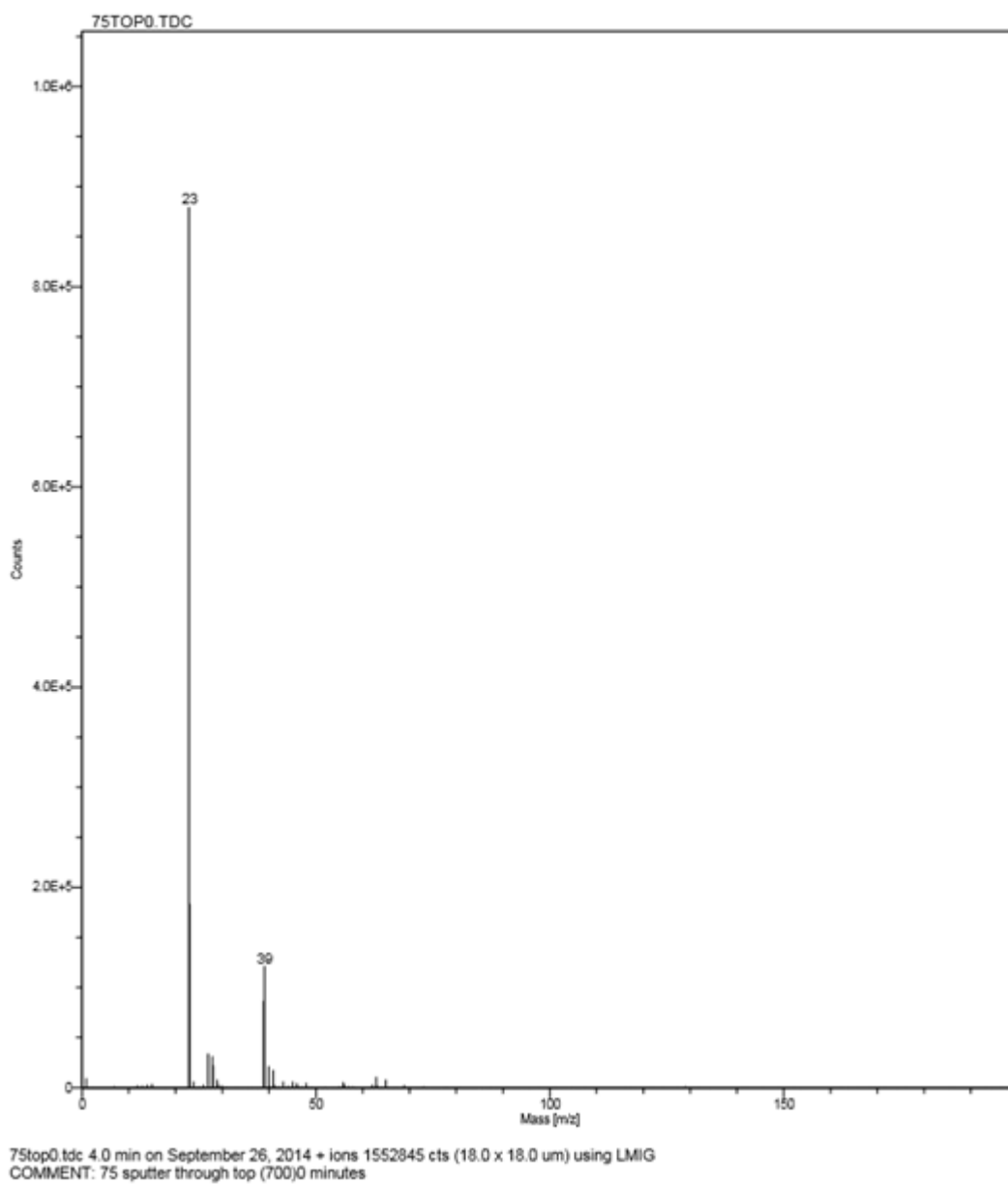


Figure 4.7 Sample 75 TOF-SIMS analysis. This sample was coated with silver layer on top and SiC, then heated at 1000 C with silver facing up in the oven. No sputtering. SiC peak can be seen at 39 but no silver peak.

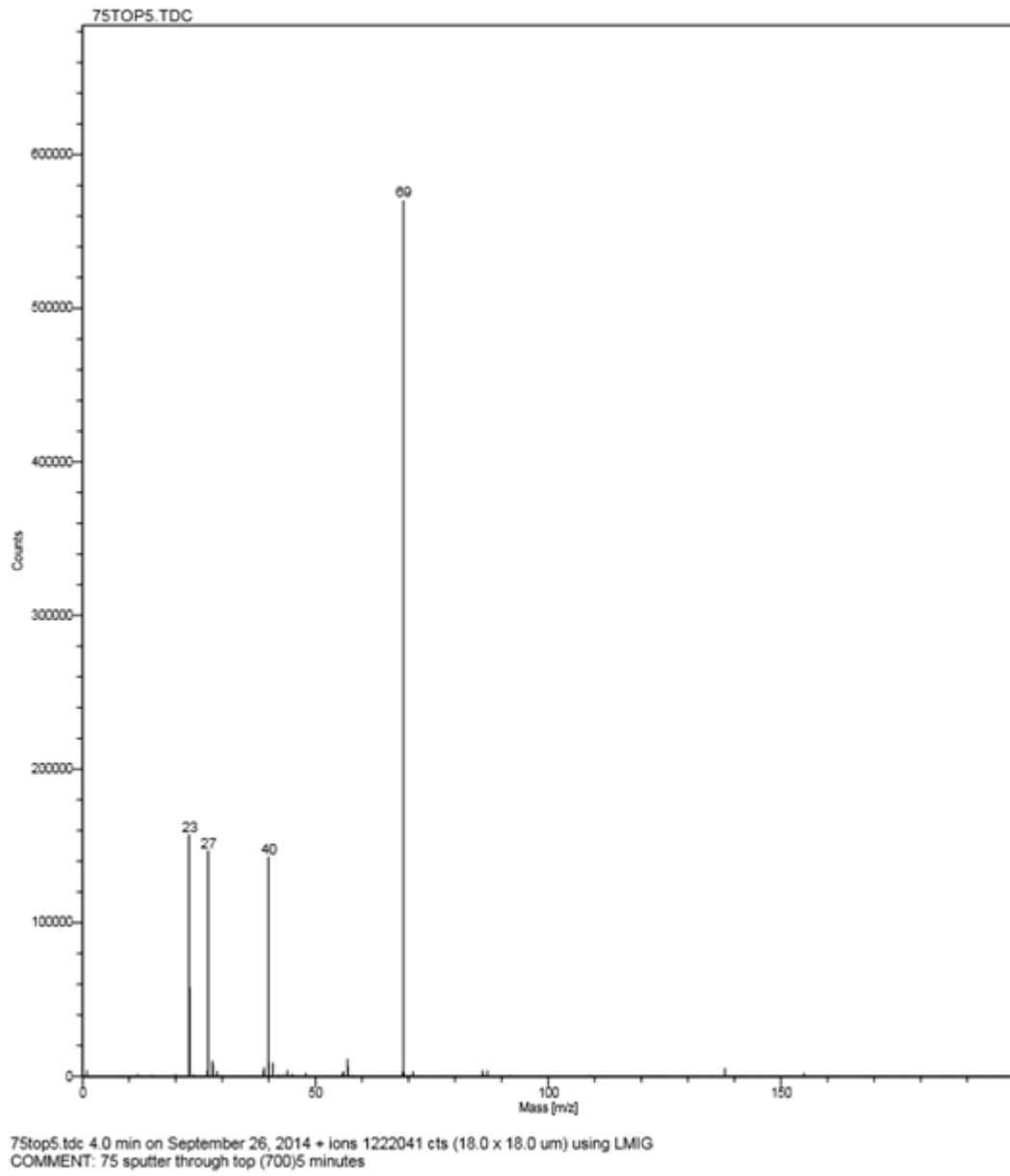
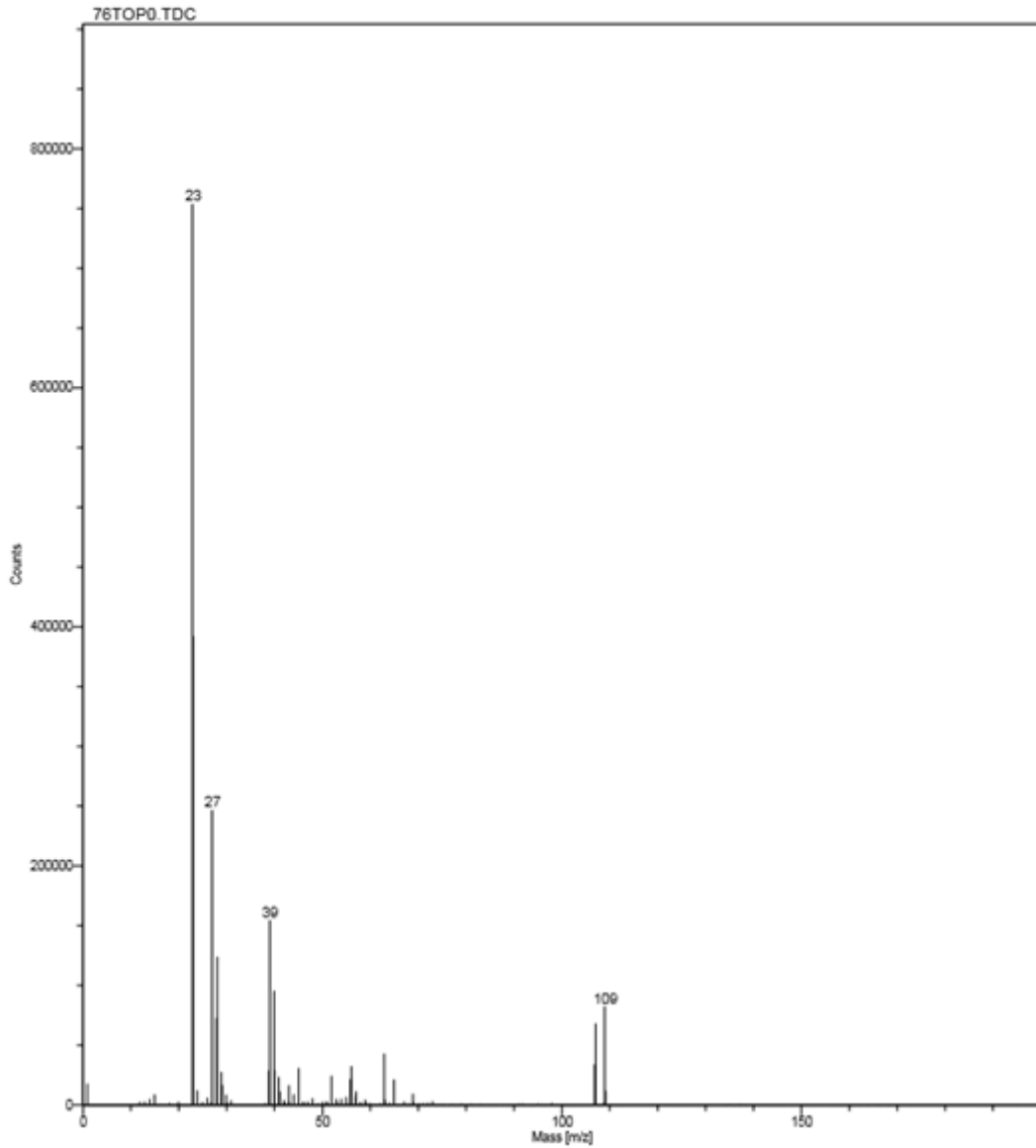


Figure 4.8 Sample 75 TOF-SIMS analysis. 5 minutes of sputtering = $0.94\mu\text{m}$. No silver peak, some SiC observable.



76top0.tdc 4.0 min on September 26, 2014 + ions 2650634 cts (18.0 x 18.0 um) using LMIG
COMMENT: 76 heated 700 silver face down sputter through silver face0 minutes

Figure 4.9 Sample 76 TOF-SIMS analysis. This sample was coated with silver layer on top and SiC, then heated at 700 C with the silver facing down in the oven. No sputtering.

Silver can be seen at 109 and SiC at 39.

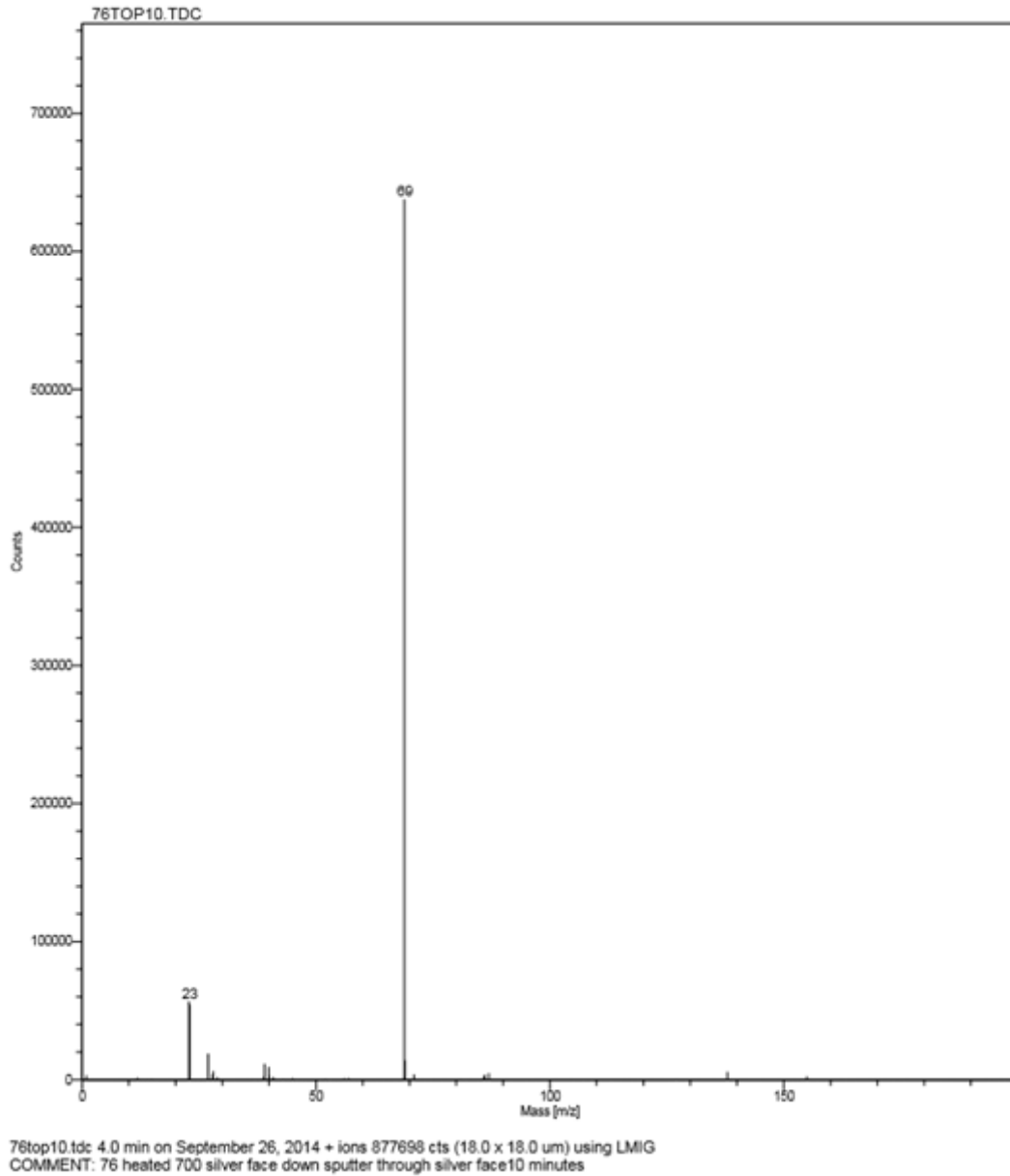


Figure 4.10 Sample 76 TOF-SIMS analysis. 10 minutes of sputtering = $1.59\mu m$. No trace of silver or SiC.

The first round of samples was intended to provide preliminary data so that another batch of similar experiments could be performed with optimal parameters. Instead of providing quantifiable data, the experiment proved that the method would not

work satisfactorily. The concept of depositing small amounts of silver by physical vapor deposition was a reasonable idea and merits consideration for further experiments. The problem lies in the SiC encapsulation layer that was supposed to keep the silver from leaving the system. The SiC encapsulation layer's failure can probably be attributed to two components – the thickness of the layer and the crystal structure of the layer. TRISO particles use significantly thicker layers of SiC, with mean thickness values around $40\mu\text{m}$ (IAEA, 1997). The crystal structure of the SiC layer is 3-C, which has been proven to be the most effective as a barrier to fission product migration. Physical vapor deposition is only capable of depositing SiC amorphously and there is no easy way to correct this deficiency.

4.2 Suggestions for Further Experimentation

The original purpose of this work was to quantify the migration of fission products, specifically silver, through matrix material. An attempt was made at obtaining experimental data and some specific lessons were learned that could be applicable for future experiments. Specifically, the inability of a physical vapor deposited SiC layer to keep silver contained inside an experimental system at 700 C was proven. This information is valuable, but the most important conclusions are at a much higher level.

There are three main problems with the published research that need to be addressed in order to provide data representative of fission product migration through fuel matrix material in a reactor. First, the majority of diffusion experiments are setup entirely differently from the conditions found inside a nuclear reactor. It is likely that most fission products, including silver, exist in a gaseous phase during the steady state

operation of a power reactor. Even if some fission products do not behave as gases, their concentrations outside TRISO particles are extremely small and, therefore, a concentration gradient is not the driving force as it is in traditional diffusion couple or “sandwich” experiments. Temperature gradients in reactors (from the location of fission product production to the reactor coolant) also are not represented in typical diffusion experiments, in which the diffusant-material couple is heated uniformly throughout. To address these differences, experiments must be designed to more closely represent what is actually happening in a reactor in terms of concentration and phase (solid vs. gas) of the diffusion species and the temperature gradient in the diffusing medium.

Secondly, an improved understanding of the species transport mechanism is necessary to inform experiment design and resulting modeling of the system. Most studies that have been published on the subject offer one of two things – a proposed mechanism supported by calculations that have not been experimentally verified, or experimental data that has not been analyzed with respect to mechanism, but rather is assumed to represent diffusion according to Fick’s Laws. Quite often, it has been deemed acceptable to apply a diffusion coefficient to an experimental system without understanding how the diffusant is migrating through the media. A diffusion coefficient in the molecular regime is calculated in a different way than a diffusion coefficient is calculated in the Knudsen regime. If experiments are done for each specific type of graphite, temperature, pressure, carrier gas, etc., then a “generic” diffusion coefficient may be adequate, but it is impossible to relate one generic diffusion coefficient determined from one set of parameters to another without knowing the diffusion regime.

The third gap in fission product migration research is a complete knowledge of the graphitic material, itself. Most of the characterization data that exist for particle fuel matrix material is specific to neutronic and durability characteristics as opposed to information related to fission product retention during operation and fission product composition at the end-of-life. Most gas-cooled reactors have operated with minimal fission product release to the coolant stream. As long as this has been the case, fission product migration through pores has been of little concern and has not warranted study. Intuitively, porosity information is the most important component for determining diffusion through porous material. In general, information regarding fuel matrix pore structure and size has been scattered and incomplete. Some researchers have compiled very specific information for their research and that information has found its way into this work to provide parameter ranges; however, the knowledge gaps that exist inhibit calculations and experiment planning. In the equations that determine diffusion regimes, for example, it is obvious that material porosity is crucial to estimating what could be happening in a porous material such as matrix graphite.

Three significant deficiencies in research addressing species' migration in particle fuel material have been identified: a disconnect between traditional diffusion studies and the conditions in a nuclear reactor, a lack of analyses linking experimental data with migration mechanisms, and a lack of information regarding the pore structure of matrix material. Each of these deficiencies can be addressed. The second and third problems can be resolved, at least partially, by collecting and analyzing existing information. The technique of discerning transport mechanisms, although complicated, is well represented in the literature. Information regarding matrix material properties exist, but with large

degrees of variability and this information has not been compiled into a useful format. Existing porosity information can be compiled and then it would become readily apparent which pieces of information are incomplete or inaccurate.

The first deficiency described, the disconnect between traditional diffusion studies and reactor conditions, can be resolved with the correct experimental approach. Boyle (2010) made one important stride by preparing silver-laden carbon powder that produced silver vapor during the experiment. Two significant improvements that can be made to his system are 1) material sectioning and analysis incorporating sample geometry and 2) adding a thermal gradient. Boyle's experiment created silver vapor that impinged on material in a hemispherical geometry, but the hemisphere was sectioned in flat layers to be analyzed. That practice violates the $1/r^2$ rule and a new sectioning mechanism or chamber design should be developed so that sections used for analysis are exposed to the same potential gradient. None of the diffusion studies that have been reviewed used a thermal gradient. When thinking of a TRISO particle in a reactor, there are at least two gradients that come to mind – concentration from the TRISO particle being a source for fission products, and a thermal gradient that exists because heat is being transferred from the fuel outwards to the coolant. A thermal gradient could be incorporated into an experiment by heating a volume that contains silver vapor and allowing that silver vapor to diffuse through matrix material towards a heat sink. This type of experiment would more closely simulate the conditions inside a reactor.

4.3 Alternate Mechanism for Silver Migration – Thermal Diffusion

A mechanism that may explain the movement of fission products through matrix graphite material is thermal diffusion. This mechanism is not driven by a concentration gradient, but rather depends on the thermal gradient within a substrate to move the diffusant. In some cases, material can be moved in the same direction as the thermal gradient, and in other cases material will move against the thermal gradient, depending on the materials in question. This concept is particularly interesting to consider for a nuclear reactor and specifically VHTRs that use TRISO coated fuel particles. The purpose of building a reactor is to create a thermal gradient that eventually will produce electricity. Because there is a steady state temperature gradient from inside the TRISO particle to the helium coolant, this gradient may be responsible for fission product movement away from fuel through other core components.

4.3.1 Soret Effect in Nuclear Applications

During the early years of mixed oxide fuel and gas cooled reactor development, thermal diffusion was thought to be a contributing factor in the separation of $PuO_2 - UO_2$ and $CeO_2 - UO_2$ (Wirtz, 1968). Separation of plutonium and uranium oxides within fuel pins was thought to be caused by a thermal gradient and could potentially become a safety concern. Migration of cerium oxide, presumably by a thermal gradient, was also seen as evidence of fission product transport by thermal diffusion. Thermal diffusion, thermophoresis, and the Soret effect are used interchangeably in literature, which can lead to confusion. Although the term “Soret effect” usually describes thermal diffusion in liquids, it is sometimes used to describe gaseous phase diffusion and is found in nuclear literature along with the term “thermal diffusion”.

In the 1960s, Wirtz and his contemporaries Beisswenger (1967), Bober (1967), Schumacher (1967), and Zebroski (1965) suspected a thermal gradient was responsible for mixed oxide fuel separation and fission product transport (Beisswenger et al., 1967) (Novak et al., 1965). The problem they encountered was describing how the heat of transfer Q^+ could be quantified. Although some data for this parameter can be found in more recent literature, the heat of transfer still has a significant degree of uncertainty. The Soret constant, S , can be determined if the separation of a two-component system in a temperature gradient reaches equilibrium.

$$S = \frac{1}{\gamma(1-\gamma)} \frac{d\gamma}{dT} \quad (4.1)$$

where γ is the molar fraction of the diffusing species. If diffusion and thermal diffusion have reached equilibrium, the coefficients for diffusion D and thermal diffusion D' are related by

$$-D \nabla \gamma - D' \gamma (1-\gamma) \nabla T = 0 \quad (4.2)$$

Combining equations 4.1 and 4.2 and solving for the Soret constant gives

$$S = \frac{-D'}{D} \quad (4.3)$$

It is known that the heat of transfer Q^+ at equilibrium is connected to the Soret constant by

$$S = \frac{Q^+}{R T^2} \quad (4.4)$$

Taking a kinetic approach and considering that the diffusion coefficient is temperature dependent,

$$D = D_o \exp(-q/RT) \quad (4.5)$$

where D_o is not strongly temperature dependent and q is the energy of activation. It was proposed that the energy of activation should consist of different components that refer to steps in the migration process. The three energy of activation components were

$q_H = \text{energy necessary at the primary position of the migrating particle}$

$q_R = \text{energy necessary to open the lattice to let the migrating particle pass}$

$q_L = \text{energy necessary to open a hole at the new position}$

and

$$Q^+ = q_H - q_L \quad (4.6)$$

For the cases of cerium oxide in uranium oxide at 2050 K and plutonium oxide in uranium oxide at 2673 K, the heats of transfer were $25 \frac{\text{kcal}}{\text{mol}}$ and $58 \frac{\text{kcal}}{\text{mol}}$, respectively. It was noted by Wirtz that more data was needed for D (non-thermal), q , and Q^+ for cerium and plutonium at different temperatures. This application of the Soret effect and thermal diffusion pertained to oxide fuels and not porous media. Despite the structural differences between oxides and graphite matrix material, this study was important because it recognized a thermal gradient as being a driving mechanism for fission product migration.

Decades after Wirtz published his findings in 1968, there was some renewed interest in the Soret effect for gas cooled reactors. In 2004, the “TRISO-Coated Particle Fuel Phenomenon Identification and Ranking Tables (PIRTs) for Fission Product Transport Due to Manufacturing, Operations, and Accidents” was published by the NRC (Morris, 2004). This publication identified the most important causes of fission product leakage from TRISO particles so that high-ranking phenomena could be investigated further. Although the focus was on “buffer” carbon and pyrolytic carbon inside the TRISO particles, this is the most relevant information available that could apply to matrix material.

Within a TRISO particle, the most probable location for a thermal gradient to move fission products would be the buffer carbon layer that surrounds the fuel. This is due to the buffer layer being porous and having a low density which reduces the thermal conductivity. These factors combine to generate the largest temperature gradient inside the TRISO particle. Reactor power directly influences the temperature gradient and the extent of thermal diffusion. In a pebble bed reactor core running at 62 MW thermal power, the temperature drop across the buffer layer inside a TRISO particle is about 10 K which corresponds to a gradient of $100 \frac{K}{cm}$.

Similar to Wirtz’s (1968) identification of a combined diffusion process, the traditional concentration gradient diffusion can be combined with thermal diffusion to predict a combined flux.

$$J = -D \left(\nabla C + \frac{C Q^+}{R T^2} \nabla T \right) \quad (4.7)$$

where the second term on the right hand side of the equation incorporates the Soret coefficient. The NRC's analytical calculations predict that the Soret effect can have an influence on the transport of fission products through TRISO carbon layers (Nuclear Regulatory Commission, 2004). A factor of 10 increase in power would increase the concentration of cesium that reaches the outer pyrolytic carbon layer by a factor of 5 to 10. The NRC identified thermal diffusion as being partially responsible for fission product transport through the carbon buffer layer, but has not identified any mechanism for fission product transport through the pyrolytic carbon.

The steady state temperature gradient that exists in a reactor is well understood, but the NRC identified another, less obvious thermal phenomena that could explain fission product migration through TRISO graphite (Nuclear Regulatory Commission, 2004). When a reactor is shut down after steady state operation, conduction cool down occurs where the peak fuel temperature rises to 1600 C. Fission products become adsorbed to the buffer and pyrolytic carbon inside the TRISO particles during steady state operation. This "trapping", as the NRC refers to adsorption, occurs in pores and crack boundaries and leads to a buildup of fission products that are loosely bound to the carbon. If the fuel temperature rises significantly, the trapped fission products can become dislodged and enter the gaseous phase where they are more likely to penetrate the SiC layer and enter matrix graphite. In a similar fashion, fission products that have entered matrix graphite during core lifetime will become more mobile if temperature increases during a conduction cool down period.

4.3.2 Thermal Diffusion in Non-Nuclear Applications

There has been a lack of experimental data for thermal diffusion in nuclear applications despite it being a probable cause of fission product migration through fuel and TRISO particles. In other areas of material science there have been more experiments and data collection that proves thermal diffusion can be quantified. Two examples were given in Paul Shewmon's book (1989) on diffusion topics.

The first example of thermal diffusion experimentation was an iron-carbon alloy annealed with a temperature gradient. When alloy annealed, the carbon concentration was found to be higher at the hot end of the alloy. Since the carbon migrated against the thermal gradient, Q_{carbon}^* was negative for the alloy. The concentration of carbon in the alloy was plotted as a function of temperature on a logarithmic scale, and since the thermal gradient was uniform, the plot also shows concentration vs. location in the alloy. The data points were linear on the log scale and the Q_{carbon}^* value was determined to be -96 kJ/mol. Note that the diffusion coefficient D_{carbon} does not need to be known to find Q_{carbon}^* experimentally.

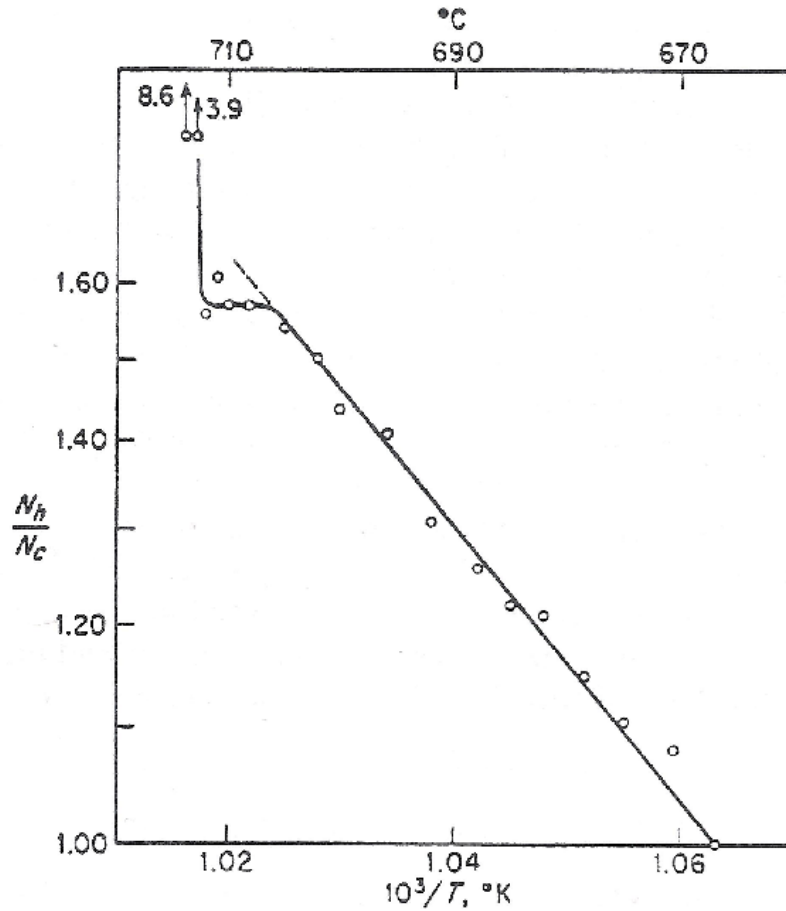


Figure 4.11 Carbon content vs. $1/T$ for carbon-iron alloy annealed in constant temperature gradient until steady state was attained.

The second example of thermal diffusion and phase distribution occurred with hydrogen in zirconium. Although these materials are present in a reactor, the comparison to a nuclear reactor should not be made. In a reactor, hydrogen is sometimes produced at the moderator – cladding interface where the temperature is low compared to the fuel – cladding interface. In the example shown in figure 4.12, hydrogen is pushed through zirconium from high temperature to low temperature. Because hydrogen is not produced at the hot side of a reactor’s thermal gradient, the example described here is not

applicable to a reactor. The reaction $Zr + H_2O \rightarrow ZrO_2 + 2H$ allows hydrogen gas to form and enter zirconium. The heat of transport for hydrogen in this system is $Q^* = 6kcal/mol$, which means the thermal gradient will push hydrogen towards the cool end of the zirconium. Before the temperature gradient exists, it may be assumed that hydrogen has reached some uniform concentration in the zirconium. When the thermal gradient is applied to the zirconium-hydrogen system, the hydrogen will be pushed away from the heat source and towards the heat sink so long as hydrogen is soluble in the zirconium. During its movement away from the hot region of the zirconium, the hydrogen solubility will decrease with temperature and precipitation may occur. This will lead to an area with low hydrogen concentration near the fuel due to thermal diffusion, a spike in concentration where hydrogen is no longer mobile and forms a precipitate, and possibly unchanged hydrogen concentration past the spike. This phenomenon has been used to explain brittle layers in zirconium.

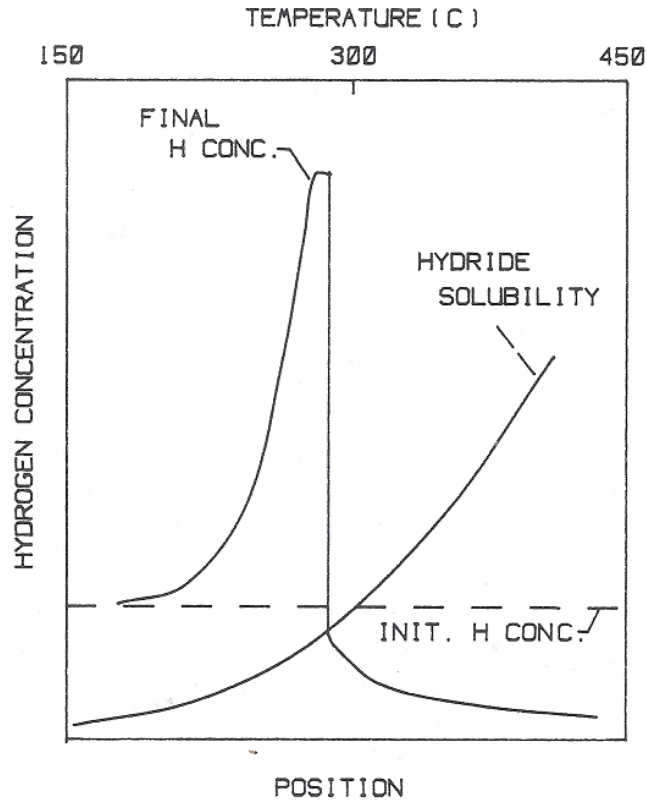


Figure 4.12 Hydrogen distribution in zirconium for an initially homogeneous sample annealed in a temperature gradient. Note the temperature – position correlation.

(Shewmon, 1989)

For a thermal diffusion – precipitation situation depicted above, the direction of diffusant migration depends on the difference between the heat of solution of the precipitate in the host material H_1 and the heat of transport of the diffusant Q^* . The solubility of diffusant in equilibrium with the precipitate is calculated with equation 4.8 and the concentration gradient in the zirconium is constrained by the second phase.

$$N_1 = N_o \exp\left(-\frac{H_1}{RT}\right) \quad (4.8)$$

where

$$H_1 = \text{heat of solution of the precipitate} \left[\frac{J}{\text{mol}} \right]$$

$$N_1 = \text{solubility in equilibrium with precipitate} \left[\frac{\text{mol}}{\text{volume}} \right]$$

$$N_o = \text{reference solubility value} \left[\frac{\text{mol}}{\text{volume}} \right]$$

The diffusant flux for this system is calculated with equation 4.9

$$J_1 = - \frac{D_1 N_1 (Q_1^* - H_1)}{RT^2} \frac{\partial T}{\partial x} \quad (4.9)$$

where

$$J_1 = \text{diffusant flux} \left[\frac{\text{mol} \times s}{m} \right]$$

$$D_1 = \text{diffusion coefficient} \left[\frac{m^2}{s} \right]$$

$$Q_1^* = \text{diffusant heat of transport} \left[\frac{J}{\text{mol}} \right]$$

Chapter 5 Conclusions

In support of fuel development for next generation nuclear reactors, the nature of fission product migration through fuel matrix material was studied from both theoretical and empirical perspectives. A simple MATLAB model was developed to estimate silver migration through A3-3 fuel matrix material. Constants for silver and helium were hardcoded into the script because helium is the coolant for high temperature gas reactor designs and silver is the most mobile of fission products in gas-cooled reactors. User inputs for time, temperature, and pressure provide the necessary parameters for calculating the Knudsen number, molecular diffusion coefficient, and the Knudsen diffusion coefficient. With this information, the script graphically shows the conditions at which the diffusion regimes take place (if at all) and estimates the migrating species concentration vs. depth in the material for the desired experimental parameters. Any experimenter should perform “back of the envelope” calculations to determine if an experiment plan can produce the desired results, and these MATLAB scripts are a quick and visual way of accomplishing this task. The structure of the scripts probably does not need to be changed, but improvements could be made with more extensive information about the porosity of the medium. The scripts could also be expanded to include more fission products, different carrier gasses, and different types of fuel matrix material.

In order to test the concept of low concentration silver migration, physical vapor deposition was used to deposit a thin (<40 nanometer) layer of silver onto one end of cylindrical matrix material samples. The silver – coated cylinders were subsequently coated on all surfaces, including on top of the silver surface, with 300 to – 500-nanometer

layers of SiC and heated for 12 hours at 700 or 1000 C in a tube furnace with argon flowing through the tube. After heating, time of flight SIMS analysis was used to sputter into the silvered surface of the graphitic matrix and detect the presence of silver. Unfortunately, silver was not detected at any significant quantity in any of the samples. This was most likely due to the amorphous structure of the SiC layer and its inability to contain the silver. It has been noted in literature that silver is the most mobile of the fission products, and this appears to have been confirmed by its complete disappearance even at 700 C heating. This type of silver – matrix material experiment would likely produce decent results if a better containment layer of SiC could be applied by using chemical vapor deposition rather than physical vapor deposition. A significantly thicker SiC layer or a 3C crystal structure or a combination of both would likely solve the problem of silver escaping from the sample.

Four main components were identified that would improve further research in this area. First, experiments need to be more representative of the conditions found in a reactor. The most promising way to achieve this would be an experiment that uses fission product vapor instead of the solid phase. Secondly, a thermal gradient should be used to more accurately model fission products being produced in hot fuel and migrating towards cooler parts of the reactor. This could be achieved by heating a silver – laden graphite powder similar to Boyle's (2010) experiment and impinging this vapor on matrix material with a heat sink on the opposite side. As of this writing, an experiment that uses a thermal gradient and gas phase diffusant has not been attempted. Thirdly, more comprehensive data for graphite and matrix material needs to be assembled, specifically regarding pore size distribution, tortuosity, and wall roughness. Finally, there should be

an attempt to explain the mechanisms of diffusion instead of applying mechanism – independent diffusion coefficients. Designing representative experiments and acquiring better porosity data are feasible with existing techniques and equipment. Explaining the mechanisms of fission product migration would be more difficult and experiment – specific than the first two objectives, but are still important for related research.

References

- Bacos, M., Dorvaux, J., Lavigne, O., & Renollet, Y. (1999). C / C Composite Oxidation Model I. Morphological Experimental Investigations. *Carbon*, 77-92.
- Beck, J., & Pincock, L. (2011). *High Temperature Gas-Cooled Reactors Lessons Learned Applicable to the Next Generation Nuclear Plant*. Idaho Falls: Idaho National Laboratory.
- Beisswenger, H., Bober, M., & Schumacher, M. (1967). Thermodiffusion in System UO₂ & CeO₂. *Journal of Nuclear Materials*, 38-52.
- Boyle, T. R. (2010). *Measurement of Fission Product Diffusion in VHTR Materials*. University of Missouri.
- Boyle, T. R. (2013). Measurement of Silver Diffusion in VHTR Graphitic Materials. *Nuclear Technology*, 149-159.
- Branney, S. (2010). *The Adsorption of Fission Products on VHTR Structural Materials*. University of Missouri - Columbia.
- Breitkopf, C. (2008, November 28). Diffusion in Porous Media. *Lectures at Fritz-Haber Institute*.
- Carman, P. (1956). *Flow of Gases Through Porous Media*. New York: Academic Press Inc.
- Chapman, S., & Cowling, T. (1970). *The Mathematical Theory of Non-Uniform Gases Third Edition*. Cambridge: Cambridge University Press.
- Copinger, D., & Moses, D. (2003). *Fort Saint Vrain Gas Cooled Reactor Operational Experience*. Oak Ridge: Oak Ridge National Laboratory.
- Cunningham, R., & Willimas, R. (1980). *Diffusion in Gases and Porous Media*. New York: Plenum Press.
- Delle, W. (1983). Influence of Fast Neutron Irradiation and Corrosion on the Porosity of Graphite and Fuel Matrix. *Hahn-Meitner-Institut fur Kernforschung Berlin GmbH* (pp. 17-25). Berlin: Hahn-Meitner-Institut fur Kernforschung Berlin GmbH.
- Duderstadt, J. J., & Hamilton, L. J. (1976). *Nuclear Reactor Analysis*. John Wiley & Sons, Inc.
- Gruener, S., & Huber, P. (2008). Knudsen Diffusion in Silicon Nanochannels. *Physical Review Letters* 100, 064502.
- Hiroshima, Nagasaki, and Subsequent Weapons Testing*. (2015, November 6). Retrieved from World Nuclear Association: <http://www.world-nuclear.org/info/Safety-and->

Security/Radiation-and-Health/Hiroshima,-Nagasaki,-and-Subsequent-Weapons-Testing/

- IAEA. (1997). *Fuel Performance and Fission Product Behavior in Gas Cooled Reactors*. Vienna: IAEA.
- Kingrey, K. I. (2003). *Fuel Summary for Peach Bottom Unit 1 High-Temperature Gas-Cooled Reactor Cores 1 and 2*. Idaho Falls: Idaho National Engineering and Environmental Laboratory.
- Knudsen, M. (1934). *The Kinetic Theory of Gases*. Methuen's Monographs on Physical Subjects.
- Krautwasser, P. E. (1983). Corrosion-Induced Changes in Pore Size Distributions of Fuel Matrix Material. *Hahn-Meitner-Institut fur Kernforschung Berlin GmbH* (pp. 33-37). Berlin: Hahn-Meitner-Institut fur Kernforschung Berlin GmbH.
- M.D. Mikhailov, M. O. (1984). *Unified Analysis and Solutions of Heat and Mass Diffusion*. Toronto: General Publishing Company.
- Mays, T., McEnaney, B., & Kelly, B. (1995). Gaseous Diffusion and Pore Structure. *Graphite Moderator Lifecycle Behavior* (pp. 329-335). Bath: International Atomic Energy Agency.
- Morris, R. P. (2004). *TRISO-Coated Particle Fuel Phenomenon Identification and Ranking Tables (PIRTs) for Fission Product Transport Due to Manufacturing, Operations, and Accidents*. Washington D.C.: Nuclear Regulatory Commission.
- Nonbol, E. (1996). *Description of the Advanced Gas Cooled Type of Reactor*. Roskilde: Nordic Nuclear Safety Research.
- Novak, P., Lauritzen, J., Prostig, J., Davies, J., & Zebroski, E. (1965). ANL-7120.
- Nuclear Regulatory Commission. (2004). *TRISO-Coated Particle Fuel Phenomenon Identification and Ranking Tables (PIRTs) for Fission Product Transport Due to Manufacturing, Operations, and Accidents*.
- Panish, M. B. (1961). Vapor Pressure of Silver. *Journal of Chemical and Engineering Data*, 592-594.
- Robens, E. (1983). Determination of Corrosion Induced Changes in Pore Size Distribution and Specific Surface of Graphitic Matrix by Gas Adsorption. *Hahn-Meitner-Institut fur Kernforschung Berlin GmbH* (pp. 26-32). Berlin: Hahn-Meitner-Institut fur Kernforschung Berlin GmbH.
- Shewmon, P. (1989). *Diffusion in Solids Second Edition*. Warrendale: Minerals, Metals & Materials Society.
- Tsoufanidis, N. (2013). *The Nuclear Fuel Cycle*. La Grange Park: American Nuclear Society.

- United States. (2015, November 6). *Electronic Code of Federal Regulations*. Retrieved from http://www.ecfr.gov/cgi-bin/text-idx?SID=695136b68147e3266740c9db10e66ccc&mc=true&node=se10.1.50_134&rgn=div8
- Vasenkov, S., Geir, O., & Karger, J. (2003). Gas Diffusion in Zeolite Beds: PFG NMR Evidence for Different Tortuosity Factors in the Knudsen and Bulk Regimes. *European Physics Journal*, 35-38.
- Wirtz, K. (1968). Thermal Diffusion in Nuclear Reactor Fuels. *Journal of the American Chemical Society*, 3098 - 3099.
- Xinli, Y., Laurent, B., Bhristian, B., & Suyuan, Y. (2008). The Modeling of Graphite Oxidation Behavior for HGTR Fuel Coolant Channels Under Normal Operating Conditions. *Nuclear Engineering and Design*, 2230-2238.
- Ziarani, A. S., & Aguilera, R. (2012, September 16). Knudsen's Permeability Correction for Tight Porous Media. *Transport in Porous Media*, pp. 239-260.

Appendix 1 MATLAB Scripts

Final V2.m

```
% Ted Pollock 2015
%
clear
clc
%
% This script will calculate:
% 1) mean free path
% 2) knudsen number
%
% Constants
%
K = 1.38*10^-23;           % boltzman constant [m^2*kg/s^2*K]
R = 8314;                 % gas constant [g-m^2/s^2-mol-k]
cdHe = 2*31*10^-12;      % collision diameter for He - He
collisions
cdHeAg = (31+144)*10^-12; % collision diameter for Ag - He
collisions
M = 107.86;              % Ag molecular weight [g/mol]
mHe = 4;                 % [amu]
mAg = 107;               % [amu]
%
% Temperature - Pressure meshgrid
%
Tlow = input('Low Temperature Value [K] > ');
Thigh = input('High Temperature Value [K] > ');
Tinterval = input('Temperature Increment [K] > ');

Plow = input('Low Pressure Value [Pa] > ');
Phigh = input('High Pressure Value [Pa] > ');
Pinterval = input('Pressure Increment [Pa] > ');
PPAg = input('# Silver atoms in He - Ag mix [ppm Ag] > ');

T = [Tlow:Tinterval:Thigh];
P = [Plow:Pinterval:Phigh];

[T,P] = meshgrid(T,P);

% PHe = ((10^6 - PPAg)/10^6).*P;
% PAg = (PPAg/10^6).*P;
%
% Calculate MFP for each spot on the meshgrid
%
MFP = (K/(3.14*((10^6 - PPAg)/10^6)*cdHe^2*2^0.5 +
(PPAg/10^6)*cdHeAg^2*(1+mHe/mAg)^0.5))* (T./P);

figure
mesh(T,P,MFP)
title('Mean Free Path [m]')
```

```

xlabel('Temperature [K]')
ylabel('Pressure [Pa]')
zlabel('Mean Free Path [m]')
%
% Calculate Knudsen number for each spot on the meshgrid
%
d = input('Pore diameter [m] > ');

KN = MFP./d;

figure
mesh(T,P,KN)
title('Knudsen Number [-]')
xlabel('Temperature [K]')
ylabel('Pressure [Pa]')
zlabel('Knudsen Number [-]')
%
```

Depth V2.m

```
% Ted Pollock 2015

clear
clc

% This script will
% 1) determine the correct silver vapor pressure for a selected
temperature
% 2) calculate the silver vapor saturation value
% 3) calculate and plot the silver concentration in matrix material

%%%%%%%%%%%%%%%%%%%%%%%%%%%%%%%%%%%%%%%%%%%%%%%%%%%%%%%%%%%%%%%%%%%%%%%%
%%%
%%%%%%%%%%%%%%%%%%%%%%%%%%%%%%%%%%%%%%%%%%%%%%%%%%%%%%%%%%%%%%%%%%%%%%%%
%%%

% Vapor Pressure Section

% This is the vapor pressure of silver as experimentally determined
% by Morton B. Panish and published in the Journal of Chemical
% and Engineering Data Vol. 6 #4 in October of 1961
% The data was obtained by Knudsen effusion, radioactive tracer,
% and mass spectrometry.

Temperature = [958 979 1010 1056 1085 1115 1123 1152 1190 1228 1237
1265 1263 ...
1287 1313 1315 1335 1349 1356 1374 1392 1393 1402 1467 1503];

mmHg = [8.30*10^-7 1.80*10^-6 6.50*10^-6 3.90*10^-5 6.20*10^-5
1.40*10^-4 ...
1.80*10^-4 4.10*10^-4 9.00*10^-4 2.30*10^-3 2.80*10^-3 6.50*10^-3
...
7.20*10^-3 6.40*10^-3 1.20*10^-2 1.73*10^-2 1.96*10^-2 2.49*10^-2
...
4.30*10^-2 5.50*10^-2 4.90*10^-2 5.21*10^-2 6.60*10^-2 2.21*10^-1
...
2.50*10^-1];

Pascals = 133.*mmHg;

Tabel = table(Temperature, mmHg, Pascals);

% Find the correct vapor pressure value for a temperature input

Temp = input('Experiment Temperature [K] > ');

if Temp < Temperature(1)
    fprintf('Selected temperature is below range for available data ')
elseif Temp >= Temperature(1) & Temp < Temperature(2)
    VP = Pascals(1);
elseif Temp >= Temperature(2) & Temp < Temperature(3)
```

```

    VP = Pascals(2);
elseif Temp >= Temperature(3) & Temp < Temperature(4)
    VP = Pascals(3);
elseif Temp >= Temperature(4) & Temp < Temperature(5)
    VP = Pascals(4);
elseif Temp >= Temperature(5) & Temp < Temperature(6)
    VP = Pascals(5);
elseif Temp >= Temperature(6) & Temp < Temperature(7)
    VP = Pascals(6);
elseif Temp >= Temperature(7) & Temp < Temperature(8)
    VP = Pascals(7);
elseif Temp >= Temperature(8) & Temp < Temperature(9)
    VP = Pascals(8);
elseif Temp >= Temperature(9) & Temp < Temperature(10)
    VP = Pascals(9);
elseif Temp >= Temperature(10) & Temp < Temperature(11)
    VP = Pascals(10);
elseif Temp >= Temperature(11) & Temp < Temperature(12)
    VP = Pascals(11);
elseif Temp >= Temperature(12) & Temp < Temperature(13)
    VP = Pascals(12);
elseif Temp >= Temperature(13) & Temp < Temperature(14)
    VP = Pascals(13);
elseif Temp >= Temperature(14) & Temp < Temperature(15)
    VP = Pascals(14);
elseif Temp >= Temperature(15) & Temp < Temperature(16)
    VP = Pascals(15);
elseif Temp >= Temperature(16) & Temp < Temperature(17)
    VP = Pascals(16);
elseif Temp >= Temperature(17) & Temp < Temperature(18)
    VP = Pascals(17);
elseif Temp >= Temperature(18) & Temp < Temperature(19)
    VP = Pascals(18);
elseif Temp >= Temperature(19) & Temp < Temperature(20)
    VP = Pascals(19);
elseif Temp >= Temperature(20) & Temp < Temperature(21)
    VP = Pascals(20);
elseif Temp >= Temperature(21) & Temp < Temperature(22)
    VP = Pascals(21);
elseif Temp >= Temperature(22) & Temp < Temperature(23)
    VP = Pascals(22);
elseif Temp >= Temperature(23) & Temp < Temperature(24)
    VP = Pascals(23);
elseif Temp >= Temperature(24) & Temp < Temperature(25)
    VP = Pascals(24);
else
    fprintf('Selected temperature is above range for available data')
end

```

```

figure
plot(Temperature(10:20),Pascals(10:20),'LineWidth',2,'Marker','*','MarkerSize',10)
title('Vapor Pressure of Silver')
xlabel('Temperature [K]')
ylabel('Vapor Pressure [Pa]')

```

```

%%%%%%%%%%%%%%%%%%%%%%%%%%%%%%%%%%%%%%%%%%%%%%%%%%%%%%%%%%%%%%%%%%%%%%%%
%%
%%%%%%%%%%%%%%%%%%%%%%%%%%%%%%%%%%%%%%%%%%%%%%%%%%%%%%%%%%%%%%%%%%%%%%%%
%%

```

```

% Diffusion Section

```

```

% Temperature - Pressure - Time

```

```

P = input('Pressure [Pa] > ');
Ti = 60*60*input('Heating Time [Hours] > ');

```

```

% Calculate diffusion coefficient appropriate for situation
% First calculate Knudsen Number
% For KN < 1 calculate the molecular diffusion coefficient
% For 1 < 5 calculate the transitional diffusion coefficient
% For KN > 5 calculate the Knudsen diffusion coefficient

```

```

K = 1.38*10^-23;           % boltzman constant [m^2*kg/s^2*K]
R = 8314;                 % gas constant [g-m^2/s^2-mol-k]
M = 107.86;              % Ag molecular weight [g/mol]
mHe = 4;                  % [amu]
mAg = 107;                % [amu]
cdHe = 2*31*10^-12;      % collision diameter for He - He
collisions
cdHeAg = (31+144)*10^-12; % collision diameter for Ag - He
collisions
d = 1.5*10^-9;           % pore diameter
por = 0.2;                % porosity [0-1]
tor = 2;                  % tortuosity

```

```

% Concentration Values

```

```

C1 = (VP/(8.314*Temp))*(mAg/1000000);

```

```

% Mean Free Path

```

```

MFP = (K/(3.14*((P-VP)*cdHe^2*2^0.5 +
VP*cdHeAg^2*(1+mHe/mAg)^0.5)))*(Temp/P);

```

```

% Knudsen Number

```

```

KN = MFP/d;

```

```

% Calculate appropriate diffusion coefficient based on KN

```

```

if KN < 1
    D = (por/tor)*(MFP/3)*((8*R*Temp)/(3.14*M))^0.5;
    fprintf('Molecular Regime Knudsen Number < 1 ')
elseif 1 < KN & KN < 5
    D =
1/(1/((por/tor)*(MFP/3)*((8*R*Temp)/(3.14*M))^0.5)+1/((por/tor)*(d/3)*
(8*R*Temp)/(3.14*M))^0.5));
    fprintf('Transitional Regime Knudsen Number between 1 and 5 ')

```

```

else KN > 5
    D = (por/tor)*(d/3)*((8*R*Temp)/(3.14*M))^0.5;
    fprintf('Knudsen Regime Knudsen Number > 5 ')
end

% Make a matrix x for the distance values
% The graphite sample length is assumed to be 1cm
% For starters, assume 100 equal divisions between 0 and 1cm

X = [0:0.0001:0.05];

% Calculate and plot Concentration as a function of depth X

C = C1*erfc(X./(2*(D*Ti)^0.5));

figure
plot(X,C,'LineWidth',2)
title('Silver Concentration Vs. Depth')
xlabel('Sample Length [m]')
ylabel('Silver Concentration [g/cm^3]')
grid on
ax.Clipping = 'off';

```

BoyleData.m

```
% Ted Pollock 2015

clear
clc

% Thomas Boyle Data

X = [4.5 13.5 24.5 37.5 49.0 57.0 64.0 71.5 78.0 85.0 92.5 98.5 ...
     102.0 105.5 113.5];

C = [9.1282 4.5984 4.0467 3.3419 4.4680 6.0568 3.9378 3.3532 2.5909 ...
     0.9780 0.7942 1.2148 1.7501 0.7412 0.1591];

figure
plot(X,C,'LineWidth',2)
title('Thomas Boyle Data')
xlabel('Depth in GR001CC Graphite [micrometers]')
ylabel('Silver Concentration [micrograms/mm^3]')

% Expected Concentration Profile

xval = [0:0.000001:0.0004];

yval = erfc(xval./(2*(1.17888*10^-14*3.456*10^5)^0.5));

figure
plot(xval,yval,'LineWidth',2)
title('Expected Concentration Profile (Boyle)')
xlabel('Depth into Graphite [m]')
ylabel('Normalized Concentration')
```

Appendix II One Practical Solution for the Diffusion Equation

There are several different solutions that can be called “the diffusion equation”. Most of these solutions start with Fick’s first or second laws and a set of boundary conditions that characterize a particular physical situation. It is preferable to obtain a solution that is both simple to use and aligns closely with experimental data. A solution that has been commonly used in diffusion publications is presented below to offer some insight into the mathematics. Although equation 13 and most of the other diffusion equations are simple to use, the procedure for obtaining the solutions is not elementary.

The boundary value problem is outlined in equations 1 through 4.

$$\frac{\partial^2 C(x, t)}{\partial^2 x} + g(x, t) = \frac{\partial C(x, t)}{\partial t} \quad x_o < x < \infty \quad t > 0 \quad (1)$$

$$C(x, 0) = f(x) \quad t = 0 \quad x_o < x < \infty \quad (2)$$

$$\alpha_o C(x_o, t) - \beta_o \frac{\partial T(x_o, t)}{\partial x} = \Phi(t) \quad x = x_o \quad (3)$$

$$\frac{\partial C(\infty, t)}{\partial x} = 0 \quad x \rightarrow \infty \quad (4)$$

The eigenfunctions and eigenvalues for the above boundary value problem along with simplifications and relations are described in Unified Analysis and Solutions of Heat

and Mass Diffusion. The complexity of the problem is beyond the scope of this work and is not presented in full detail.

The boundary condition from equation 3 states that $C(0, t) = \Phi(t)$ if $\alpha_o = 1$ $\beta_o = 0$ $x_o = 0$, then the solution to the boundary value problem in equations 1-4 becomes equation 5.

$$\begin{aligned}
C(x, t) = & \frac{1}{\pi} \int_{x'=x_o}^{\infty} f(x') \int_{\mu=0}^{\infty} e^{-\mu^2 t} \left[\cos(\mu(x - x_o)) \right. \\
& + \frac{\beta_o^2 \mu^2 - \alpha_o^2}{\beta_o^2 \mu^2 + \alpha_o^2} \cos(\mu(x + x' - 2x_o)) \\
& + \left. \frac{2\alpha_o \beta_o}{\beta_o^2 \mu^2 + \alpha_o^2} \mu \sin(\mu(x + x' - 2x_o)) \right] d\mu dx' \\
& + \frac{1}{\pi} \int_{t'=0}^t \Phi(t') \int_{\mu=0}^{\infty} e^{-\mu^2(t-t')} \frac{2\mu}{\beta_o^2 + \alpha_o^2} \left[\beta_o \mu \cos(\mu(x \right. \\
& - x_o)) + \alpha_o \sin(\mu(x - x_o)) \left. \right] d\mu dt' \\
& + \frac{1}{\pi} \int_{t'=0}^t \int_{x'=x_o}^{\infty} g(x', t') \int_{\mu=0}^{\infty} e^{-\mu^2(t-t')} \left[\cos(\mu(x - x')) \right. \\
& + \frac{\beta_o^2 \mu^2 - \alpha_o^2}{\beta_o^2 \mu^2 + \alpha_o^2} \cos(\mu(x + x' - 2x_o)) \\
& + \left. \frac{2\alpha_o \beta_o}{\beta_o^2 \mu^2 + \alpha_o^2} \mu \sin(\mu(x + x' - 2x_o)) \right] d\mu dx' dt'
\end{aligned} \tag{5}$$

$$\begin{aligned}
C(x, t) = & \frac{1}{\pi} \int_{x'=0}^{\infty} f(x') \int_{\mu=0}^{\infty} e^{-\mu} [\cos(\mu(x - x')) - \cos(\mu(x + x'))] d\mu dx' \\
& + \frac{2}{\pi} \int_{t'=0}^t \Phi(t') \int_{\mu=0}^{\infty} e^{-\mu^2(t-t')} \mu \sin(\mu x) d\mu dt' \\
& + \frac{1}{\pi} \int_{t'=0}^t \int_{x'=0}^{\infty} g(x', t') \int_{\mu=0}^{\infty} e^{-\mu^2(t-t')} [\cos(\mu(x - x')) \\
& - \cos(\mu(x + x'))] d\mu dx' dt'
\end{aligned} \tag{6}$$

The integrations with respect to μ in equation 6 are done by using equations 7 and 8 to yield equation 9.

$$\int_0^{\infty} x e^{-ax^2} \sin bx dx = \frac{b\sqrt{\pi}}{4a^{\frac{3}{2}}} e^{-\frac{b^2}{4a}} \quad a > 0 \quad b > 0 \tag{7}$$

$$\int_0^{\infty} e^{-ax^2} \cos bx dx = \frac{1}{2} \sqrt{\frac{\pi}{a}} e^{-\frac{b^2}{4a}} \quad a > 0 \quad b > 0 \tag{8}$$

$$\begin{aligned}
C(x, t) = & \frac{1}{2\sqrt{\pi t}} \int_{x'=0}^{\infty} f(x') \left[e^{-\frac{(x-x')^2}{4t}} - e^{-\frac{(x+x')^2}{4t}} \right] dx' \\
& + \frac{x}{2\sqrt{\pi}} \int_{t'=0}^t \frac{\Phi(t')}{(t-t')^{\frac{3}{2}}} e^{-\frac{x^2}{4(t-t')}} dt' \\
& + \frac{1}{2\sqrt{\pi}} \int_{t'=0}^t \frac{1}{\sqrt{t-t'}} \int_{x'=0}^{\infty} g(x', t') \left[e^{-\frac{(x-x')^2}{4(t-t')}} \right. \\
& \left. - e^{-\frac{(x+x')^2}{4(t-t')}} \right] dx' dt'
\end{aligned} \tag{9}$$

$$C(x, t) = \frac{x}{2\sqrt{\pi}} \int_{t'=0}^t \frac{\Phi(t')}{(t-t')^{\frac{3}{2}}} e^{-\frac{x^2}{4(t-t')}} dt' \tag{10}$$

If

$$\eta = \frac{x}{2\sqrt{t-t'}}$$

and

$$dt = \frac{2}{\eta} (t-t') d\eta$$

Equation 10 becomes

$$C(x, t) = \frac{2}{\sqrt{\pi}} \int_{\frac{x}{2\sqrt{t}}}^{\infty} e^{-\eta^2} \Phi \left(t - \frac{x^2}{4\eta^2} \right) d\eta \tag{11}$$

For constant surface concentration at the boundary surface

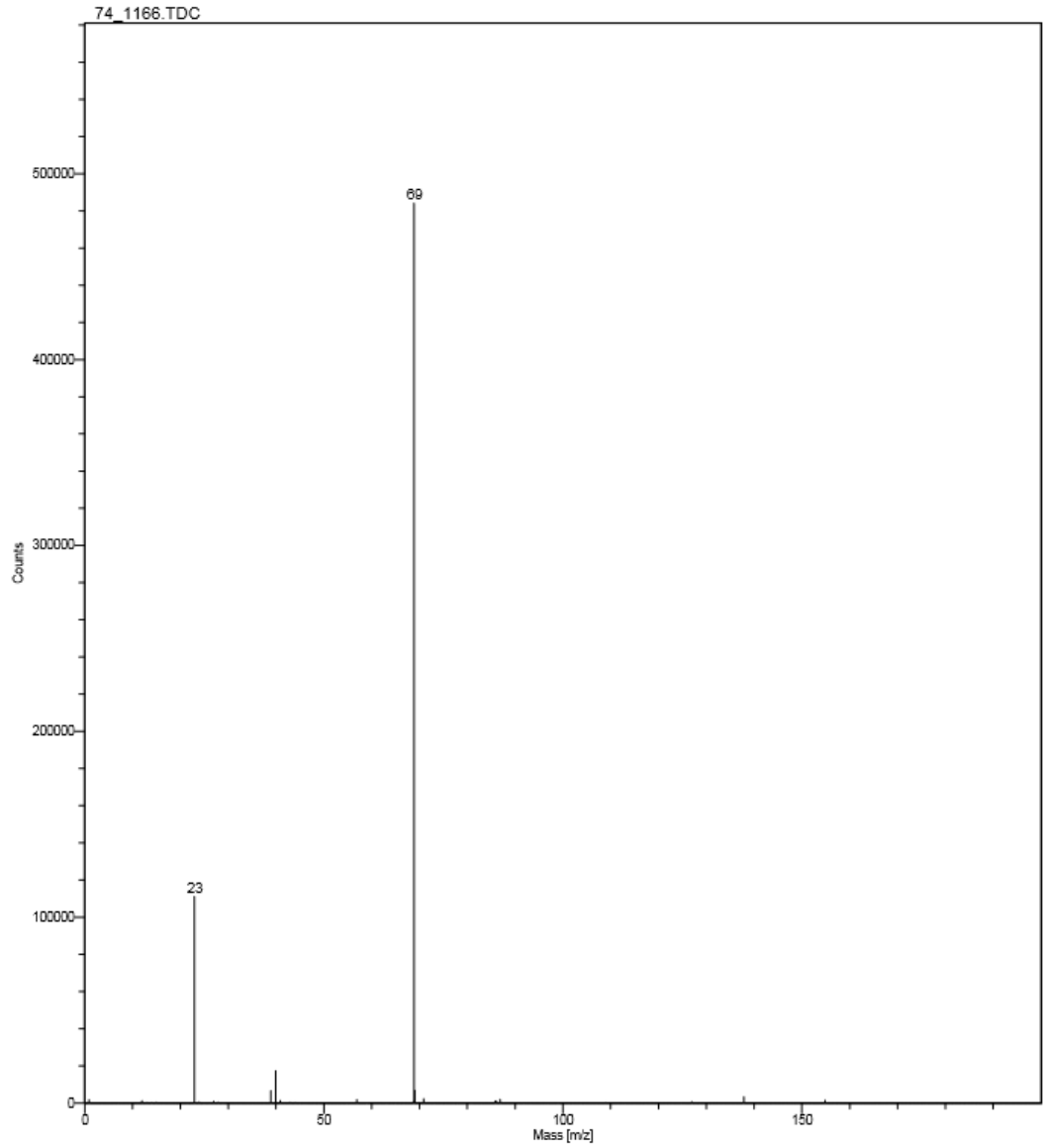
$$C(x, t) = \frac{2}{\sqrt{\pi}} \int_{\frac{x}{2\sqrt{t}}}^{\infty} e^{-\eta^2} d\eta \quad (12)$$

Recognizing that the integral is the error function, equation 12 can be rewritten as

$$C(x) = \operatorname{erfc}\left(\frac{x}{2\sqrt{t}}\right) \quad (13)$$

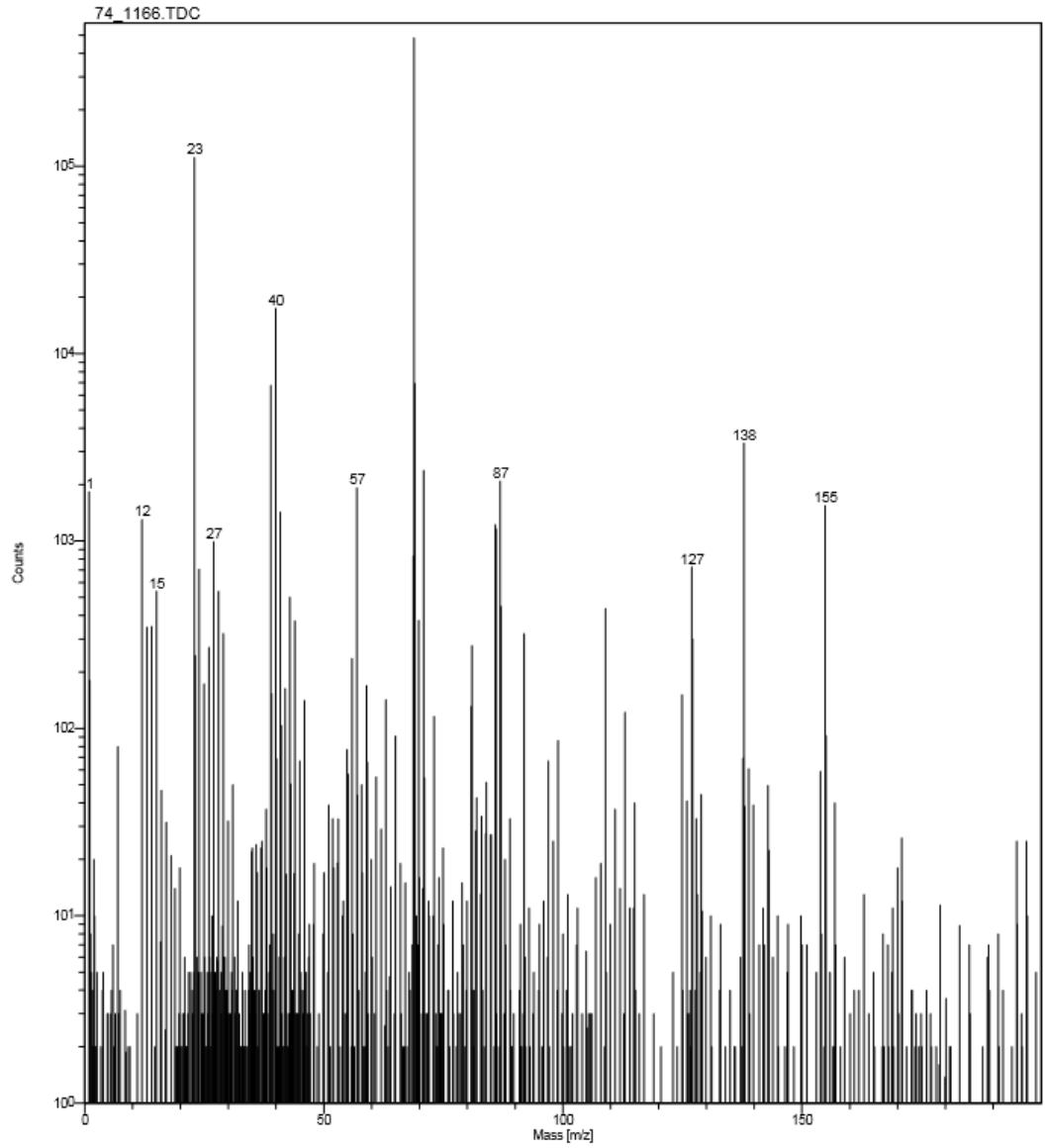
Appendix III TOF-SIMS Files Linear and Log Y-axis Scales

Physical Electronics, Inc.
6509 Flying Cloud Drive
Eden Prairie, MN 55344



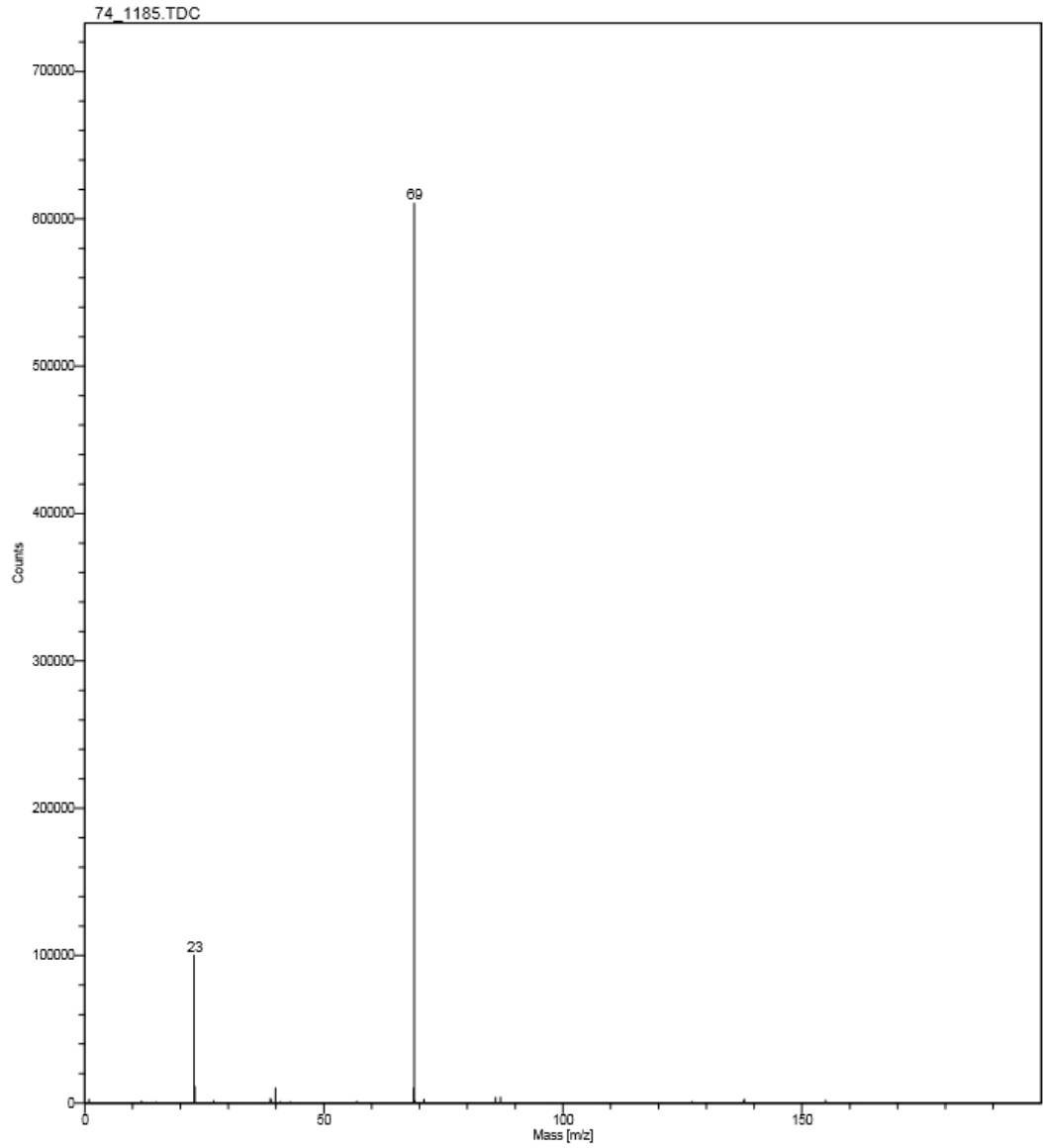
Figure__

Physical Electronics, Inc.
6509 Flying Cloud Drive
Eden Prairie, MN 55344



Figure__

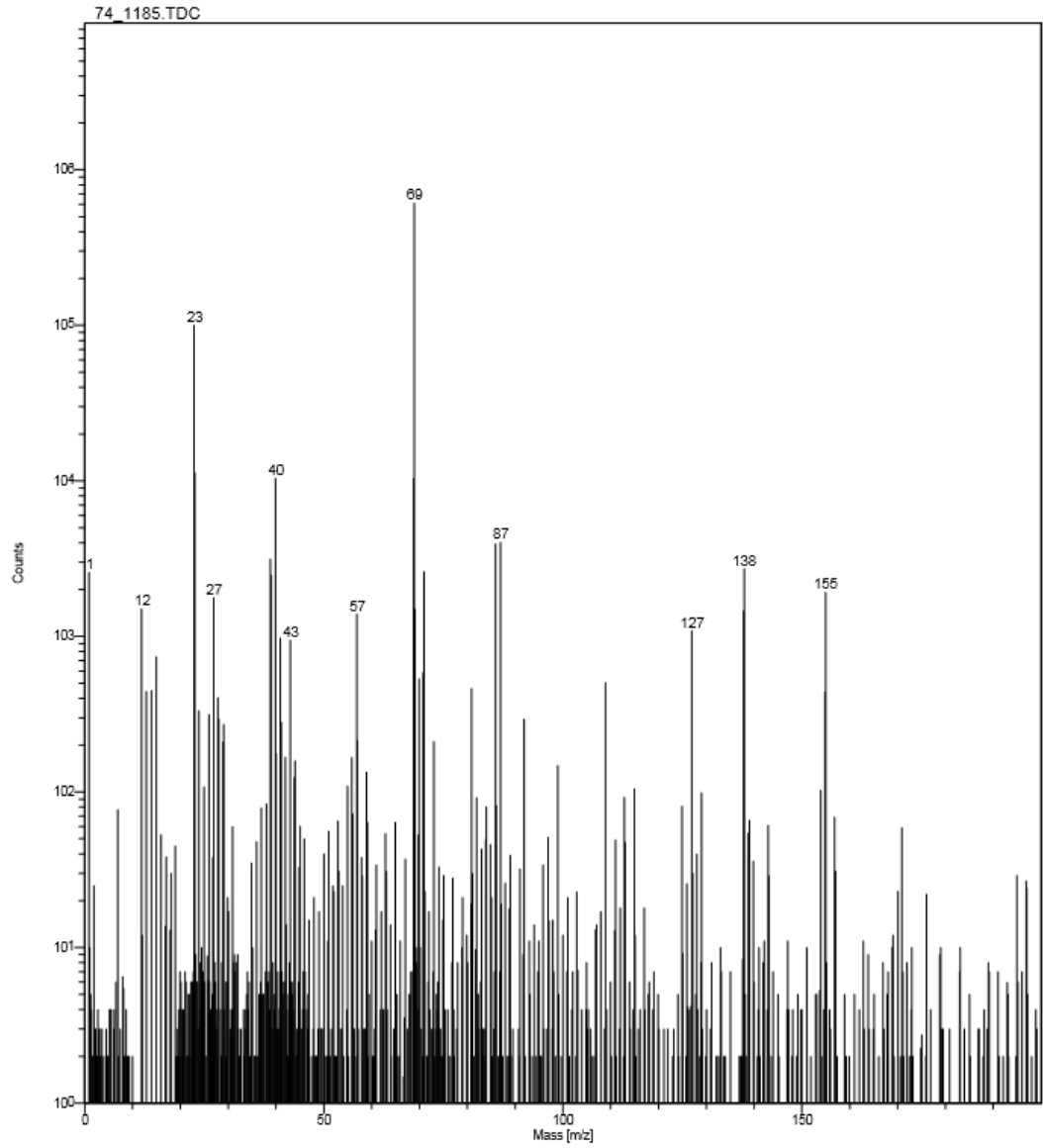
Physical Electronics, Inc.
6509 Flying Cloud Drive
Eden Prairie, MN 55344



74_1185.tdc 5.0 min on September 25, 2014 + ions 792585 cts (18.0 x 18.0 um) using LMIG
COMMENT: 11.85 position#74 not heated

Figure__

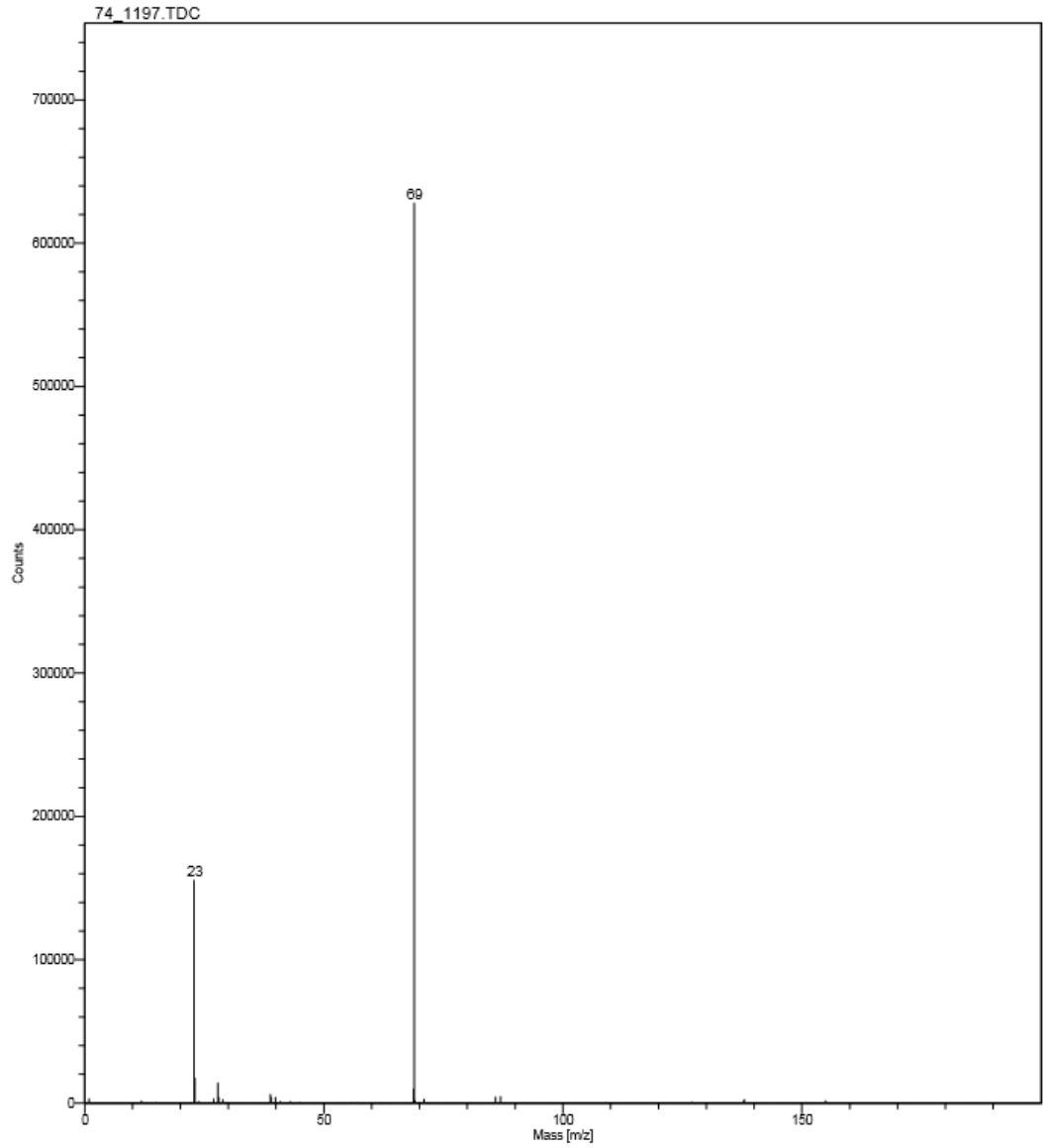
Physical Electronics, Inc.
6509 Flying Cloud Drive
Eden Prairie, MN 55344



74_1185.tdc 5.0 min on September 25, 2014 + ions 792585 cts (18.0 x 18.0 um) using LMIG
COMMENT: 11.85 position#74 not heated

Figure__

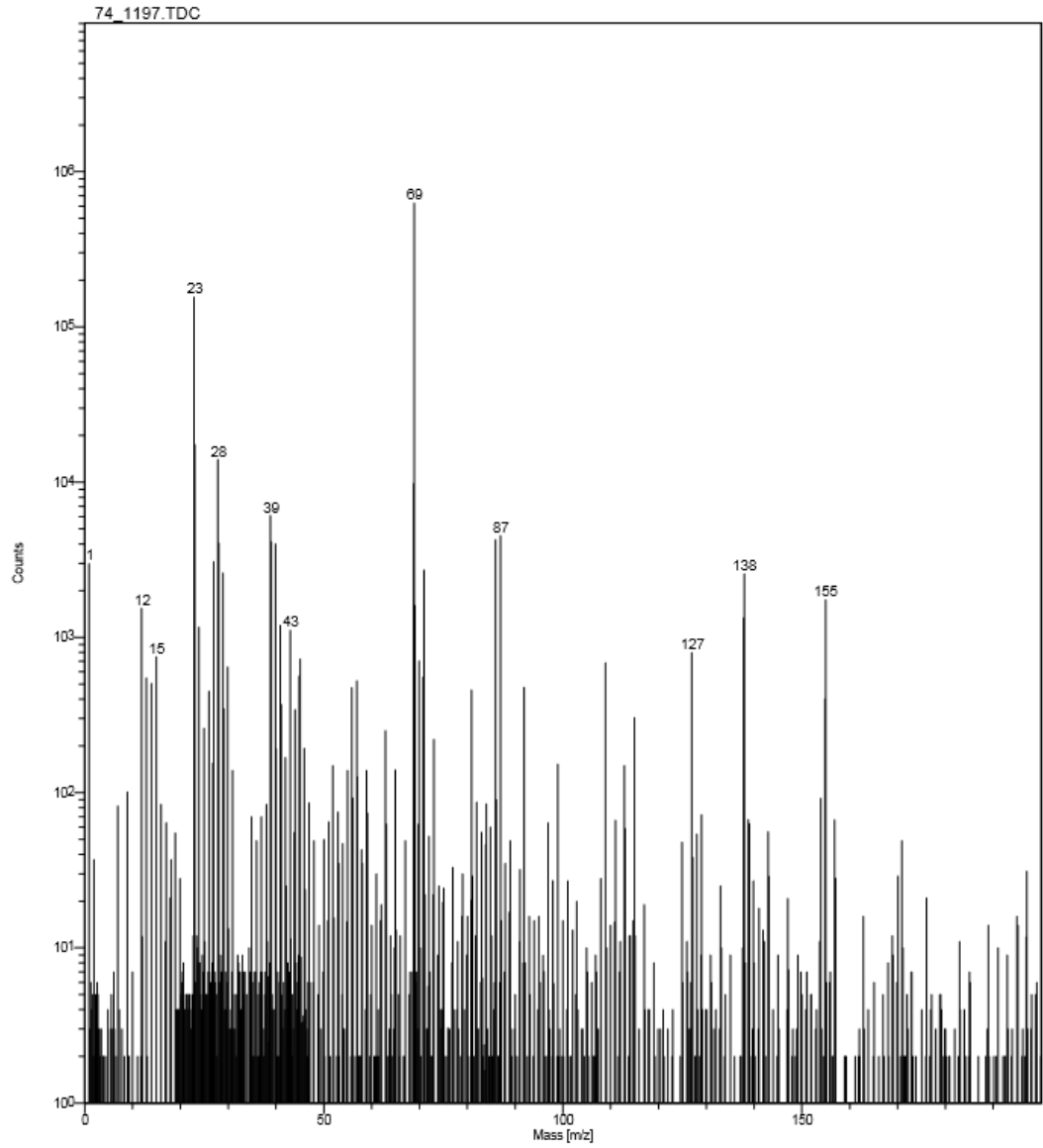
Physical Electronics, Inc.
6509 Flying Cloud Drive
Eden Prairie, MN 55344



74_1197.tdc 5.0 min on September 25, 2014 + ions 896081 cts (18.0 x 18.0 um) using LMIG
COMMENT: 11.97 starting position#74 not heated

Figure__

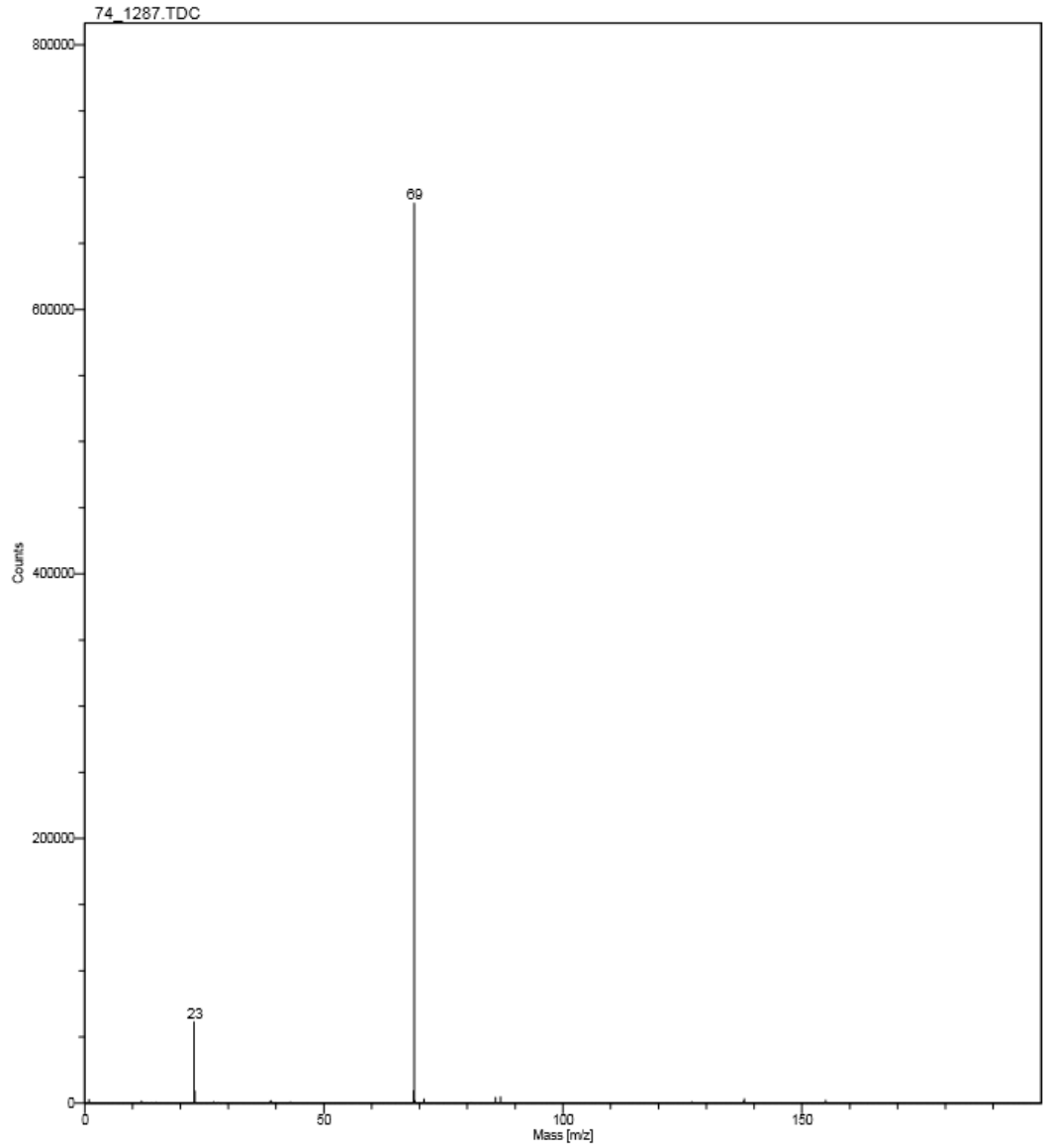
Physical Electronics, Inc.
6509 Flying Cloud Drive
Eden Prairie, MN 55344



74_1197.tdc 5.0 min on September 25, 2014 + ions 896081 cts (18.0 x 18.0 um) using LMIG
COMMENT: 11.97 starting position#74 not heated

Figure__

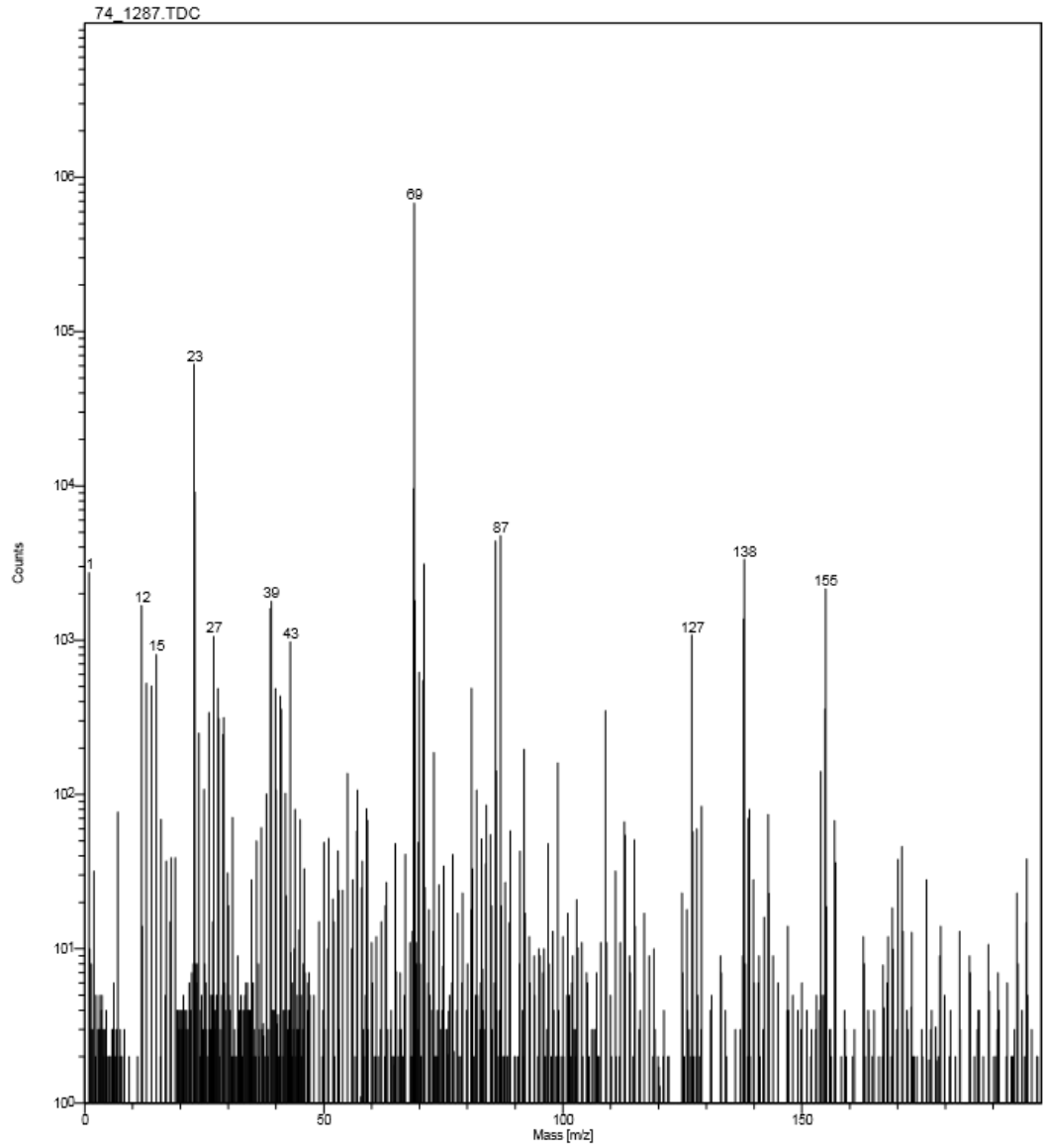
Physical Electronics, Inc.
6509 Flying Cloud Drive
Eden Prairie, MN 55344



74_1287.tdc 5.0 min on September 25, 2014 + ions 808001 cts (18.0 x 18.0 um) using LMIG
COMMENT: 12.87 starting position#74 not heated

Figure__

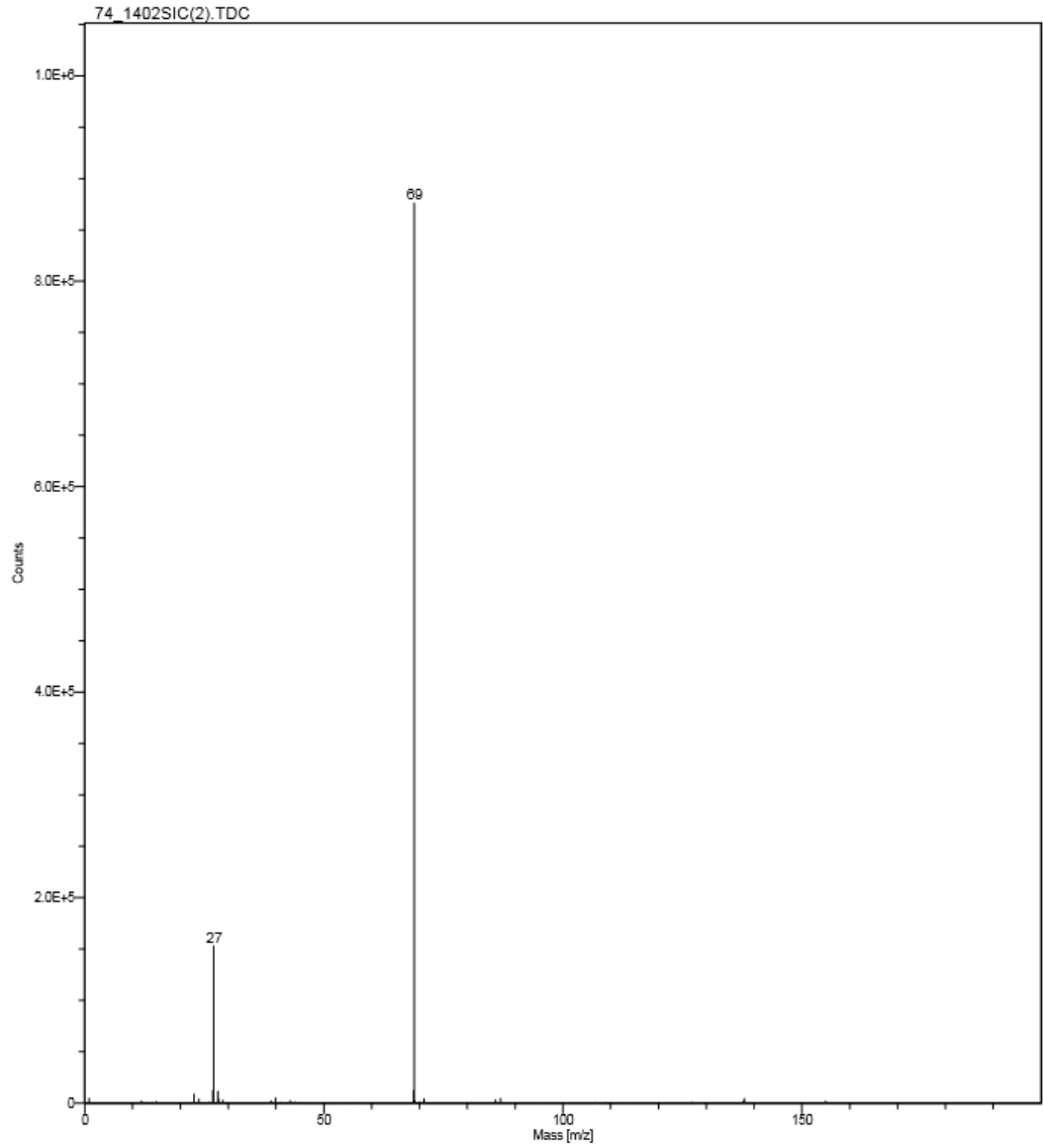
Physical Electronics, Inc.
6509 Flying Cloud Drive
Eden Prairie, MN 55344



74_1287.tdc 5.0 min on September 25, 2014 + ions 808001 cts (18.0 x 18.0 um) using LMIG
COMMENT: 12.87 starting position#74 not heated

Figure__

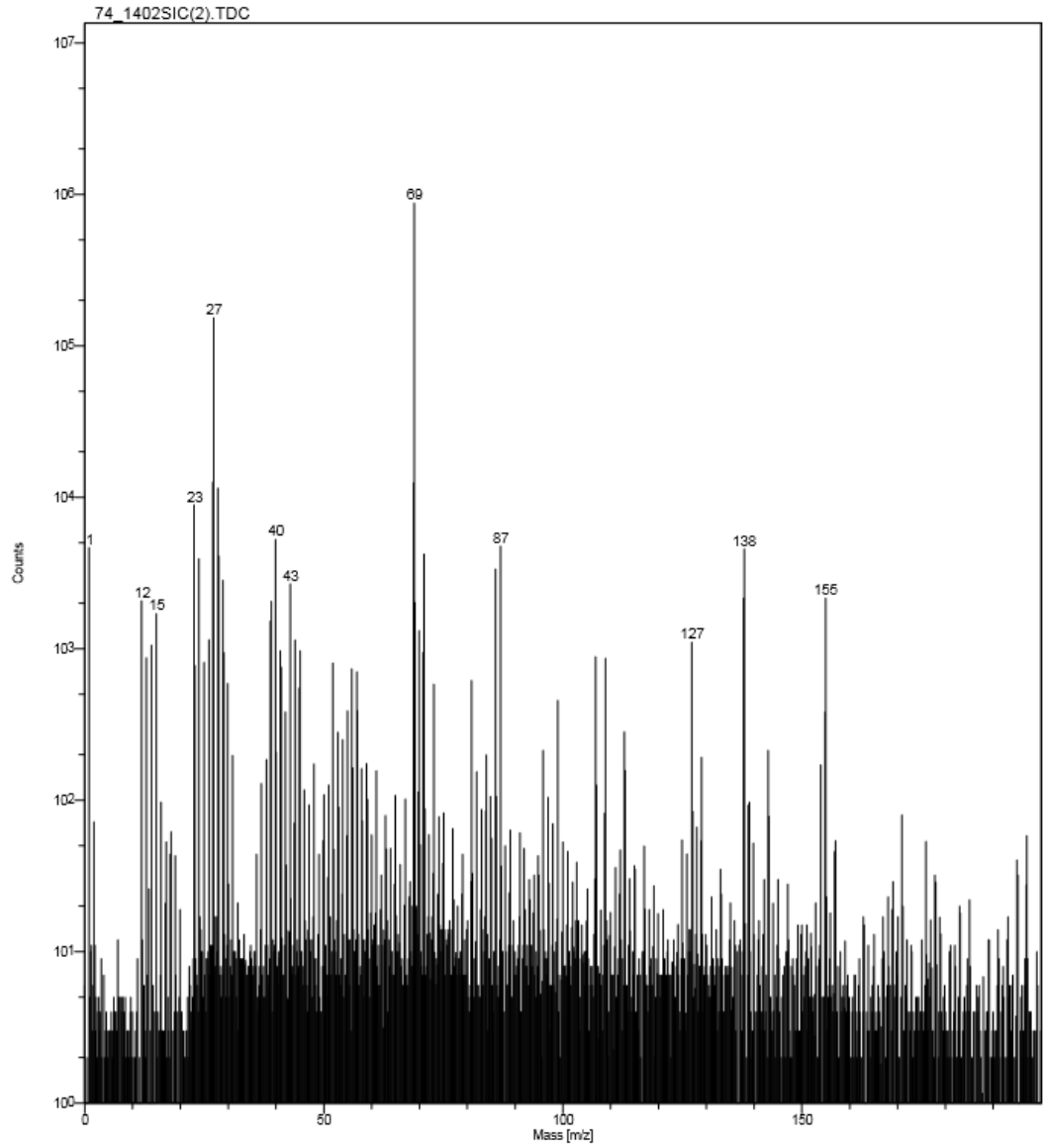
Physical Electronics, Inc.
6509 Flying Cloud Drive
Eden Prairie, MN 55344



74_1402SIC(2).tdc 5.3 min on September 25, 2014 + ions 1168540 cts (18.0 x 18.0 um) using LMIG
COMMENT: 74 14.02 second rastering at same spot

Figure__

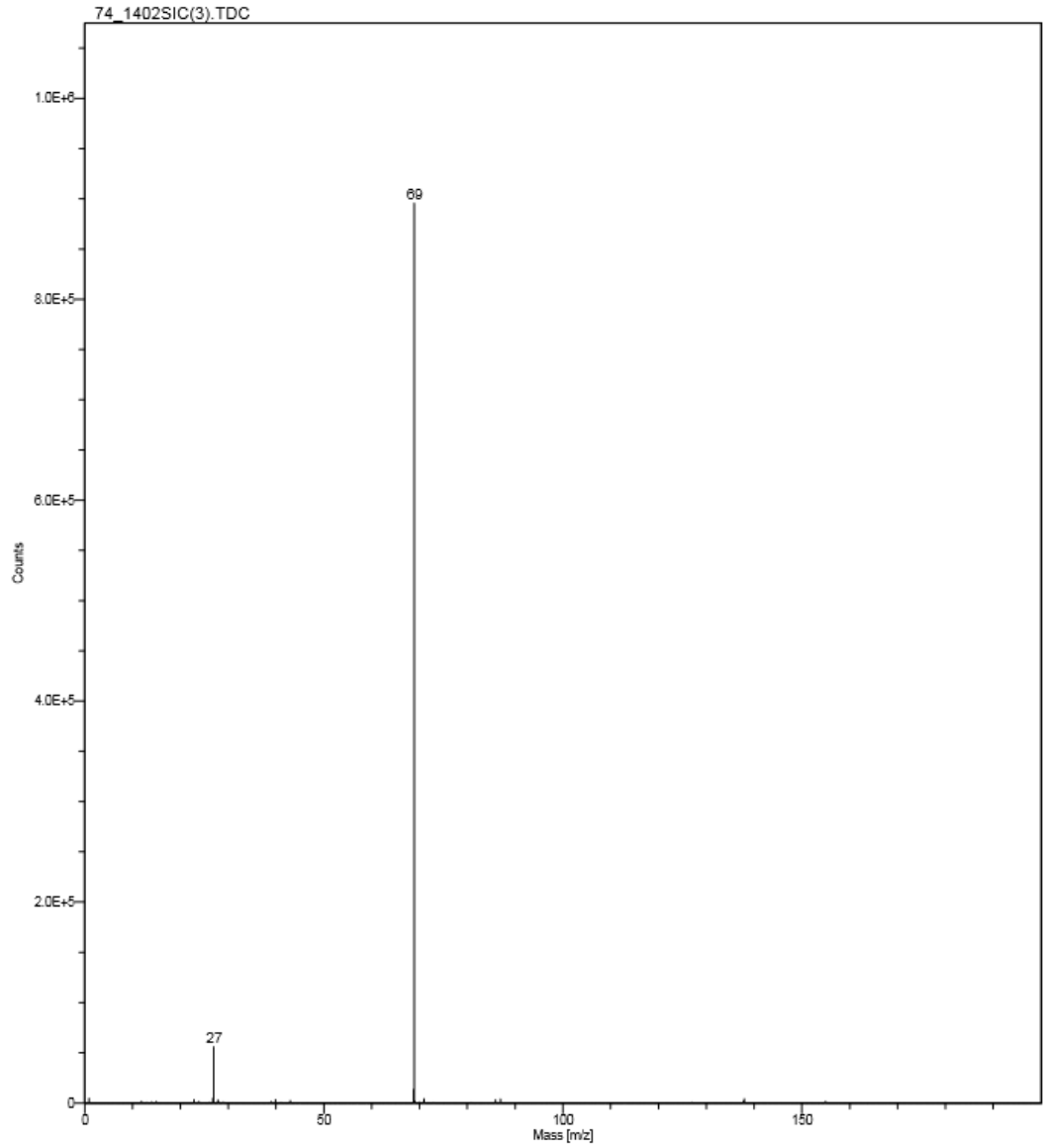
Physical Electronics, Inc.
6509 Flying Cloud Drive
Eden Prairie, MN 55344



74_1402SIC(2).tdc 5.3 min on September 25, 2014 + ions 1168540 cts (18.0 x 18.0 um) using LMIG
COMMENT: 74 14.02 second rastering at same spot

Figure__

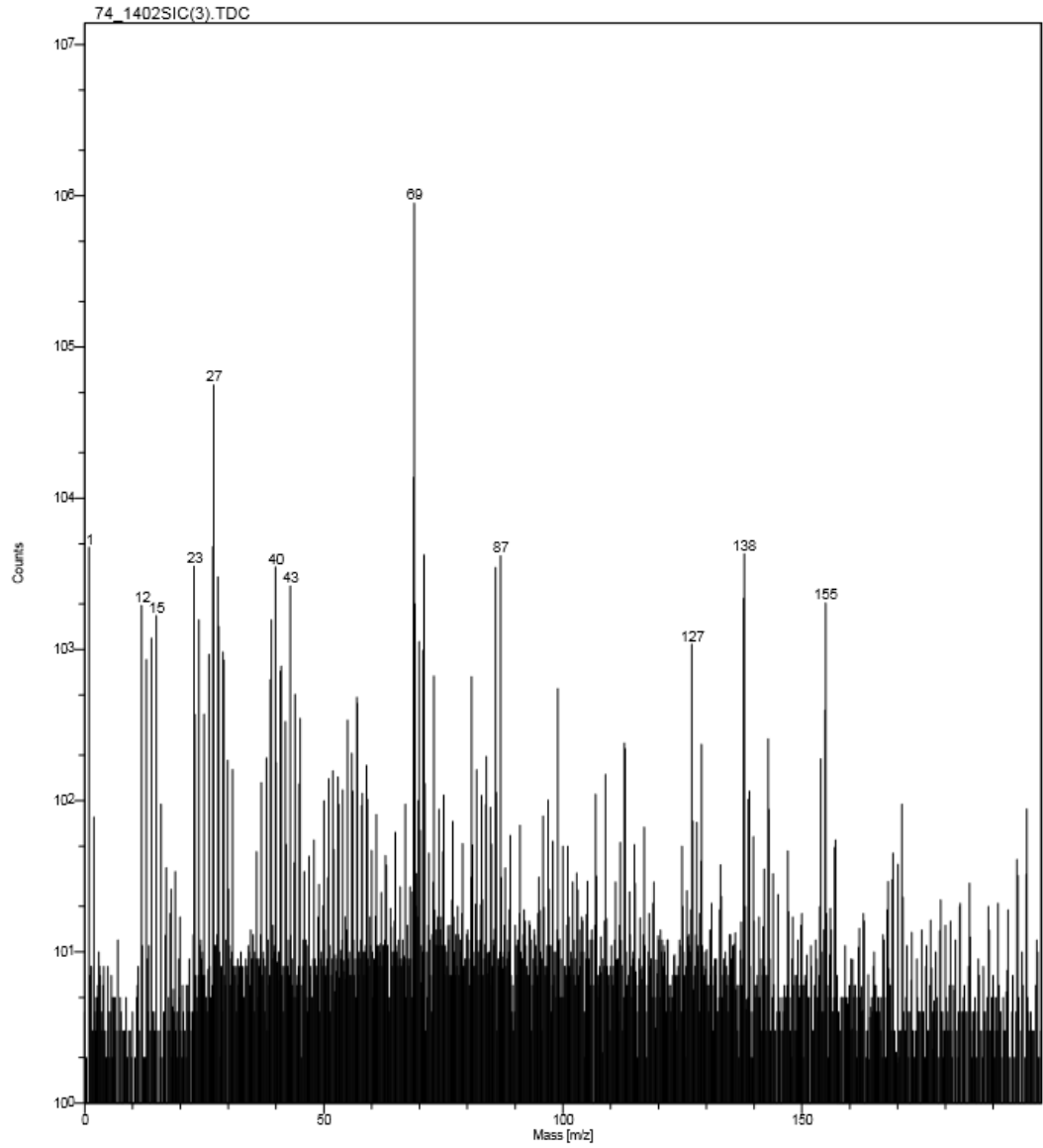
Physical Electronics, Inc.
6509 Flying Cloud Drive
Eden Prairie, MN 55344



74_1402SIC(3).tdc 5.3 min on September 25, 2014 + ions 1052748 cts (18.0 x 18.0 um) using LMIG
COMMENT: 74 14.02 third rastering at same spot

Figure__

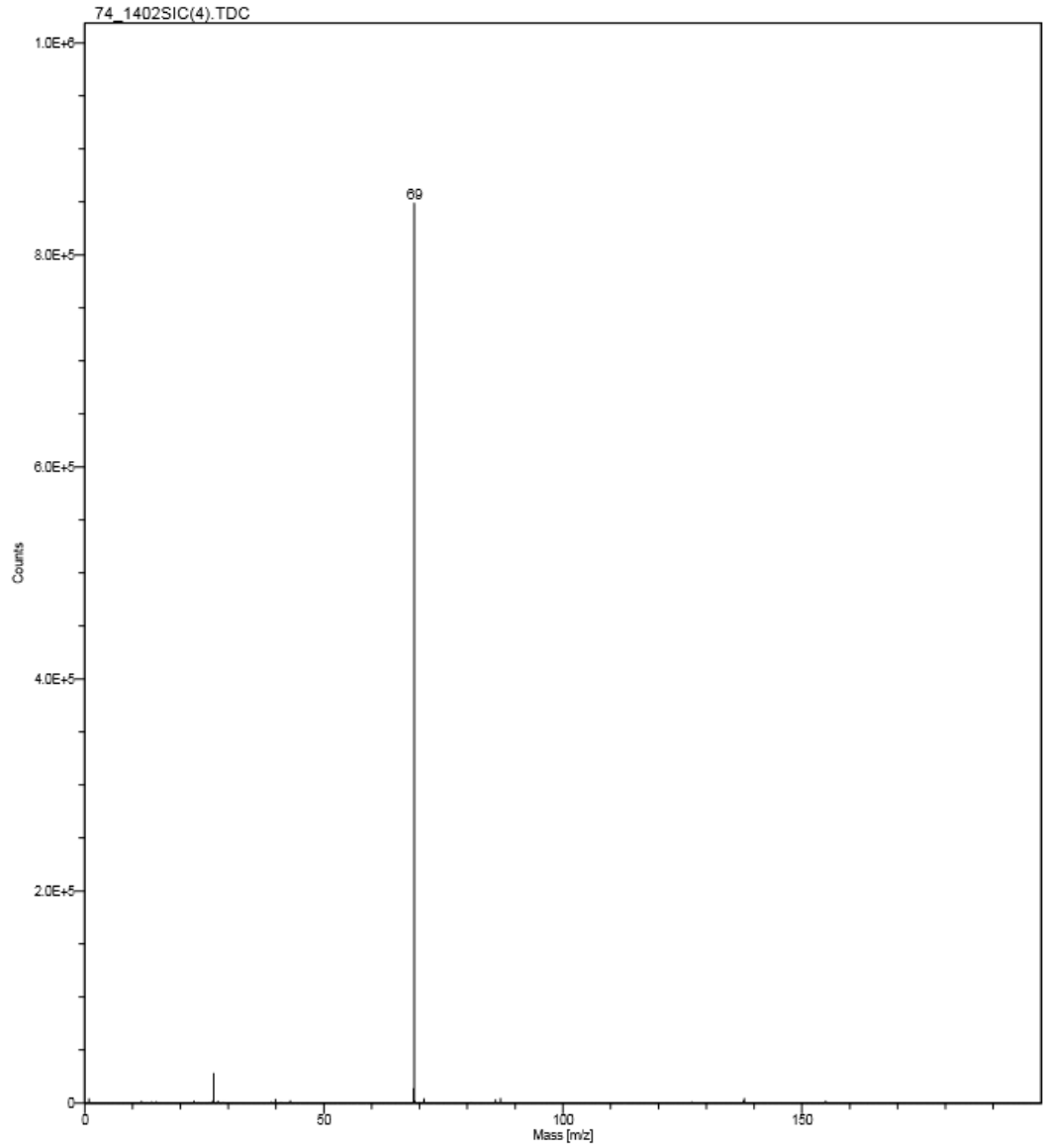
Physical Electronics, Inc.
6509 Flying Cloud Drive
Eden Prairie, MN 55344



74_1402SIC(3).tdc 5.3 min on September 25, 2014 + ions 1052748 cts (18.0 x 18.0 um) using LMIG
COMMENT: 74 14.02 third rastering at same spot

Figure__

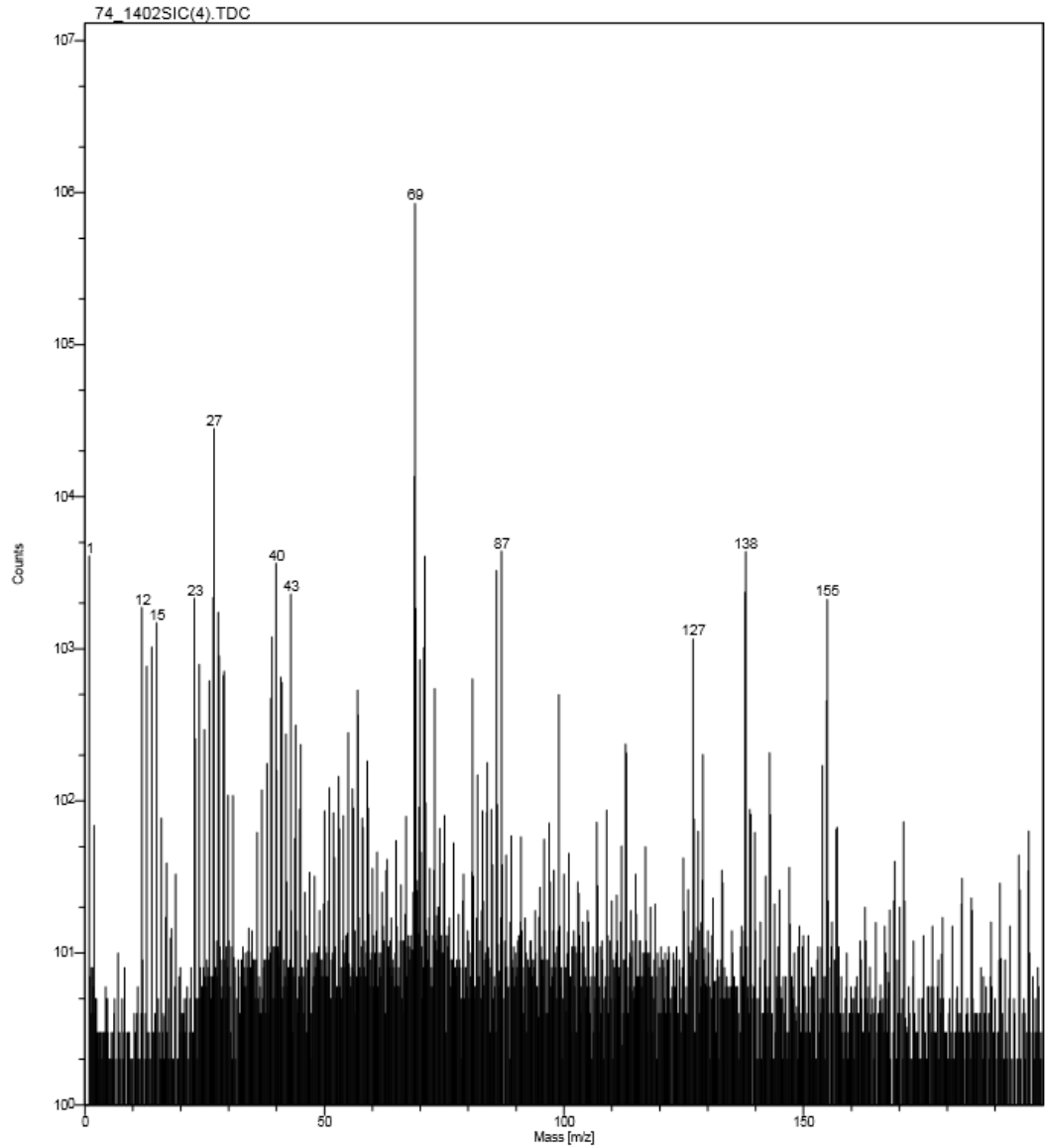
Physical Electronics, Inc.
6509 Flying Cloud Drive
Eden Prairie, MN 55344



74_1402SIC(4).tdc 5.0 min on September 25, 2014 + ions 964682 cts (18.0 x 18.0 um) using LMIG
COMMENT: 74 14.02 fourth rastering at same spot

Figure__

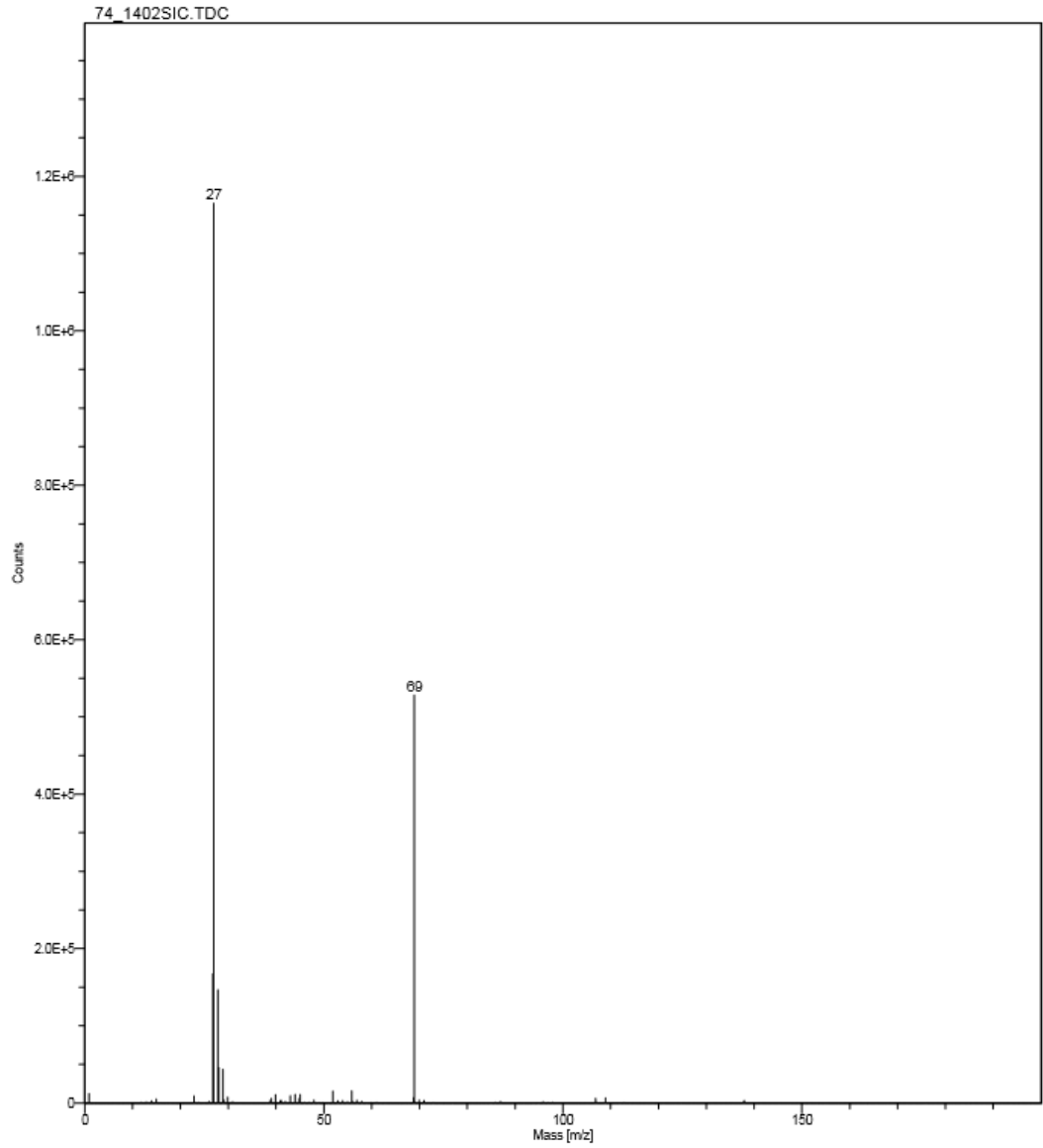
Physical Electronics, Inc.
6509 Flying Cloud Drive
Eden Prairie, MN 55344



74_1402SIC(4).tdc 5.0 min on September 25, 2014 + ions 964682 cts (18.0 x 18.0 um) using LMIG
COMMENT: 74 14.02 fourth rastering at same spot

Figure__

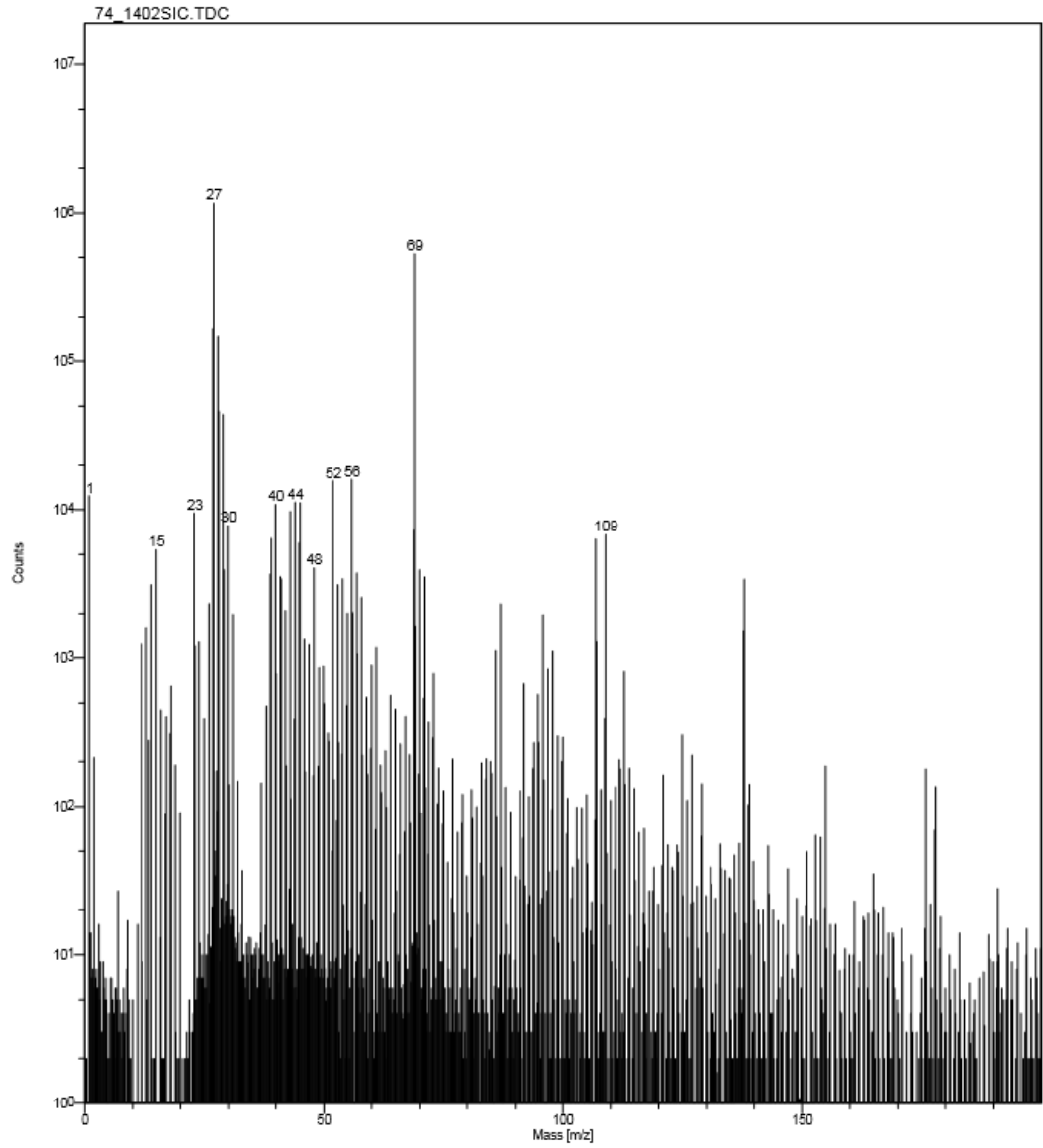
Physical Electronics, Inc.
6509 Flying Cloud Drive
Eden Prairie, MN 55344



74_1402SIC.tdc: 5.0 min on September 25, 2014 + ions 2355812 cts (18.0 x 18.0 um) using LMIG
COMMENT: 14.02#74 not heated outside SiC

Figure__

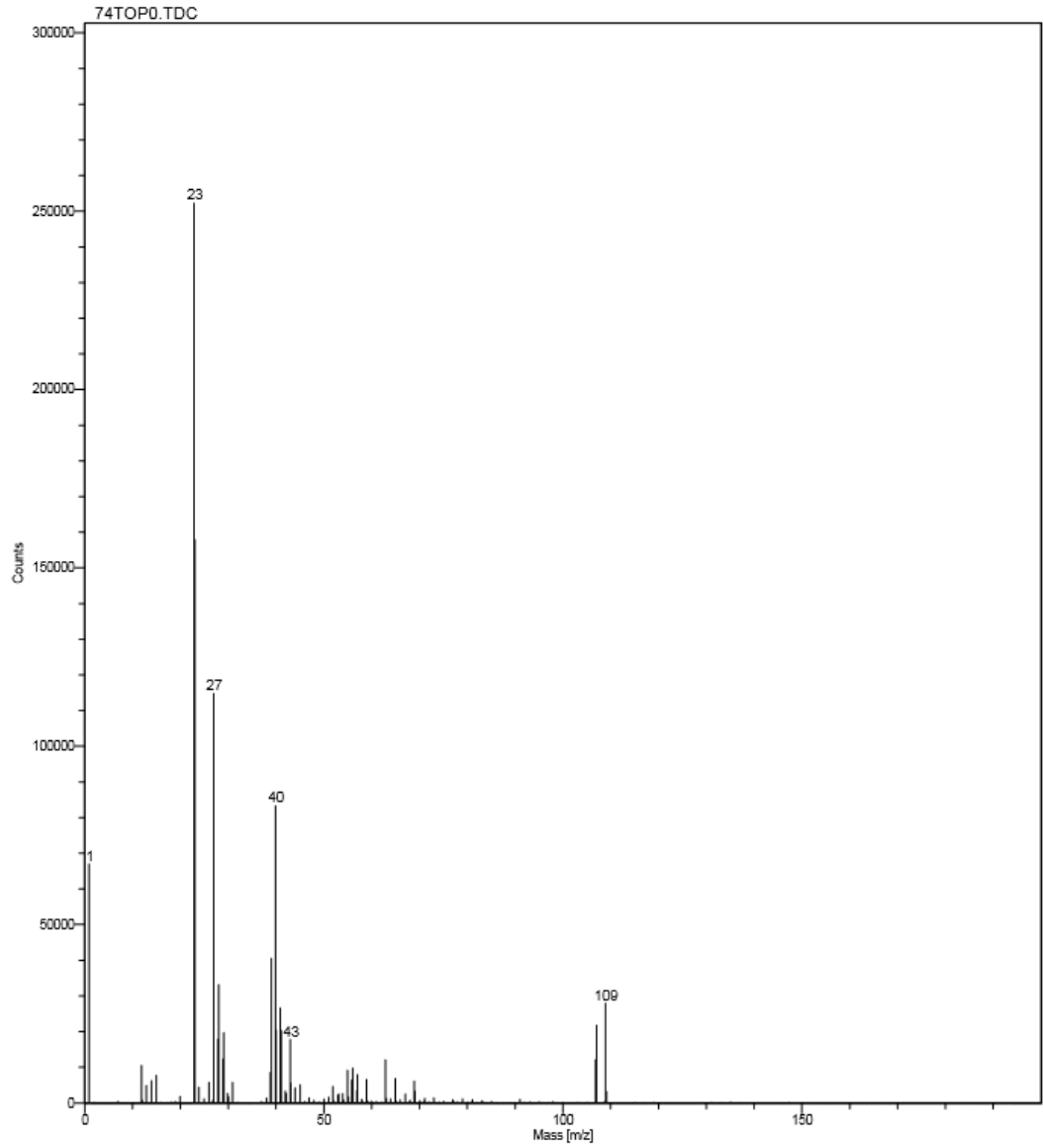
Physical Electronics, Inc.
6509 Flying Cloud Drive
Eden Prairie, MN 55344



74_1402SIC.tdc: 5.0 min on September 25, 2014 + ions 2355812 cts (18.0 x 18.0 um) using LMIG
COMMENT: 14.02#74 not heated outside SIC

Figure__

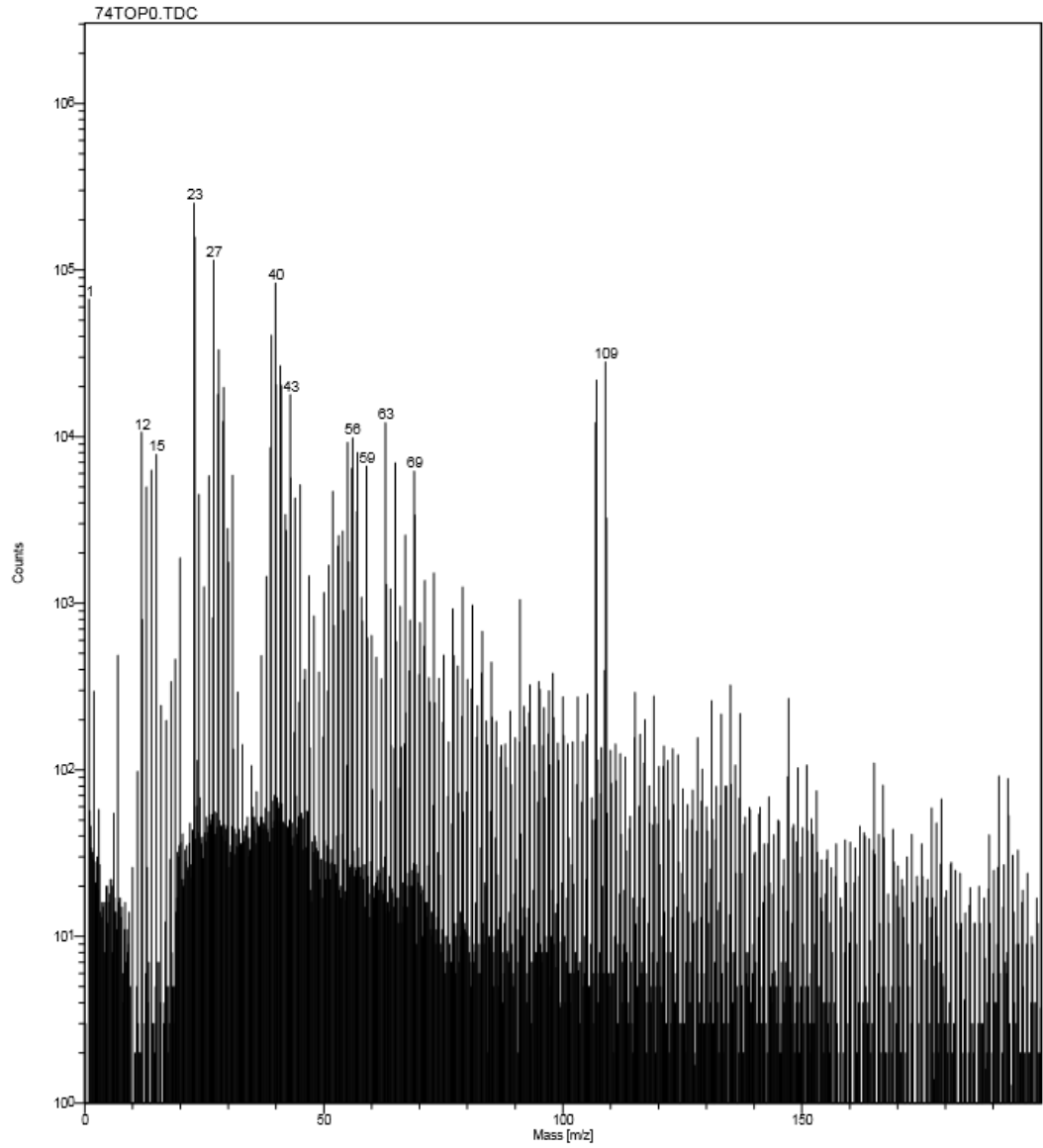
Physical Electronics, Inc.
6509 Flying Cloud Drive
Eden Prairie, MN 55344



74top0.tdc 4.0 min on September 26, 2014 + ions 1198146 cts (18.0 x 18.0 um) using LMIG
COMMENT: 74 sputter through topno sputtering yet

Figure__

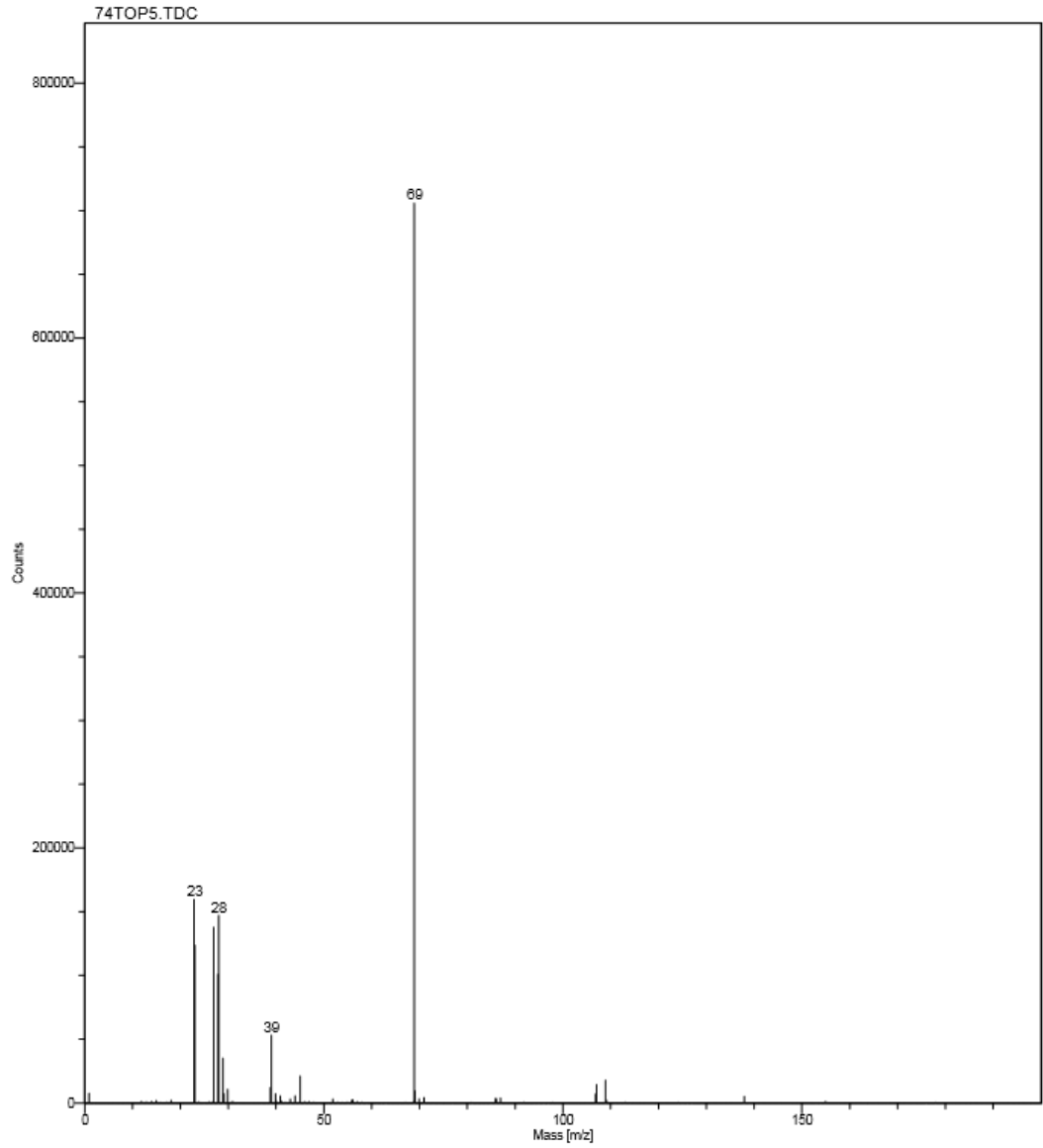
Physical Electronics, Inc.
6509 Flying Cloud Drive
Eden Prairie, MN 55344



74top0.tdc 4.0 min on September 26, 2014 + ions 1198146 cts (18.0 x 18.0 um) using LMIG
COMMENT: 74 sputter through topno sputtering yet

Figure__

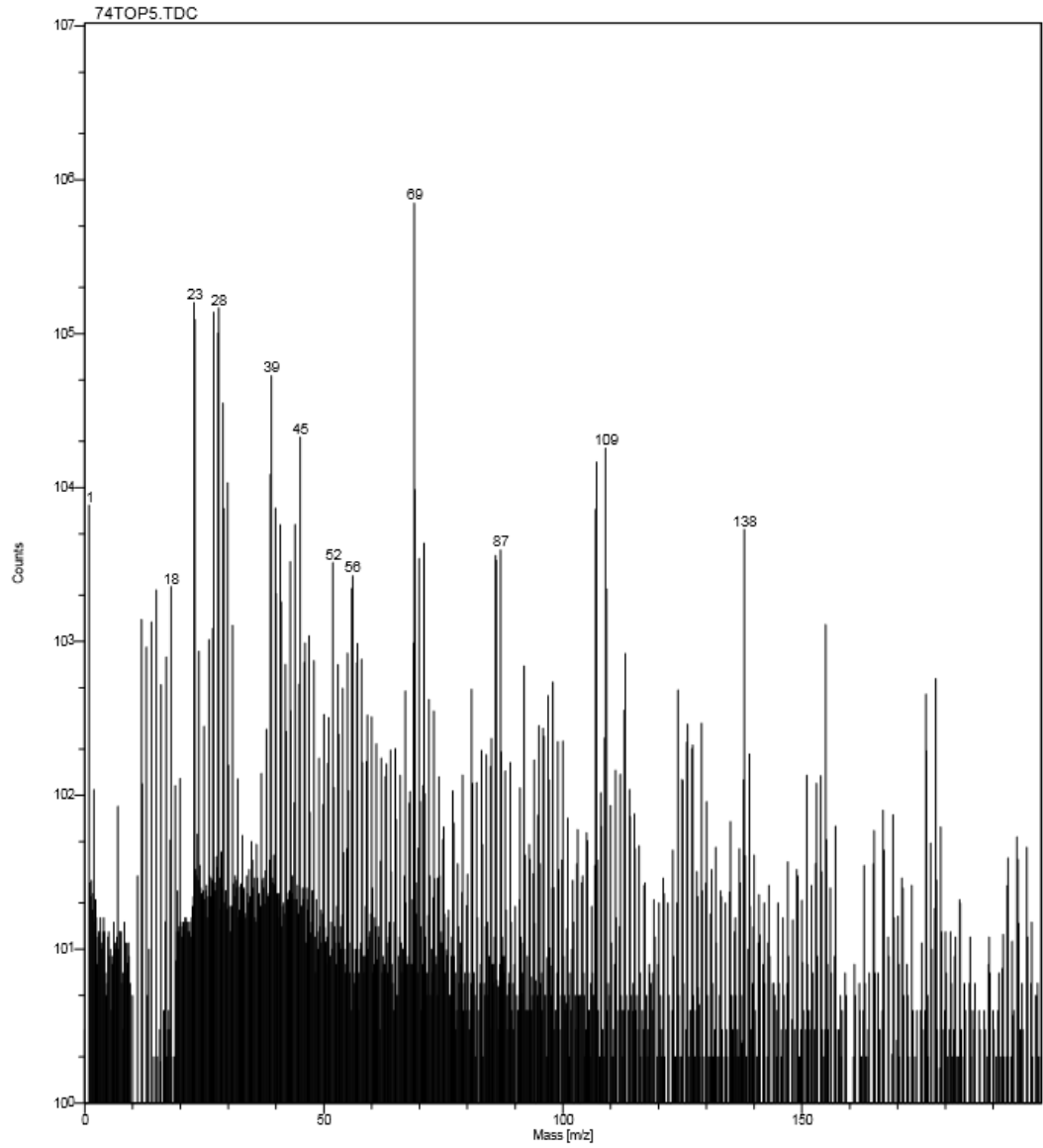
Physical Electronics, Inc.
6509 Flying Cloud Drive
Eden Prairie, MN 55344



74top5.tdc 4.0 min on September 26, 2014 + ions 1693193 cts (18.0 x 18.0 um) using LMIG
COMMENT: 74 sputter through top5 minutes

Figure__

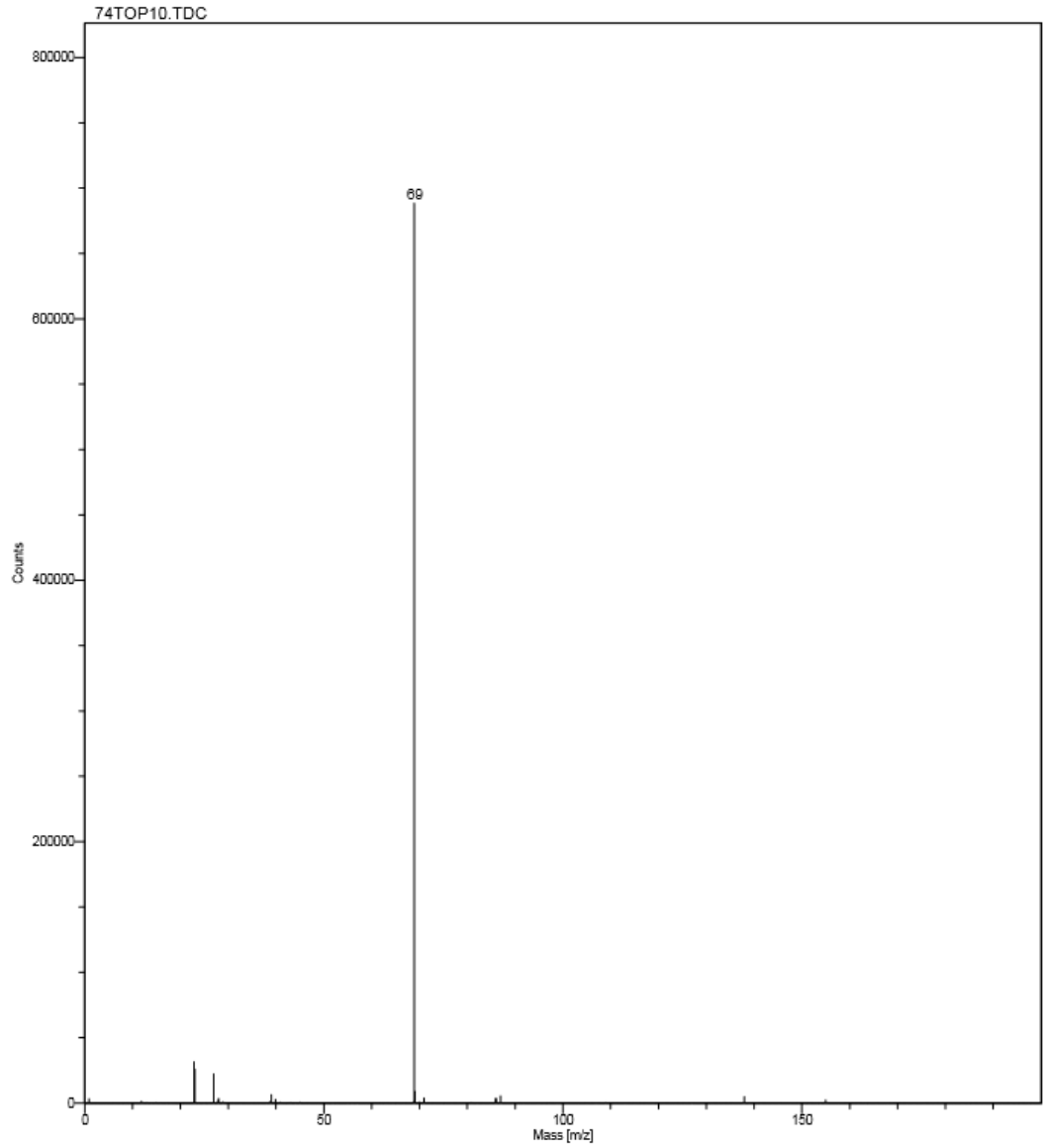
Physical Electronics, Inc.
6509 Flying Cloud Drive
Eden Prairie, MN 55344



74top5.tdc 4.0 min on September 26, 2014 + ions 1693193 cts (18.0 x 18.0 um) using LMIG
COMMENT: 74 sputter through top5 minutes

Figure__

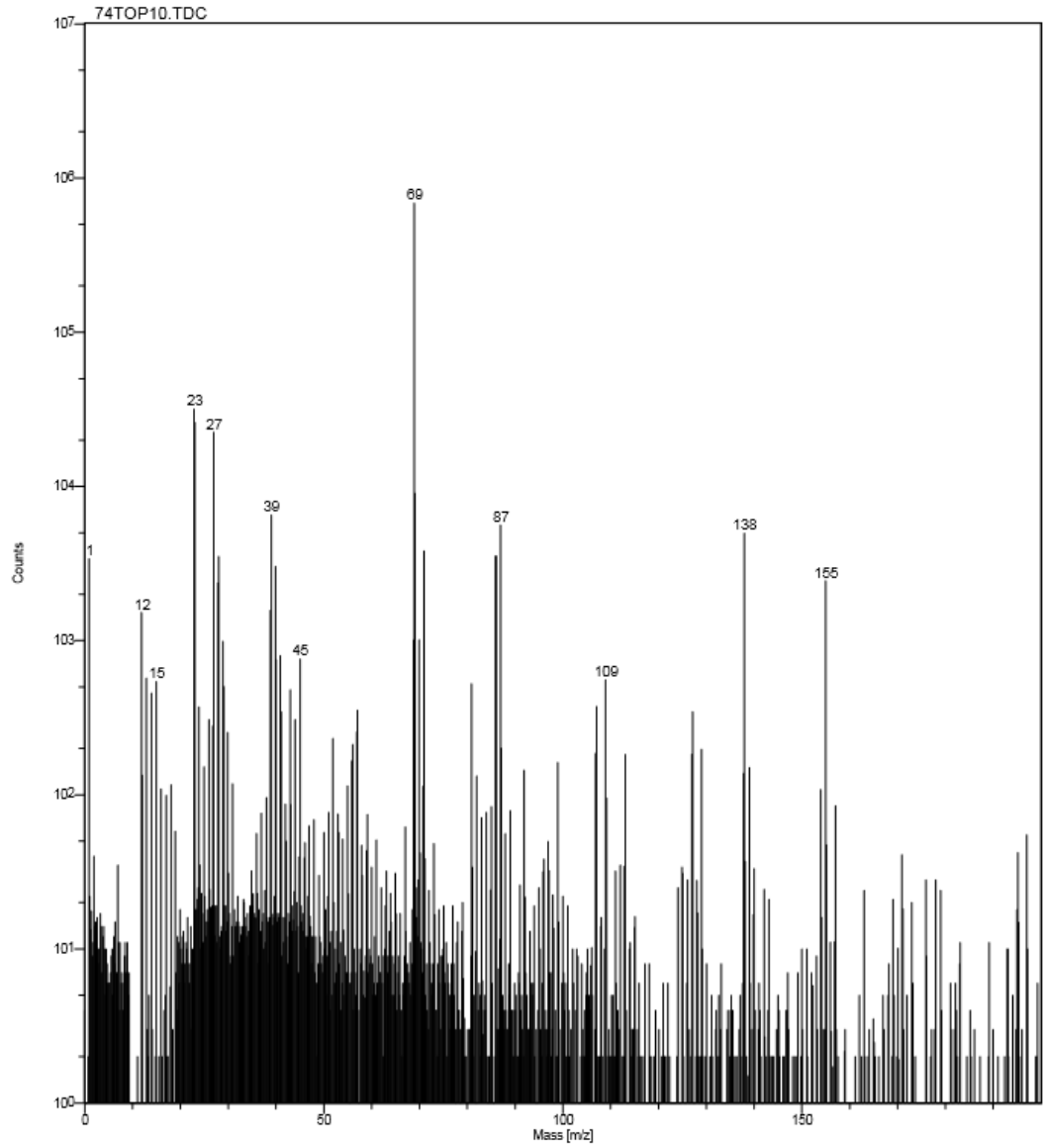
Physical Electronics, Inc.
6509 Flying Cloud Drive
Eden Prairie, MN 55344



74top10.tdc 4.0 min on September 26, 2014 + ions 848959 cts (18.0 x 18.0 um) using LMIG
COMMENT: 74 sputter through top10 minutes

Figure__

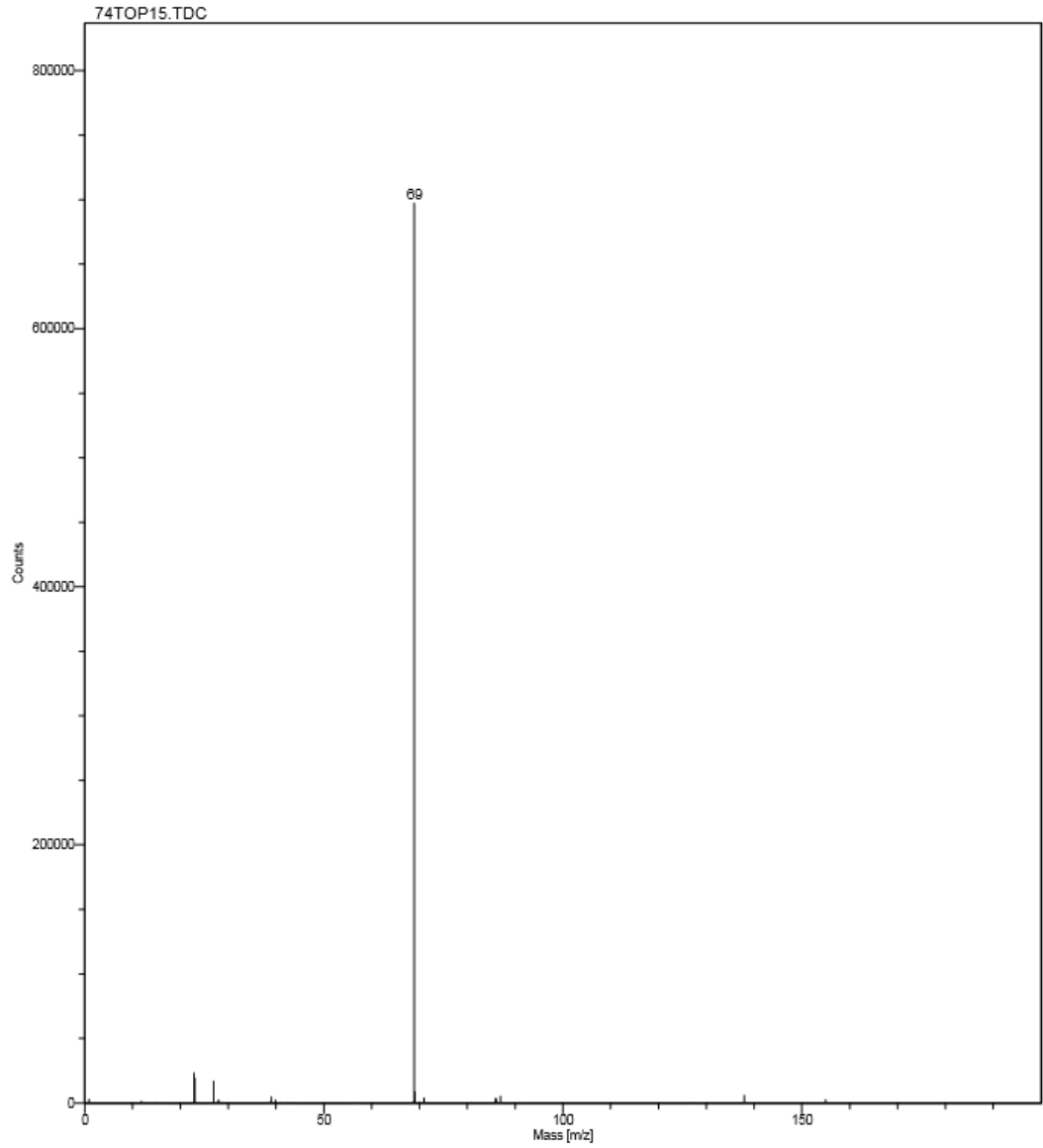
Physical Electronics, Inc.
6509 Flying Cloud Drive
Eden Prairie, MN 55344



74top10.tdc: 4.0 min on September 26, 2014 + ions 848959 cts (18.0 x 18.0 um) using LMIG
COMMENT: 74 sputter through top10 minutes

Figure__

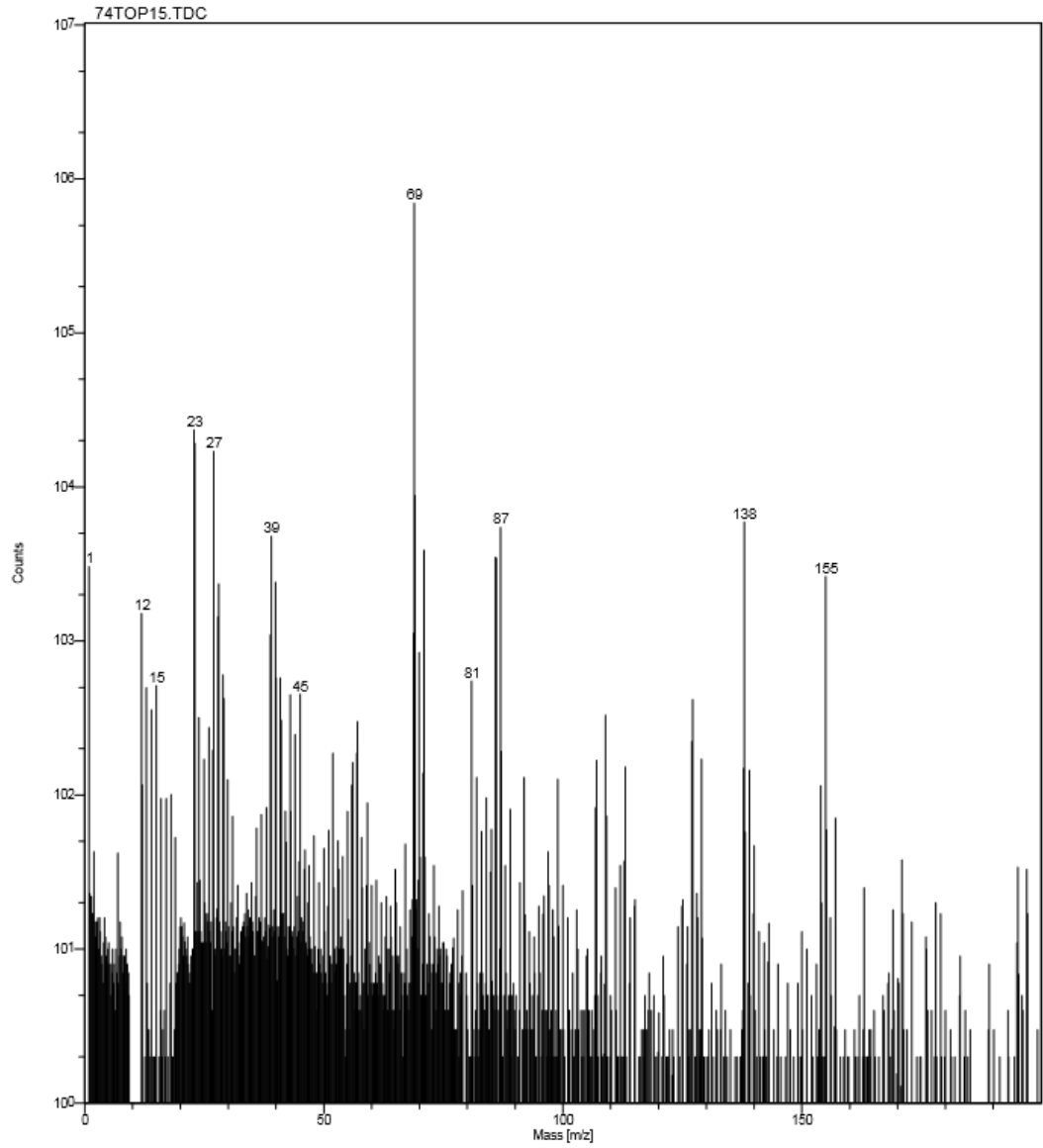
Physical Electronics, Inc.
6509 Flying Cloud Drive
Eden Prairie, MN 55344



74top15.tdc 4.0 min on September 26, 2014 + ions 829102 cts (18.0 x 18.0 um) using LMIG
COMMENT: 74 sputter through top15 minutes

Figure__

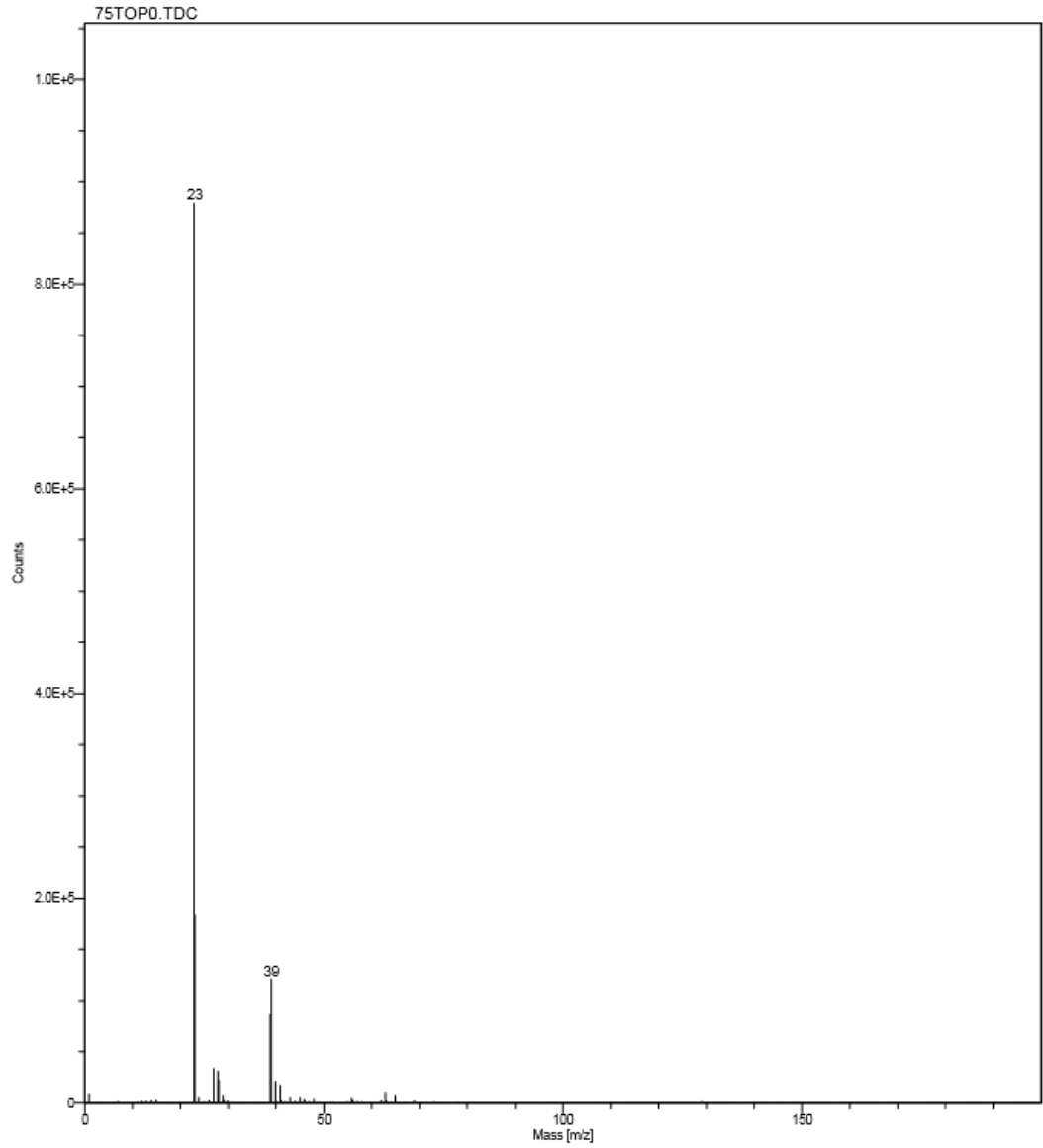
Physical Electronics, Inc.
6509 Flying Cloud Drive
Eden Prairie, MN 55344



74top15.tdc: 4.0 min on September 26, 2014 + ions 829102 cts (18.0 x 18.0 um) using LMIG
COMMENT: 74 sputter through top15 minutes

Figure__

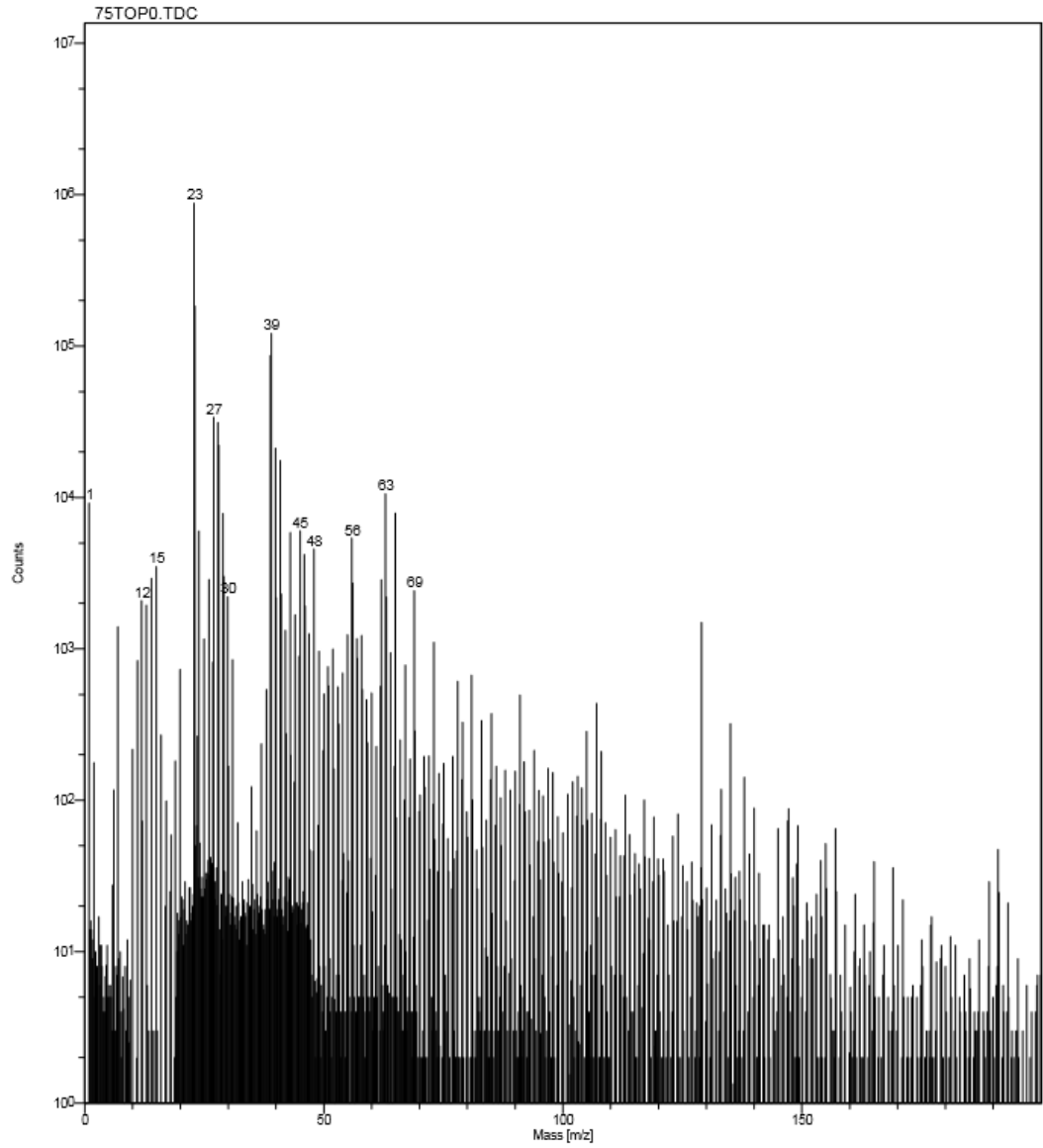
Physical Electronics, Inc.
6509 Flying Cloud Drive
Eden Prairie, MN 55344



75top0.tdc 4.0 min on September 26, 2014 + ions 1552845 cts (18.0 x 18.0 um) using LMIG
COMMENT: 75 sputter through top (700)0 minutes

Figure__

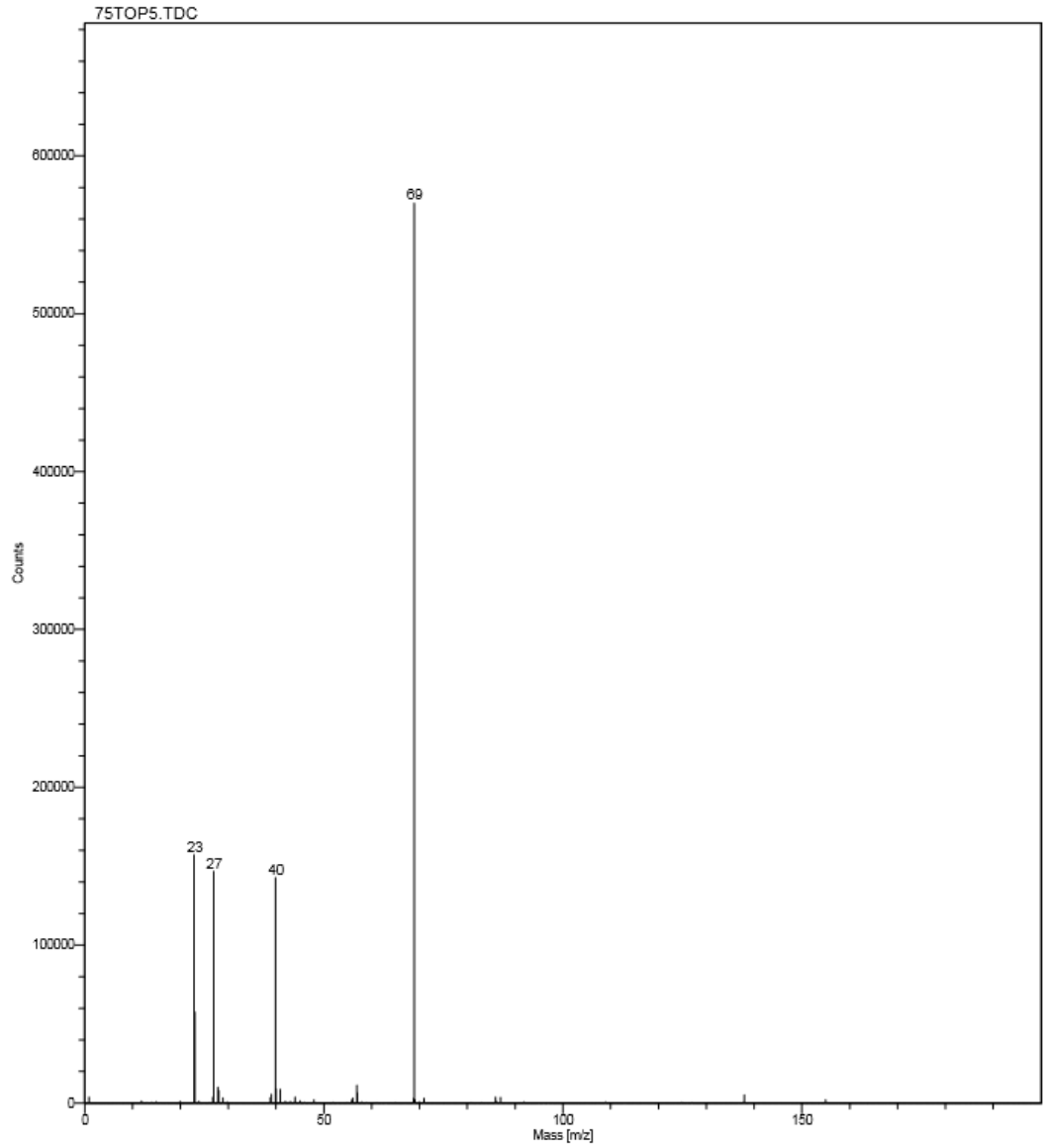
Physical Electronics, Inc.
6509 Flying Cloud Drive
Eden Prairie, MN 55344



75top0.tdc 4.0 min on September 26, 2014 + ions 1552845 cts (18.0 x 18.0 um) using LMIG
COMMENT: 75 sputter through top (700)0 minutes

Figure__

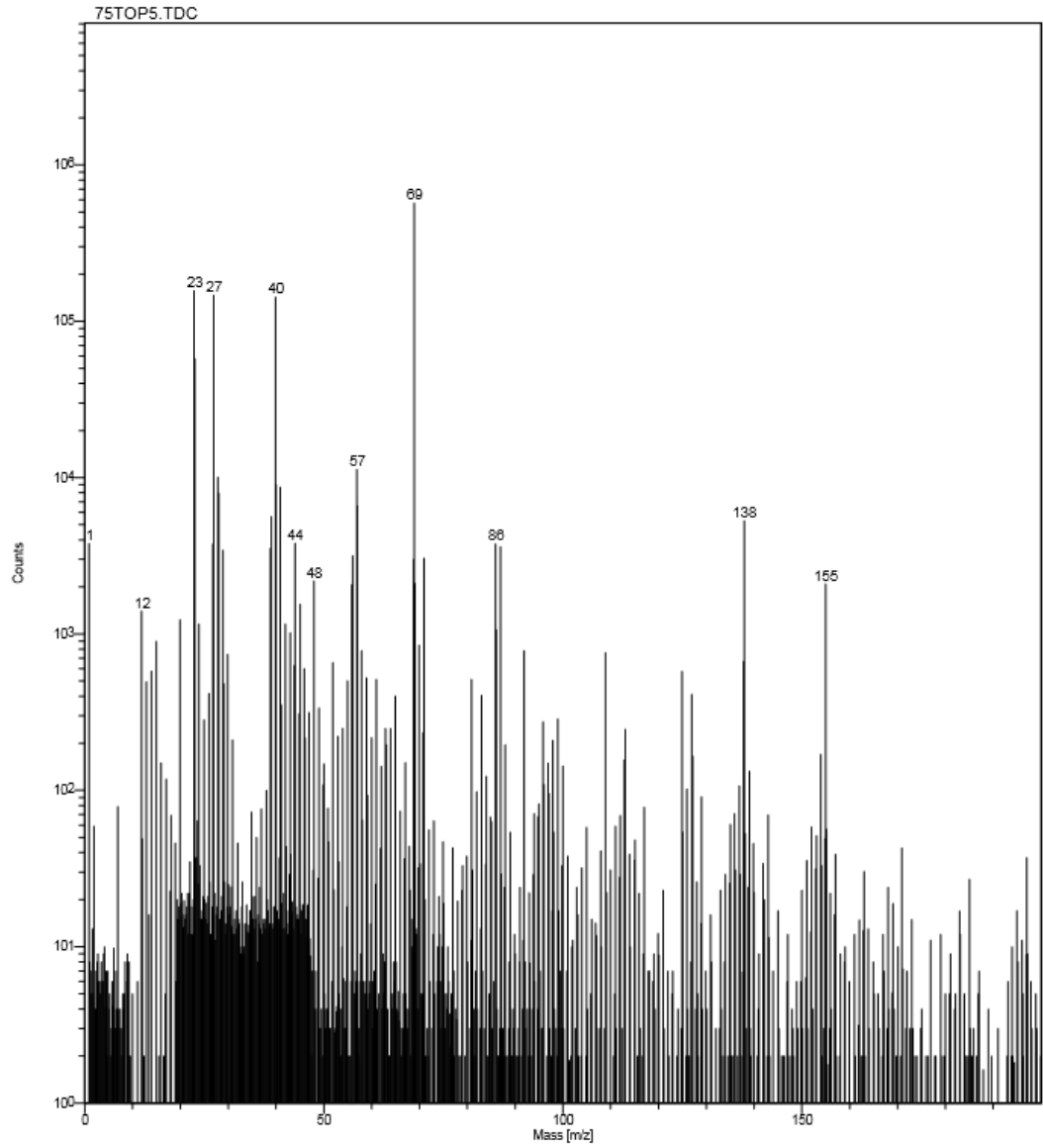
Physical Electronics, Inc.
6509 Flying Cloud Drive
Eden Prairie, MN 55344



75top5.tdc 4.0 min on September 26, 2014 + ions 1222041 cts (18.0 x 18.0 um) using LMIG
COMMENT: 75 sputter through top (700)5 minutes

Figure__

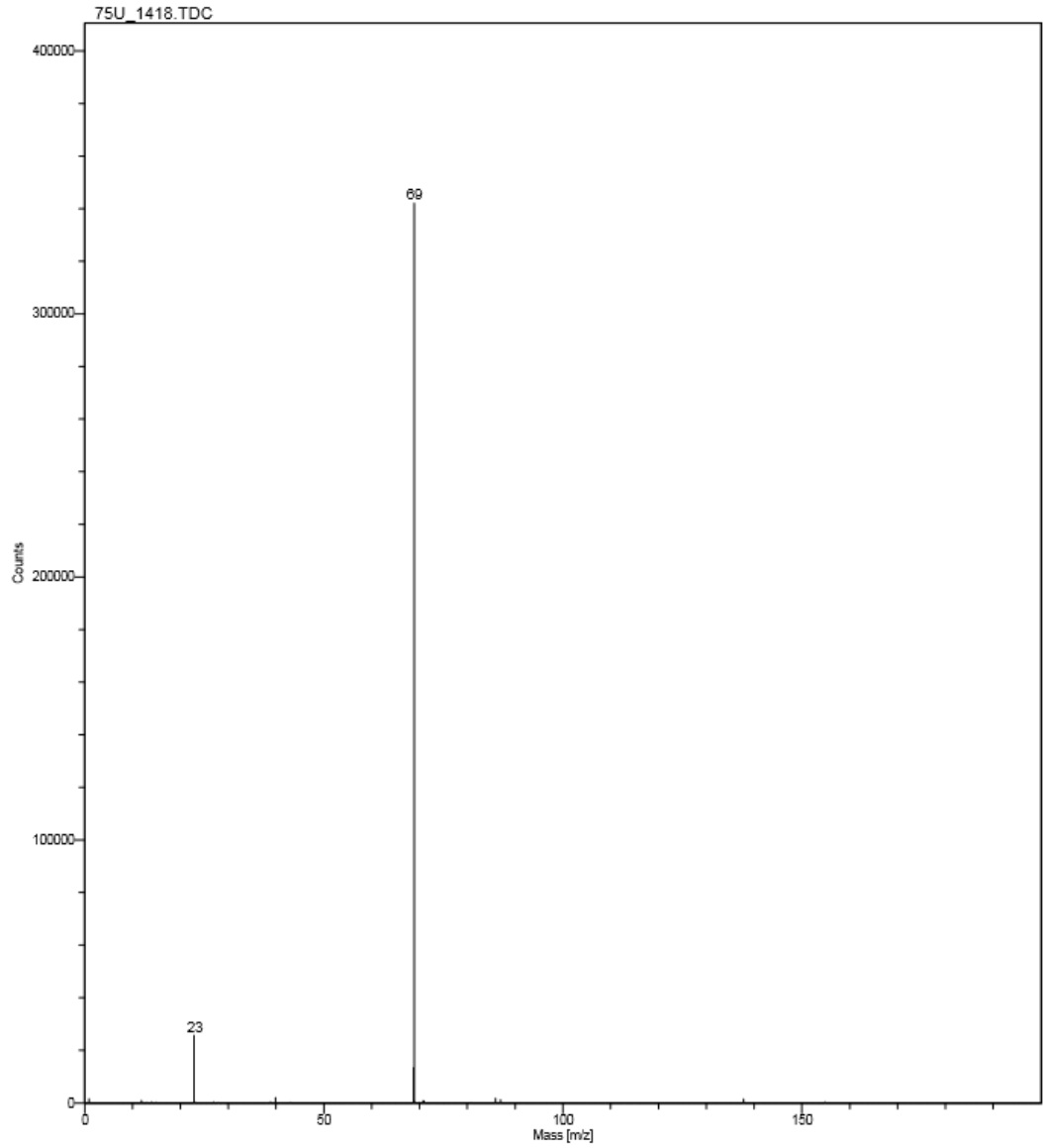
Physical Electronics, Inc.
6509 Flying Cloud Drive
Eden Prairie, MN 55344



75top5.tdc 4.0 min on September 26, 2014 + ions 1222041 cts (18.0 x 18.0 um) using LMIG
COMMENT: 75 sputter through top (700)5 minutes

Figure__

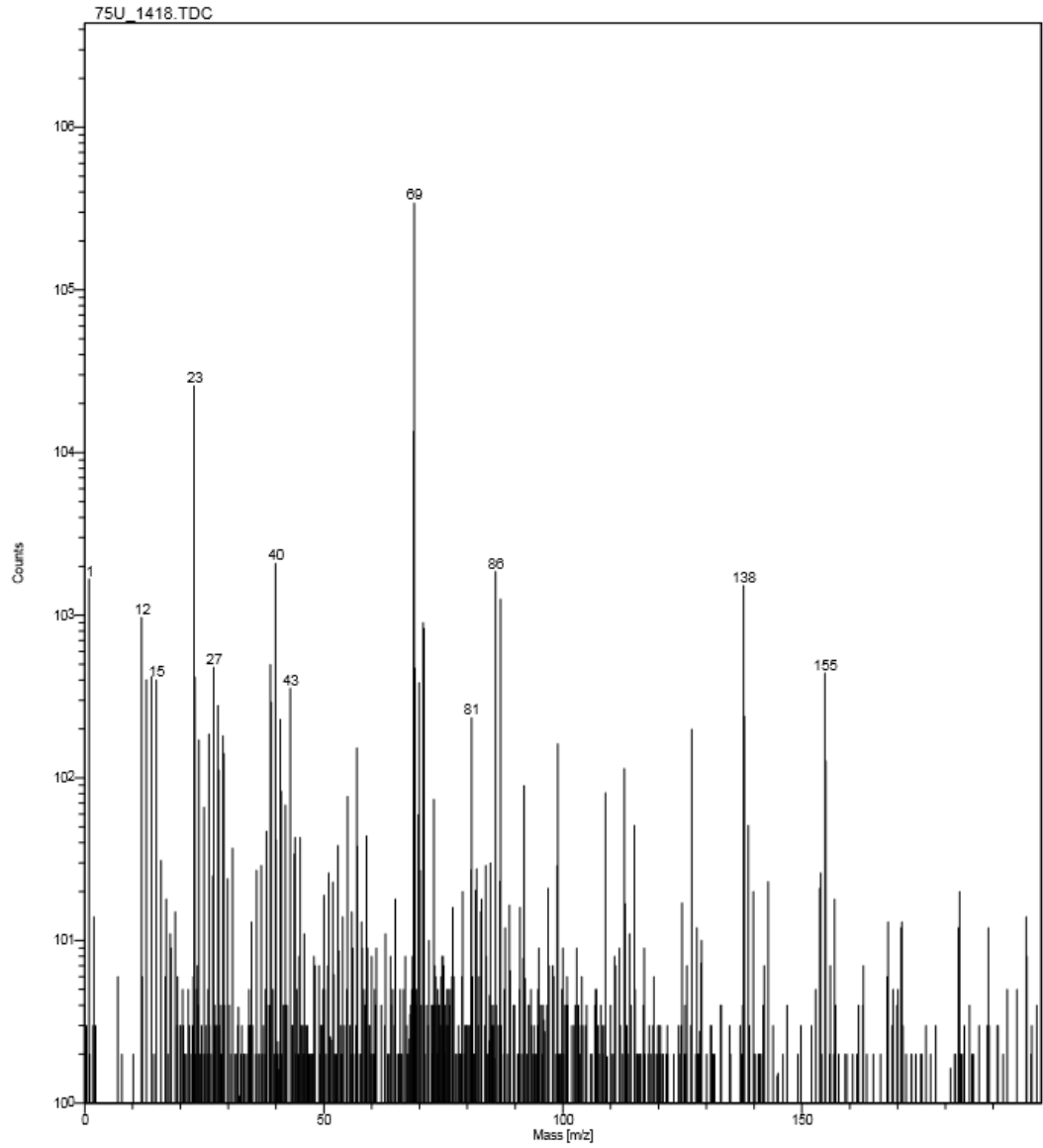
Physical Electronics, Inc.
6509 Flying Cloud Drive
Eden Prairie, MN 55344



75u_1418.tdc 5.0 min on September 26, 2014 + ions 403971 cts (18.0 x 18.0 um) using LMIG
COMMENT: 75 heated silver up

Figure__

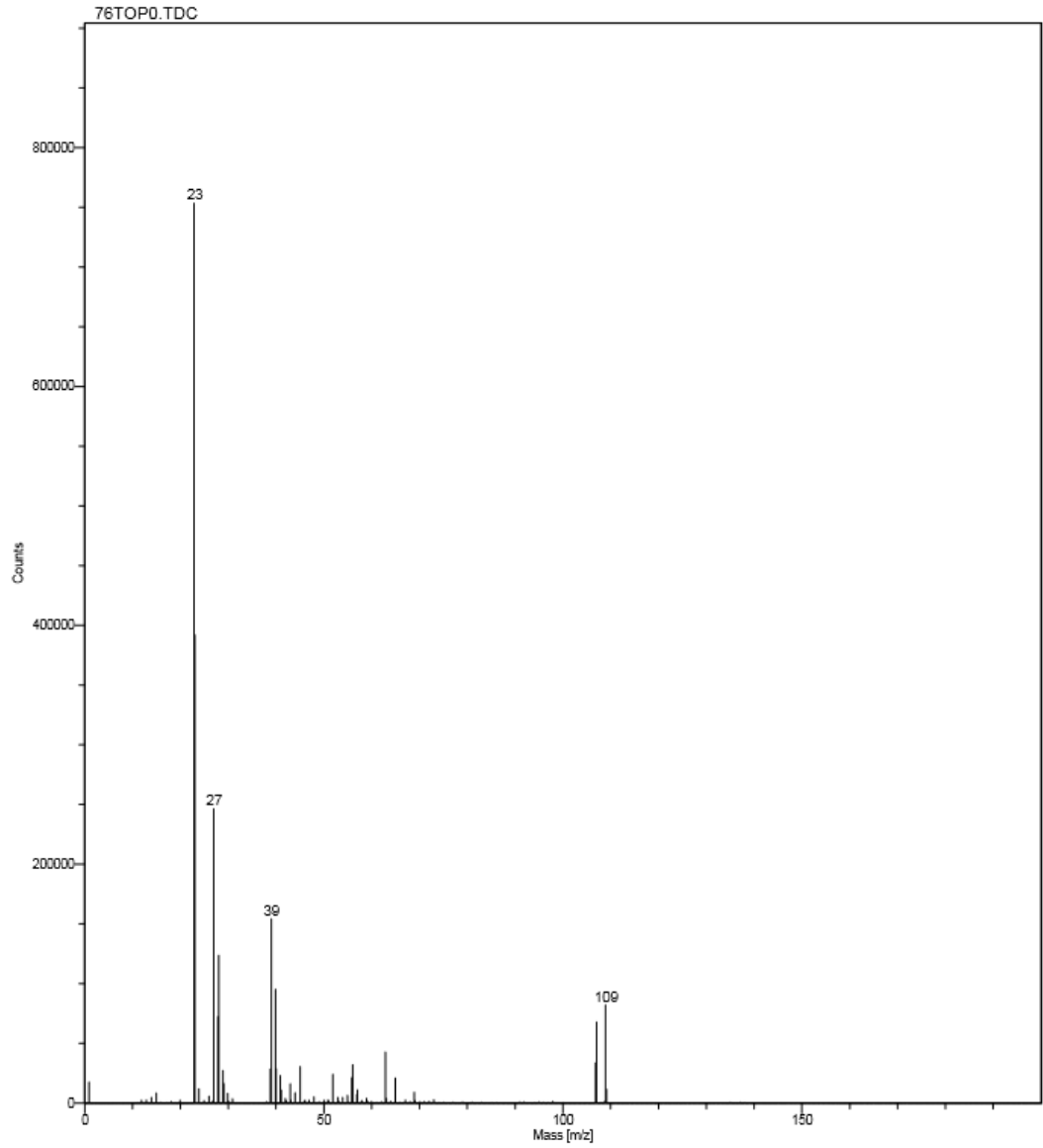
Physical Electronics, Inc.
6509 Flying Cloud Drive
Eden Prairie, MN 55344



75u_1418.tdc 5.0 min on September 26, 2014 + ions 403971 cts (18.0 x 18.0 um) using LMIG
COMMENT: 75 heated silver up

Figure__

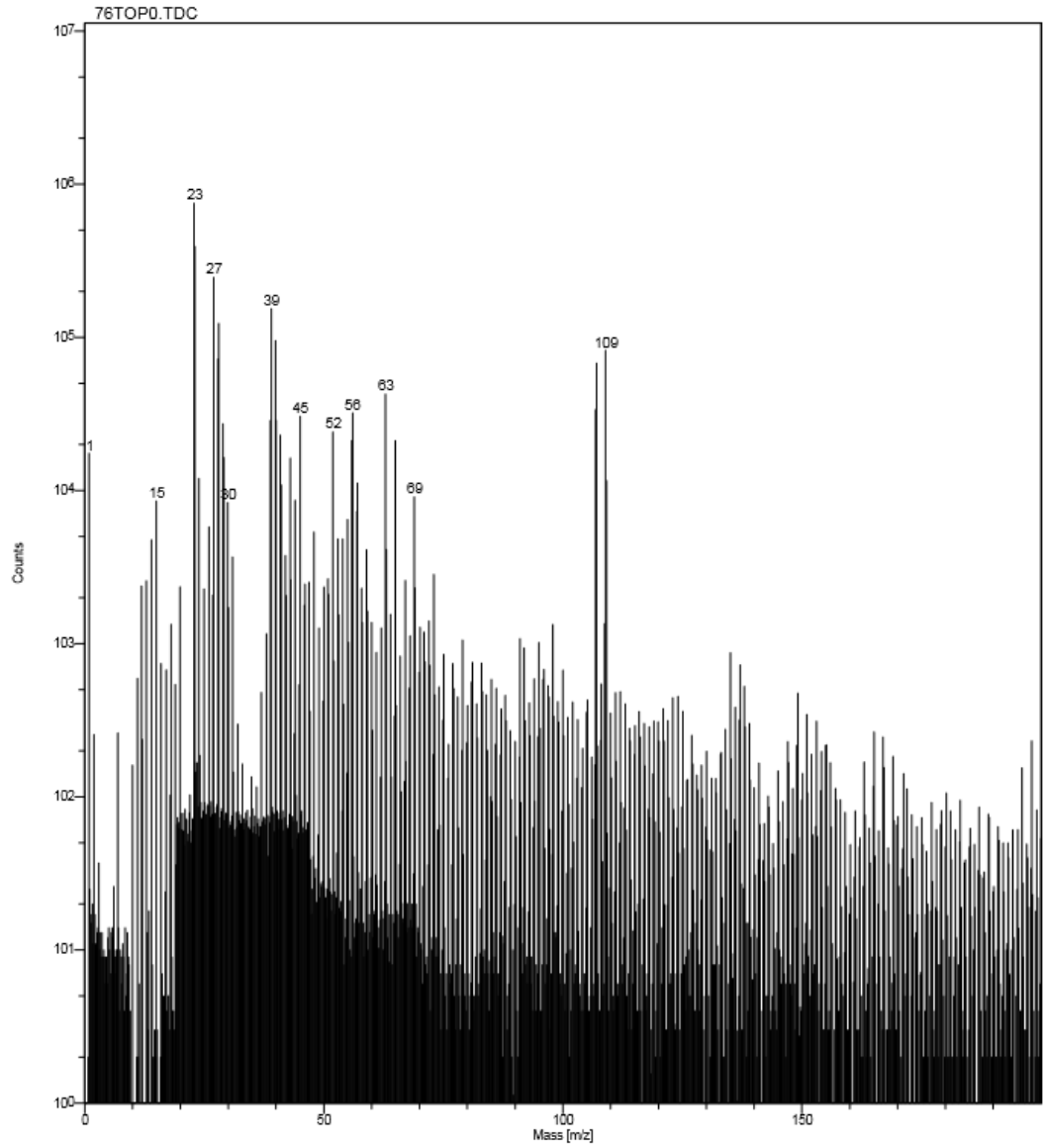
Physical Electronics, Inc.
6509 Flying Cloud Drive
Eden Prairie, MN 55344



76top0.tdc 4.0 min on September 26, 2014 + ions 2650634 cts (18.0 x 18.0 um) using LMIG
COMMENT: 76 heated 700 silver face down sputter through silver face0 minutes

Figure__

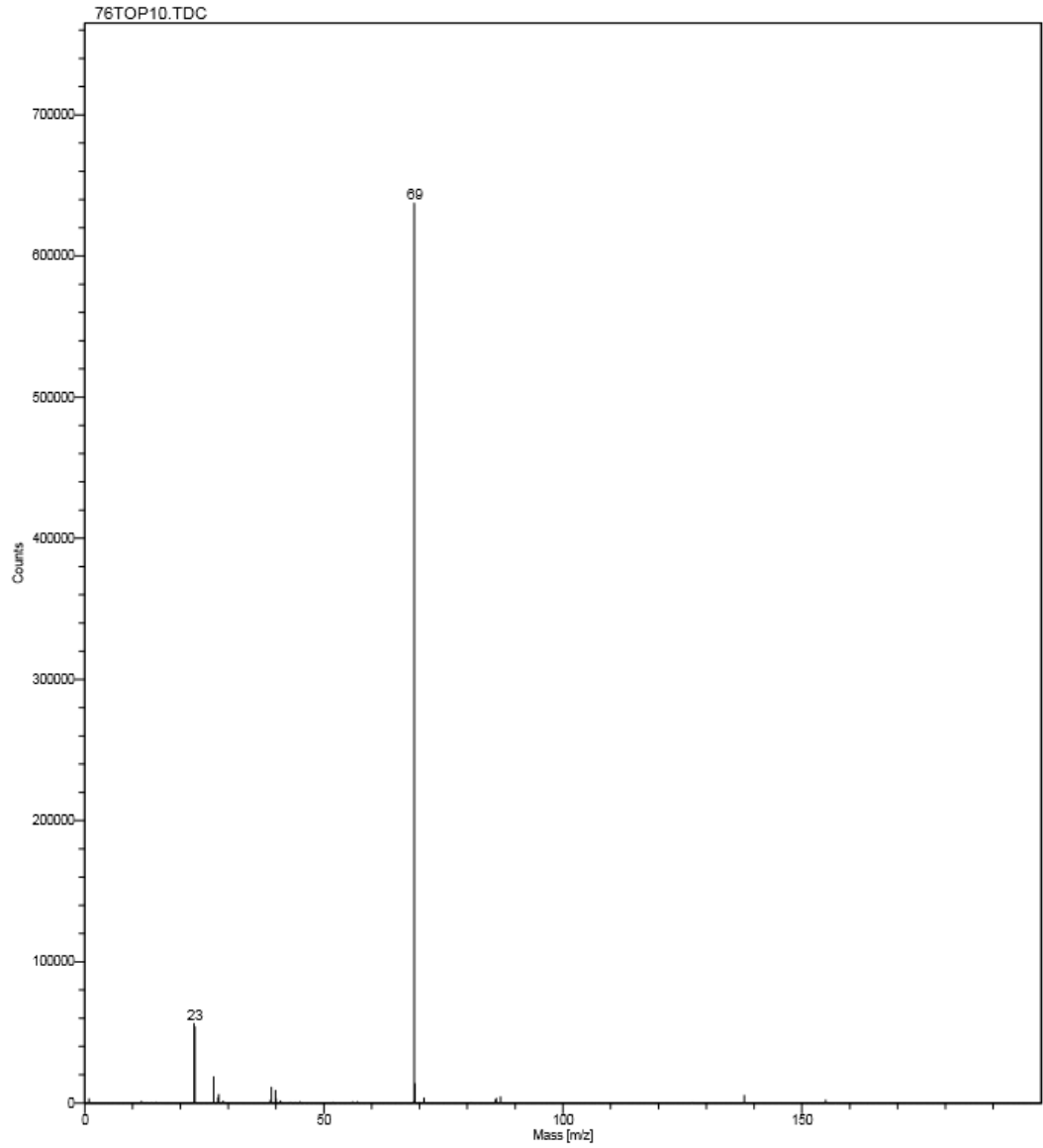
Physical Electronics, Inc.
6509 Flying Cloud Drive
Eden Prairie, MN 55344



76top0.tdc 4.0 min on September 26, 2014 + ions 2650634 cts (18.0 x 18.0 um) using LMIG
COMMENT: 76 heated 700 silver face down sputter through silver face0 minutes

Figure__

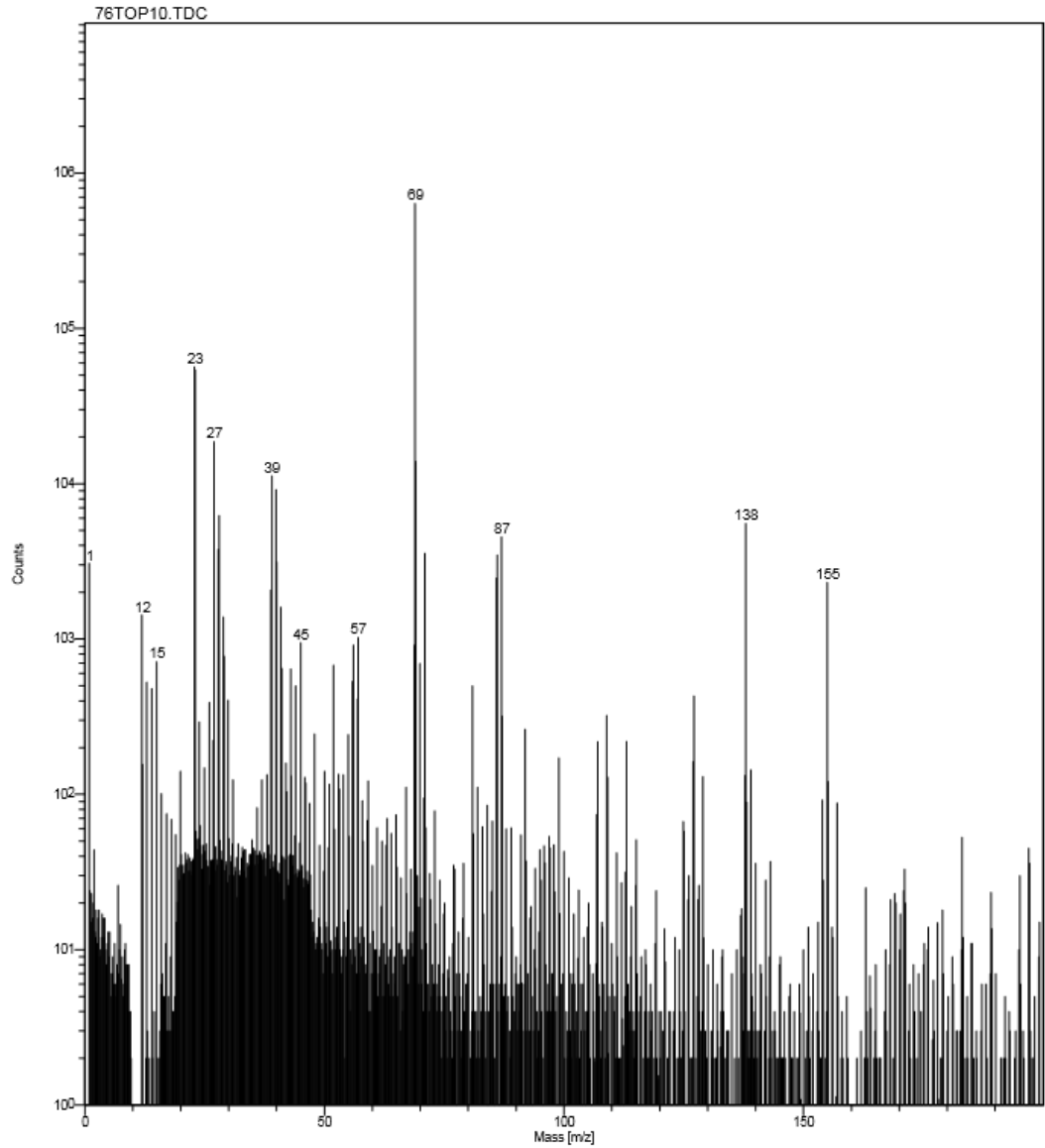
Physical Electronics, Inc.
6509 Flying Cloud Drive
Eden Prairie, MN 55344



76top10.tdc 4.0 min on September 26, 2014 + ions 877698 cts (18.0 x 18.0 um) using LMIG
COMMENT: 76 heated 700 silver face down sputter through silver face10 minutes

Figure__

Physical Electronics, Inc.
6509 Flying Cloud Drive
Eden Prairie, MN 55344



76top10.tdc: 4.0 min on September 26, 2014 + ions 877698 cts (18.0 x 18.0 um) using LMIG
COMMENT: 76 heated 700 silver face down sputter through silver face 10 minutes

Figure__